

FRP-CONCRETE-STEEL COMPOSITE COLUMNS

RETROFIT OF STRUCTURAL STEEL COLUMNS USING FRP-CONCRETE
COMPOSITE SYSTEMS

By JOEL LINDE, B.ENG.&MGT.

A Thesis Submitted to the School of Graduate Studies in Partial Fulfilment of the
Requirements for the Degree Master of Applied Science

McMaster University © Copyright by Joel Linde, April 2013

McMaster University MASTER OF APPLIED SCIENCE (2013) Hamilton,
Ontario

TITLE: Retrofit of Structural Steel Columns using FRP-Concrete
Composite Systems

AUTHOR: Joel Linde, B.Eng.&Mgt. (McMaster University)

SUPERVISOR: Professor M.J. Tait; Professor S.N. Razavi

NUMBER OF PAGES: xix, 203

Abstract

Fiber reinforced polymer (FRP) - confined concrete-steel composite columns have been recently introduced as a retrofit technique for structural steel columns. This technique involves placing an FRP tube around an in situ steel column and subsequently filling the void between the steel section and the FRP tube with concrete to create a composite column. The composite action occurs due to the concrete encasing the steel section and the FRP confining the concrete. An experimental investigation has been undertaken to evaluate: the effect of adding a steel W section to confined concrete; the effect of using a split tube system as a practical application technique; and the effect of shrinkage reducing admixture in confined concrete. A total of eighteen stub columns, consisting of six different column types were tested to meet these objectives. It was found that the load-displacement response of confined concrete that includes a steel W section is similar to the response of confined concrete plus the elastic-perfectly plastic steel contribution. Experimental findings demonstrate the enhanced performance of the proposed split tube retrofit technique. An analytical model was used to predict the response of the different column types. A method is proposed to incorporate the increased stiffness of the FRP jacket in the split tube system and is shown to be an improvement on the original model. A parametric study was also performed on the revised model.

Acknowledgements

This thesis would not have been possible without the help and guidance of several individuals who contributed and extended their valuable assistance in the completion of this study.

First, I would like to sincerely thank my supervisor, Dr. Michael Tait, for his guidance and assistance throughout the entire process. The encouragement, suggestions, and direction I received at all stages of this study were of unparalleled value. In addition, I would like to thank my co-supervisor, Dr. Saiedeh Razavi, for her insightful reviews and suggestions.

I would like to thank Dr. Kian Karimi for the help he has given me. The assistance he provided by helping me construct my initial test specimens, explaining his modelling work to me, and providing direction for my research was of immense benefit.

I would also like to thank the technical staff at the Applied Dynamics Lab (ADL) for the help I received in completing the experimental portion of this study. I would like to thank Mr. Kent Wheeler for his assistance and suggestions in the preparation of the test specimens and Mr. David Perrett for his help testing the column specimens. The help I received from Mr. Peter Koudys, Mrs. Connie Barry, and Dr. Michael Bruhis is also much appreciated.

Finally, I would like to thank my wife, Annemarie, and my daughter, Amy, for their unwavering support and encouragement to see this study through to the end.

Joel Linde

Department of Civil Engineering

McMaster University

Table of Contents

Abstract	iii
Acknowledgements	iv
Table of Contents	vi
List of Tables	xi
List of Figures	xii
List of all Abbreviations and Symbols	xvii
Chapter 1 - Introduction.....	1
1.1 General Introduction.....	1
1.2 Research Background.....	2
1.2.1 Steel Column Retrofit Background.....	2
1.2.2 Split Tube System for FRP-Confined Concrete.....	9
1.2.3 Shrinkage Reducing Admixture Concrete used in FRP- Confined Concrete	10
1.3 Significance of Research.....	12
1.4 Research Objectives	14
1.5 Methodology.....	15
Chapter 2 - Experimental Program.....	23
2.1 Introduction.....	23
2.2 Testing Matrix.....	24

2.3	Composite Column Components.....	26
2.3.1	Steel Section.....	26
2.3.2	FRP Tube	26
2.3.3	Concrete	33
2.4	Composite Column Construction.....	34
2.5	Test Setup and Instrumentation	35
2.5.1	Specimen Preparation	35
2.5.2	Specimen Instrumentation	36
2.5.3	Test Setup	36
2.6	Test Results	37
2.6.1	Load-Displacement Response.....	37
2.6.2	Failure Modes.....	39
2.6.3	Ultimate Experimental Measures	44
2.6.4	Hoop Strain.....	45
2.6.5	Enhancement Factors.....	46
2.6.6	Confinement Effects.....	49
2.7	Experimental Findings.....	50
2.7.1	Effect of Adding a Steel Section to Confined Concrete.....	50
2.7.2	Split Tube Effects.....	51
2.7.3	Shrinkage Reducing Admixture Effects.....	53

2.8	Conclusions.....	56
Chapter 3 - Modelling		102
3.1	Introduction.....	102
3.2	Composite Column Response.....	103
3.3	Steel Section Response	103
3.4	Concrete Parameters	104
3.5	Biaxial State of Stress	105
3.6	Uniaxial State of Stress	108
3.7	Design-Orientated Model.....	109
3.7.1	Design-Orientated Model Framework	109
3.7.2	Modelling of Column Type C2: CFRP-Confined Concrete .	111
3.7.3	Modelling of Column Type C4: CFRP-Confined Concrete-Steel Composite.....	118
3.7.4	Modelling of Column Type C6: CFRP-Wrapped Split-GFRP-Confined Concrete-Steel Composite.....	119
3.7.5	Comparison of All Design-Orientated Model Responses ...	122
3.8	Analysis-Orientated Model	122
3.8.1	Analysis-Orientated Model Framework	125
3.8.2	Modelling of Column Type C2: CFRP-Confined Concrete .	127
3.8.3	Modelling of Column Type C4: CFRP-Confined Concrete-Steel Composite.....	128

3.8.4	Modelling of Column Type C6: CFRP-Wrapped Split-GFRP-Confined Concrete-Steel Composite.....	129
3.8.5	Comparison of All Analysis-Orientated Model Responses.	136
3.9	Conclusion.....	136
Chapter 4	- Retrofit Design.....	162
4.1	Introduction.....	162
4.2	Parametric Study.....	165
4.2.1	Number of Plies of GFRP in the Split Tube.....	166
4.2.2	Number of Plies in the CFRP Wrap	167
4.2.3	Concrete Strength.....	168
4.2.4	Steel Ratio	169
4.2.5	Parametric Study Results	171
4.3	Code Predictions Comparison.....	171
4.3.1	The ACI440.2R-08.....	172
4.3.2	The CAN/CSA S6-06	174
4.3.3	The CAN/CSA S806-12	176
4.3.4	Comparison	177
4.4	Conclusions.....	179
Chapter 5	- Summary and Conclusions.....	191
5.1	Summary.....	191

5.2	Conclusion.....	193
5.3	Recommendations for Future Work.....	194
Chapter 6	References	196

List of Tables

Table 2.1: Testing Matrix	58
Table 2.2: Steel Section W150x14 Properties	59
Table 2.3: FRP Composite Laminate Properties from Data Sheets.....	60
Table 2.4: Coupon Test Material Properties	61
Table 2.5: Concrete Mix Design	62
Table 2.6: Concrete Cylinder Test Results	63
Table 2.7: Experimental Results.....	64
Table 2.8: Enhancement Factors.....	65

List of Figures

Figure 1.1: Proposed Composite Columns (Images from Karimi et al. (2011)).....	18
Figure 1.2: Snap-Tite FRP Jacketing System.....	19
Figure 1.3: Proposed Slotted Tube System by Liu et al. (2005)	20
Figure 1.4: Proposed Onion Skin Jacket System by Liu et al. (2005) and Karimi et al. (2010)	21
Figure 1.5: Proposed CFRP-Wrapped Split-GFRP-Confined Concrete-Steel Composite System	22
Figure 2.1: Column Types	66
Figure 2.2: CFRP Fiber Directions.....	67
Figure 2.3: CFRP Coupon Tensile Response Curves	68
Figure 2.4: Failed CFRP Coupons.....	69
Figure 2.5: Direction Definitions.....	70
Figure 2.6: FRP Tube Construction Process	71
Figure 2.7: Column Type C6 Split Tube Construction Process.....	72
Figure 2.8: CFRP-Wrapped Split-GFRP-Confined Concrete-Steel Composite Specimen Cross-Section	73
Figure 2.9: FRP Tubes Prior to Placing Concrete.....	74
Figure 2.10: Tube Instrumentation.....	75
Figure 2.11: Failed CFRP Tube.....	76
Figure 2.12: CFRP Tube Response Curves	77

Figure 2.13: Wooden Spacer.....	78
Figure 2.14: Specimen Preparation.....	79
Figure 2.15: Instrumentation.....	80
Figure 2.16: Test Setup.....	81
Figure 2.17: Axial Load vs. Axial Strain Column Specimen Response....	82
Figure 2.18: Axial Load vs. Axial Displacement Column Type Response	83
Figure 2.19: Comparison of Column Type Load – Strain Response.....	84
Figure 2.20: C1 – Steel Section Failed Specimen (From Karimi et al. (2010)).....	85
Figure 2.21: CFRP-Confined Concrete Failed Specimens	86
Figure 2.22: CFRP-Confined Shrinkage Reducing Admixture Concrete Failed Specimens.....	87
Figure 2.23: Steel, Rupture, and Overlap Location Orientation	88
Figure 2.24: C4-2 CFRP Rupture Location.....	89
Figure 2.25: CFRP-Confined Concrete-Steel Composite Failed Specimens	90
Figure 2.26: CFRP-Confined Shrinkage Reducing Admixture Concrete-Steel Composite Failed Specimens.....	91
Figure 2.27: CFRP-Wrapped Split-GFRP-Confined Concrete-Steel Composite Failed Specimens.....	92
Figure 2.28: CFRP-Wrapped Split-GFRP-Confined Concrete-Steel Composite Failed Specimen Components	93

Figure 2.29: Ultimate Hoop Strain	94
Figure 2.30: Hoop Strain Distribution around Circumference at Ultimate Capacity	95
Figure 2.31: Definition of Energy Dissipation Capacity Idealization	96
Figure 2.32: Energy Dissipation Capacity	97
Figure 2.33: Effect of Adding Steel W Section to CFRP Confined Concrete	98
Figure 2.34: Split Tube Effects	99
Figure 2.35: Shrinkage Reducing Admixture Effects on Confined Concrete	100
Figure 2.36: Shrinkage Reducing Admixture Effects Compared.....	101
Figure 3.1: Column Types	138
Figure 3.2: Biaxial State of Stress in CFRP Jacket.....	139
Figure 3.3: CFRP Secondary Direction Material Response Curve	140
Figure 3.4: Model Framework	141
Figure 3.5: Confining Action	142
Figure 3.6: Design-Orientated Model for Column Type C2.....	143
Figure 3.7: Design-Orientated Model for Column Type C4.....	144
Figure 3.8: Confining Pressure Distribution around Circumference	145
Figure 3.9: Design-Orientated Model for Column Type C6.....	146
Figure 3.10: Design-Orientated Model Comparison Plot	147

Figure 3.11: Generation of a Passive Confinement Model from a Family of Active Confinement Models with the Properties of Column Type C2.....	148
Figure 3.12: Analysis-Orientated Model Flowchart.....	149
Figure 3.13: Column Type C2 Axial-Hoop Strain Relationship	150
Figure 3.14: Column Type C2 Load vs. Strain Response.....	151
Figure 3.15: Column Type C4 Axial-Hoop Strain Relationship	152
Figure 3.16: Column Type C4 Load vs. Strain Response.....	153
Figure 3.17: Column Type C6 Axial-Hoop Relationship for 2 Ply CFRP Jacket.....	154
Figure 3.18: Column Type C6 Load vs. Strain Response Assuming 2 Ply CFRP Jacket	155
Figure 3.19: Comparison of Axial-Hoop Strain Relationship for Column Types C2, C4, and C6.....	156
Figure 3.20: Column Type C6 Jacket Locations	157
Figure 3.21: Column Type C6 Axial-Hoop Strain Relationship Comparison	158
Figure 3.22: Influence of the number of GFRP Plies on the factor β	159
Figure 3.23: Column Type C6 Load vs. Strain Response Incorporating Increased Jacket Stiffness.....	160
Figure 3.24: Analysis-Orientated Model Comparison	161
Figure 4.1: Effect of the Number of GFRP Plies on the Load vs. Strain Response	180

Figure 4.2: Influence of the Number of GFRP Plies.....	181
Figure 4.3: Effect of the Number of CFRP Plies on the Load vs. Strain Response	182
Figure 4.4: Influence of the Number of CFRP Plies.....	183
Figure 4.5: Effect of the Concrete Strength on the Load vs. Strain Response	184
Figure 4.6: Influence of the Concrete Strength	185
Figure 4.7: Influence of Concrete Strength on Split Tube FRP Jacket Confinement Effectiveness.....	186
Figure 4.8: Effect of the Steel Ratio on the Load vs. Strain	187
Figure 4.9: Influence of the Steel Ratio	188
Figure 4.10: Comparison of Experimental Response to Code Determined Resistance Values for Column Type C2.....	189
Figure 4.11: Comparison of Experimental Response to Code Determined Resistance Values for Column Type C4.....	190

List of all Abbreviations and Symbols

α	=	analysis-orientated model constant;
α_1	=	compressive concrete factor;
β	=	ratio of the rupture hoop strain of the hybrid jacket compared to the 2 ply CFRP region;
γ_{ah}	=	shear strain;
γ_c	=	density of concrete;
δ_u	=	ultimate axial displacement;
δ_y	=	axial yield displacement;
ε_a	=	strain in the axial direction;
ε_c	=	axial strain;
ε_{co}	=	strain of unconfined concrete at peak compressive stress;
ε_{cc}^*	=	axial strain at peak axial stress in the active confinement model;
ε_{cc}	=	ultimate axial strain of confined concrete;
ε_{fe}	=	effective strain level;
ε_{frp}	=	ultimate strain of FRP as determined by coupon tests;
ε_h	=	strain in the hoop direction;
$\varepsilon_{h,rupt}$	=	maximum hoop strain at rupture of FRP tube;
$\varepsilon_{h,rupt,CFRP}$	=	maximum hoop strain at rupture of CFRP jacket;
$\varepsilon_{h,rupt,Hybrid}$	=	maximum hoop strain at rupture of hybrid jacket;
ε_p	=	strain in primary fiber direction;
ε_s	=	strain in secondary fiber direction;
ε_t	=	transition strain;
κ_a	=	geometry efficiency factor;
κ_ε	=	FRP strain efficiency factor;
ν	=	Poisson's ratio;
ν_{ah}	=	Poisson's ratio for CFRP corresponding to a contraction in the hoop direction due to an extension in the axial direction;
ν_{ha}	=	Poisson's ratio for CFRP corresponding to a contraction in the axial direction due to an extension in the hoop direction;
ν_{ps}	=	Poisson's ratio for CFRP corresponding to a contraction in the secondary fiber direction due to an extension in the primary fiber direction;
ν_{sp}	=	Poisson's ratio for CFRP corresponding to a contraction in the primary fiber direction due to an extension in the secondary fiber direction;
ρ_k	=	confinement stiffness ratio;
ρ_e	=	strain ratio;
σ_a	=	stress in the axial direction;
σ_h	=	stress in the hoop direction;

- σ_l = confining pressure;
- $\sigma_l(\varepsilon_h)$ = confining pressure as a function of hoop strain;
- τ_{ah} = shear stress;
- ϕ = material strength reduction factor;
- ϕ_c = concrete strength reduction factor;
- ϕ_F = FRP strength reduction factor;
- ϕ_{FRP} = FRP strength reduction factor;
- ϕ_s = steel strength reduction factor;
- Ω_{CFRP} = FRP efficiency factor for the CFRP jacket;
- ψ_f = confined concrete strength reduction factor;
- Ω_{frp} = FRP efficiency factor;
- Ω_{Hybrid} = FRP efficiency factor for the hybrid jacket;
- A = analysis-orientated model constant of 0.85;
- A_c = cross-sectional area of concrete;
- A_s = cross-sectional area of steel;
- B = analysis-orientated model constant of 0.75;
- c = normalized ultimate strain of unconfined concrete;
- C = analysis-orientated model constant of 0.7;
- C.A.I. = composite action index;
- CES = concrete encased steel;
- CFFT = concrete filled FRP tube;
- CFRP = carbon fiber reinforced polymer;
- CFST = concrete filled steel tubular;
- C.O.V. = coefficient of variation;
- C.R. = confinement ratio;
- d = inner diameter of FRP tube;
- D = analysis-orientated model constant of 7;
- DIC = digital image correlation;
- E_2 = slope of second portion of model response;
- E_a = Young's modulus in the axial direction;
- E_c = Young's modulus for unconfined concrete;
- E_{CFRP} = Young's modulus for the CFRP jacket;
- E_d = energy dissipation capacity;
- E_{GFRP} = Young's modulus for the GFRP jacket;
- E_h = Young's modulus in the hoop direction;
- E_{Hybrid} = Young's modulus for the hybrid jacket;
- E_p = Young's modulus for CFRP in the primary fiber direction;
- E_s = Young's modulus for CFRP in the secondary fiber direction;
- f = 1 MPa;
- f_c = axial stress;
- f_c = compressive strength of unconfined concrete;
- f_{cc}^* = peak axial stress in the active confinement model;
- f_{cc} = compressive strength of confined concrete;

$f_c(\varepsilon)$ = confined concrete stress as a function of axial strain;
 f_F = tensile stress in the FRP in the hoop direction;
FRP = fiber reinforced polymer;
 f_{FRPu} = tensile strength of the FRP in the hoop direction;
 f_l = maximum confining pressure;
 f_L = confining pressure;
 $f_{l,FRP}$ = confinement pressure due to FRP strengthening;
 $f_s(\varepsilon)$ = steel stress as a function of axial strain;
 f_{Fu} = ultimate tensile strength of FRP components;
 f_y = yield strength of steel;
G = shear modulus;
GFRP = glass fiber reinforced polymer;
HSS = hollow steel section;
 k_1 = confinement effectiveness ratio;
 k_2 = strain enhancement coefficient;
 k_c = confinement coefficient;
 k_l = confinement factor;
 I_x = moment of inertia about primary axis;
 I_y = moment of inertia about secondary axis;
 $P(\varepsilon)$ = column capacity as a function of axial strain;
 P_r = factored column capacity;
 $P_{ult.}$ = ultimate axial capacity;
r = constant to account for concrete brittleness;
RC = reinforced concrete;
SRA = shrinkage reducing agent;
t = thickness of the FRP tube;
 t_{CFRP} = thickness of the CFRP jacket;
 t_{GFRP} = thickness of the GFRP jacket;
 t_{Hybrid} = thickness of the hybrid jacket;

Chapter 1 - Introduction

1.1 General Introduction

As of December 2011, the Federal Highway Administrative Bridge Programs National Bridge Inventory (2012) reported 67,525 of the 605,098 bridges in the United States as structurally deficient. The average direct cost of corrosion on these bridges was reported as \$8.3 billion per year (Lee, 2012) and the indirect costs were estimated as ten times this amount. Steel bridges comprise 133,839 of these and account for 30,806 of the structurally deficient bridges (Federal Highway Administrative Bridge Programs National Bridge Inventory, 2012). Work is ongoing to repair these structurally deficient bridges and over the last decade around 1200 steel bridges per year have been rehabilitated (Federal Highway Administrative Bridge Programs National Bridge Inventory, 2012). One of the main types of deterioration of steel bridges is coating failure which exposes the structural steel. It was suggested that the current state of the U.S. bridge deterioration can be improved if more maintenance resources and attention is given to preserve many old small steel bridges (Lee, 2012).

Indeed, a significant amount of aging civil infrastructure in North America has been constructed with steel columns. Some of these columns have deteriorated due to corrosion while others have been over stressed as a

result of overloading. Various methods have been employed to restore the original carrying capacity or increase it to deal with higher load demands. For existing infrastructure, substantial cost savings can be realized through an effective retrofit technique compared to column replacement.

Strengthening techniques should increase the corrosion resistance of the steel column to delay or prevent future corrosion. In addition, the technique should provide resistance against local and cross-sectional buckling. Finally, it is beneficial if the retrofit technique can improve the fire-rating of the steel section although this is not a concern for steel structural members in bridge structures.

1.2 Research Background

1.2.1 Steel Column Retrofit Background

1.2.1.1 *FRP Laminate*

Retrofit of steel members using fiber reinforced polymers (FRP) has been mainly limited to beams and girders. For example, Liu et al. (2005) used epoxy to attach FRP laminates to the tensile flange of flexural members in areas where loss of section had occurred due to corrosion. They found this retrofit scheme to increase the stiffness and capacity of corroded steel members. Shear strengthening has been investigated by Patnaik et al. (2004) by attaching FRP strips to the web of a steel section with fibers

orientated vertically. However, little work has been done using FRP to strengthen steel compression members. What has been done has been limited to hollow steel sections (HSS). Shaat and Fam (2006) investigated wrapping HSS columns with FRP. For short columns they found that FRP orientated transversely confined the steel member and prevented outward local buckling. Longer columns are more susceptible to overall buckling therefore FRP orientated longitudinally on the member was found to increase load capacity by resisting this failure mechanism.

1.2.1.2 Concrete Encased Steel

Composite column systems may be used as a retrofit technique in some cases. For example, Mirza et al. (2004) describe a concrete encased steel (CES) column technique in which concrete is cast around in situ steel columns. The concrete delays the onset of local buckling in the steel column and the overall buckling capacity is increased as a result of the larger cross sectional area. For this composite system, the steel is not exposed, which reduces corrosion concerns. In addition, the outer surface of the composite column is concrete, which leads to a higher fire rating than the original unencased steel section. However, the concrete is not confined, so reinforced concrete (RC) hoops or spiral ties are required to prevent spalling. Finally, formwork is required to place the concrete, which incurs substantial costs.

1.2.1.3 Concrete-Filled Steel Tubular

Another type of composite column retrofit technique involves filling steel tubular columns with concrete. This type of composite column is referred to as a concrete-filled steel tubular (CFST) column (Yang, Lam, & Gardner, 2008). The infill concrete prevents inward local buckling of the steel section and delays the overall buckling due to the increased cross sectional area. The tubular steel confines the concrete and allows the concrete to achieve greater compressive strengths than unconfined concrete. The steel section also acts as a stay in place formwork for the concrete. However, these columns have exposed steel which makes them susceptible to corrosion and leads to a lower fire rating than CES columns.

1.2.1.4 FRP Confined Concrete

FRP has been widely utilized as an alternative confining material to tubular steel in composite columns. FRP has a higher corrosion resistance than steel, which increases its durability and life span, particularly in harsh saline environments. FRP-confinement has been used extensively as a retrofit scheme on existing RC columns. FRP confined concrete can be classified into two types. In the first, the FRP fabric is impregnated with epoxy on site and is wrapped around the concrete column in situ. In the second type, manufactured FRP tubes act as formwork and are filled with concrete. The latter are referred to as concrete-filled FRP tubes (CFFT).

FRP wrapping is generally used as a retrofitting technique for RC columns whereas CFFT is generally used for composite columns in new construction such as piles. Both methods create FRP-confined concrete composite columns in which the confined concrete can reach up to 3.5 times the original concrete strength. Several commercial companies, such as Fyfe and Sika, produce FRP fabric for wrapping applications. The FRP fabric is impregnated with an epoxy resin and then wrapped around the RC column. Several commercial companies, such as Ameron and Amiantit, manufacture FRP tubes. Researchers have utilized these commercially available tubes and filled them with concrete to construct CFFT specimens. Much research has been done on FRP confined concrete constructed by both types of application. Although a study by Lam and Teng (2003) reported a significant difference between the two types of application, a more recent study by Mohamed and Masmoudi (2010) reported that the behaviours of FRP wrapped concrete and CFFT are similar. The main difference between the two is the bond between the concrete and the FRP jacket. In FRP wrapped applications, the wet epoxy cures against the concrete core and forms a strong bond. In CFFT specimens the concrete cures against the inside of the tube with minimal bonding. Mirmiran et al. (1998) tested and compared FRP wrapped concrete specimens to CFFT specimens. They cut specimens of each type open and reported that the concrete and the FRP tube in the CFFT

specimens separated with ease but the FRP wrapped concrete specimens resulted in a cracked concrete core with a significant amount of concrete attached to the FRP jacket due to the strong epoxy bond. However, they reported no significant difference in the response of FRP wrapped concrete and CFFT specimens.

1.2.1.5 FRP Confined Concrete encasing Pultruded FRP Section

Mirmiran et al. hold U.S. patents 5599599 and 6123485. These patents cover CFFT which includes an interior FRP reinforcement. This reinforcement can include FRP pultruded shapes such as an H section or FRP longitudinal reinforcing bars with additional FRP cross ties.

1.2.1.6 Rectangular FRP-Confined Concrete-Steel Composite

Karimi et al. (2011) recognized the benefits of FRP in retrofit application and applied it to steel columns. The steel W section was first wrapped with a single ply of glass fiber reinforced polymer (GFRP) to prevent galvanic corrosion, which occurs when steel and carbon fiber are in direct contact. A carbon fiber reinforced polymer (CFRP) sheet was subsequently wrapped around the GFRP ply. The unidirectional CFRP was orientated in the transverse direction in order to provide confinement. The wrapped column is shown in Figure 1.1 (a). The dry sheets were impregnated with a two part epoxy before being applied to the specimens. A 250 mm

overlap ensured that debonding would not occur before the fiber sheets reach their ultimate strength. The void between the FRP wrap and the steel section was filled with concrete creating rectangular FRP-confined concrete-steel composite columns. The concrete restrained local buckling of the steel section and overall buckling was delayed due to the increased cross sectional area. This method improved the corrosion resistance of the initial steel section since the outermost material is FRP which has higher corrosion resistance than the original steel section. The confining FRP allowed the confined concrete to reach up to three times its unconfined compressive strength. Ultimate failure in the retrofitted specimens was caused by rupture of the FRP. Increases in stiffness and ductility and a 200-300% increase in load capacity demonstrated the effectiveness of this technique. Karimi et al. (2011) also investigated the effect of high stress concentrations in the FRP at the corners of the rectangular section. Reinforcing bars were placed in the four corners of the rectangular columns at the edges of the flanges to reduce the influence of stress concentrations as shown in Figure 1.1 (b).

1.2.1.7 Circular FRP-Confined Concrete-Steel Composite

Circular FRP tubes were introduced as an alternative to directly wrapping the steel section with FRP. This technique eliminates the development of stress concentrations at the corners of the steel section since the steel is not in direct contact with the FRP. The steel column to be retrofitted is

surrounded with an FRP tube and the void between the steel column and the FRP tube is subsequently filled with concrete. Results presented by Karimi et al. (2010) demonstrated increased load capacity of the composite columns of up to 5.5 times that of the original steel section. The results also showed an increase in axial elastic stiffness of 4.4 times compared to the original stiffness of the steel column. Furthermore, the ultimate axial strain of the composite columns was twice that of the original steel section. The outermost material is FRP which protects the steel from corrosion. The FRP confines the concrete and the encasing action of the concrete postpones the onset of local buckling in the steel web and flanges. Finally, the FRP acts as stay in place formwork reducing construction time and expense. Karimi et al. (2010) present this method as a retrofit technique for existing steel columns to restore or increase load carrying capacity.

Liu et al. (2005) investigated a similar technique for strengthening corroded steel columns. They simulated the loss of section due to corrosion on steel W sections by notching a portion of the flanges. The retrofit technique involved surrounding the steel W section with a GFRP tube in the vicinity of the notch and filling the void between the tube and the steel section with concrete. The length of the retrofitted portion was suggested as the length of the corroded portion of the member plus two times the development length required. The retrofit was shown to restore

and exceed the carrying capacity of the member and forced failure due to overall bending to occur outside the retrofitted region.

1.2.2 Split Tube System for FRP-Confined Concrete

A commercial system called Snap-Tite, invented by N.C. Fawley and owned by NCF Industries, was introduced in 1995. The system utilizes a series of pre-manufactured GFRP cylindrical shells each with a single longitudinal slit (Xiao & Ma, 1997). Each shell component is 3.2 mm thick and “snaps on” to RC columns as a retrofit solution. A typical column requires 4-5 shell elements. The column is coated with urethane adhesive before the first shell is applied and then between subsequent shells. The nested shells are bound with belt clamps until the adhesive cures. The slit for each ply is not butt bonded and the continuity relies on the subsequent ply. Therefore, the effective number of plies is considered as the total ply number less the last ply. A schematic of a retrofitted column with 4 shell elements is shown in Figure 1.2. A study by Xiao et al. (1999) reported that the prefabricated shell system had minimal impact on flexural stiffness or flexural strength compared to FRP wrapped retrofit techniques. The Snap-Tite system was approved for highway RC column retrofit projects by the California Department of Transportation (Caltrans) and was used to strengthen 3,480 concrete columns of the Yolo County Causeway (International Institute for FRP in Construction, 1998).

Liu et al. (2005) proposed two retrofit techniques for the application of an FRP jacket around an in situ steel column. The first is a slotted tube system similar to the Snap-Tite system used for retrofitting RC columns. A schematic of the system is shown in Figure 1.3. The second technique involves bonding open shapes together with epoxy to form an onion skin jacket as shown in Figure 1.4. Karimi et al. (2010) suggested the onion skin retrofit technique as a practical application to strengthen steel W sections with FRP-concrete-steel composite columns. Liu et al. (2005) and Karimi et al. (2010) both propose application techniques, but due to simplicity of construction they both use solid, pre-manufactured GFRP tubes in their studies.

1.2.3 Shrinkage Reducing Admixture Concrete used in FRP-Confined Concrete

El Chabib et al. (2005) tested concrete confined in short GFRP tubes. They compared concrete with ordinary Portland cement to concrete with expansive cement that also included a commercial shrinkage reducing admixture. They reported that the use of expansive cement in concrete delayed the occurrence of slip between the GFRP tube and the concrete core however it did not fully prevent slippage. They reported that no significant change was observed in the confinement effect on concrete strength and ductility under uniaxial compression.

Yang et al. (2008) investigated the effects of concrete shrinkage on elliptical steel tubular confined concrete. The inner surfaces of the steel tubes for 6 of the 21 specimens were coated with grease before the concrete was poured in an effort to simulate the loss of contact due to concrete shrinkage. It was reported that shrinkage has negative effects on the bond between concrete and the steel tube and can even prevent the composite action from occurring. They reported less than 5% deviation in ultimate load between the greased and the ungreased specimens and concluded the effects to be negligible.

Harries et al. (2003) used a small gap created by plastic wrap to study the effect of FRP jackets which were bonded versus unbonded to the concrete core. They reported a lower confined concrete strength in the unbonded specimens which they attributed to the fact that the unbonded cylinders must initially dilate to close the gap and engage the FRP jacket. Strain gauges on the FRP jacket provided axial strain measurements. It was reported that these measurements were incorrect since the initial gap did not ensure strain compatibility between the FRP jacket and the concrete core at the beginning of the test. They found the overall efficiency of the jacket not to be affected by the gap. If one assumes that the gap simulates concrete shrinkage, the results can be extended to suggest that concrete shrinkage causes a decrease in compressive strength over concrete with reduced shrinkage.

Karimi et al. (2010) tested a single GFRP-confined concrete-steel composite column specimen that utilized concrete with shrinkage reducing admixture and found an increase in performance in this specimen over a similar specimen that did not include shrinkage reducing admixture. They reported a 20% increase in load carrying capacity, a 23% increase in elastic axial stiffness, a 24% increase in ultimate axial strain, and a 23% increase in the confined concrete strength for the specimen that contained shrinkage reducing admixture in the concrete.

1.3 Significance of Research

Review of the literature reveals that retrofit techniques for steel compressive members using FRP are limited. The two studies which utilize FRP-confined concrete columns report the technique as beneficial to increase load carrying capacity, axial stiffness, and ductility. However, a more comprehensive database of testing needs to be assembled before this technique can be employed.

The response of confined concrete has been studied and modelled extensively by others. In addition, Karimi et al. (2010) and Liu et al. (2005) both investigated the response of composite columns comprised of a steel W section encased in confined concrete. However, neither of them tested confined concrete without a steel section as a comparison. The current study investigates the direct effect of adding a steel W section to the

confined concrete. This is accomplished by testing and contrasting confined concrete with and without a steel *W* section.

Experimental testing of the Snap-Tite FRP jacketing technique focused on flexural and shear enhancements but did not test the technique for compressive qualities. Liu et al. (2005) and Karimi et al. (2010) both propose application techniques, but due to simplicity of construction they both use solid, premade tubes in their studies. The current study investigates a practical application technique to apply the system in a retrofit scenario on an in situ steel *W* section column. A 2 ply thick, GFRP tube is constructed and then cut longitudinally into two half-tube elements. In a retrofit scenario, these two half-tube elements are brought together to surround an in situ steel *W* section. They are subsequently wrapped with two plies of wet layup CFRP. The CFRP cures and is incorporated with the split GFRP tube to create a solid FRP jacket. The void between the steel *W* section and the FRP jacket is subsequently filled with concrete to complete the composite column. This process is shown in Figure 1.5. The technique provides a straight forward method of applying the retrofit technique reported by Karimi et al. (2010).

A review of the literature regarding the effect of shrinkage reducing admixture in concrete used in confined concrete columns is conflicting. El Chabib et al. (2005) and Yang et al. (2008) reported that the addition of

shrinkage reducing admixture had no significant effect. However, Karimi et al. (2010) reported an increase in performance for a specimen containing concrete with shrinkage reducing admixture over a similar specimen that did not include shrinkage reducing admixture. These studies use different techniques to explore the effect of shrinkage reducing admixture and reach opposing conclusions. The current study directly investigates the effect of using concrete with shrinkage reducing admixture in a confined concrete application.

1.4 Research Objectives

The main objectives of this research are to:

- Conduct an experimental program to investigate the cross-sectional compressive behaviour of composite columns by testing different column types. The experimental program investigates:
 - The influence of adding a steel W section to confined concrete.
 - The influence of using a split tube as a practical application technique.
 - The influence of using concrete with shrinkage reducing admixture in confined concrete column applications.
- Develop an analytical model to predict the cross-sectional compressive behaviour of the different column types.

- Conduct a parametric study with the analytical model to investigate:
 - The influence of the number of plies of GFRP in the split tube elements on the response.
 - The influence of the number of plies of CFRP used to wrap the split tube elements on the response.
 - The influence of the concrete strength on the response.
 - The influence of the steel ratio on the response.
- Examine the ability of North American codes to predict the capacity of retrofitted composite columns.

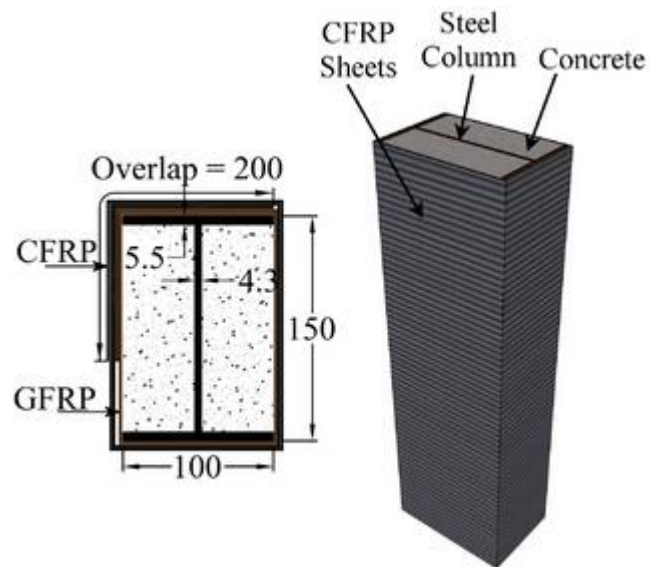
1.5 Methodology

A total of 15 column specimens are studied in the current experimental program. Experimental results from three of the test specimens have been reported elsewhere (Linde, 2011). The 15 column specimens are supplemented by three similar columns tested by Karimi et al. (2010). They comprise six different column types, with three specimens per column type. The column types allow evaluation of the retrofitting technique, the influence of adding a steel *W* section to confined concrete, the influence of using a split tube system, and the influence of using shrinkage reducing admixture in the concrete. Analytical predictions are made with models for confined concrete and the contributions of the different composite column components are added together to obtain the

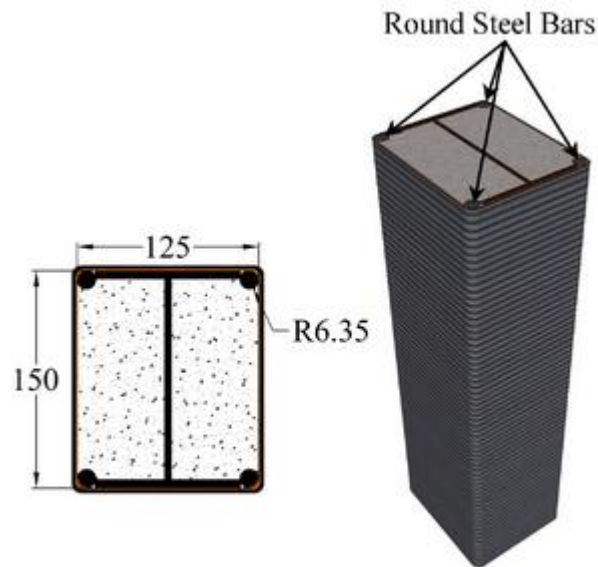
composite column response. To meet the research objectives, the following are carried out:

- Obtain data regarding three steel W section specimens from Karimi et al. (2010) to use for evaluation of the retrofitting technique.
- Design and construct 15 column specimens. These include three confined concrete specimens with normal concrete, three confined concrete specimens with concrete that includes shrinkage reducing admixture, three confined concrete specimens with normal concrete that also include an encased steel W section, three confined concrete specimens with concrete that includes shrinkage reducing admixture that also include an encased steel W section, and three confined concrete specimens with normal concrete that also include an encased steel W section and which utilizes a split tube system.
- Analyze test results.
- Apply an analytical model to describe the compressive cross-sectional behaviour of the column types which use normal concrete.
- Perform a parametric study.
- Compare the column capacity from three North American codes to the experimental results.

This thesis consists of three main chapters. Chapter 2 focuses on the experimental program. Chapter 3 deals with the development and application of an analytical model to the column types tested in Chapter 2. Chapter 4 includes a parametric study using the model developed in Chapter 3 and also includes a review of three North American codes.



(a)



(All dimensions in mm)

(b)

Figure 1.1: Proposed Composite Columns (Images from Karimi et al. (2011))

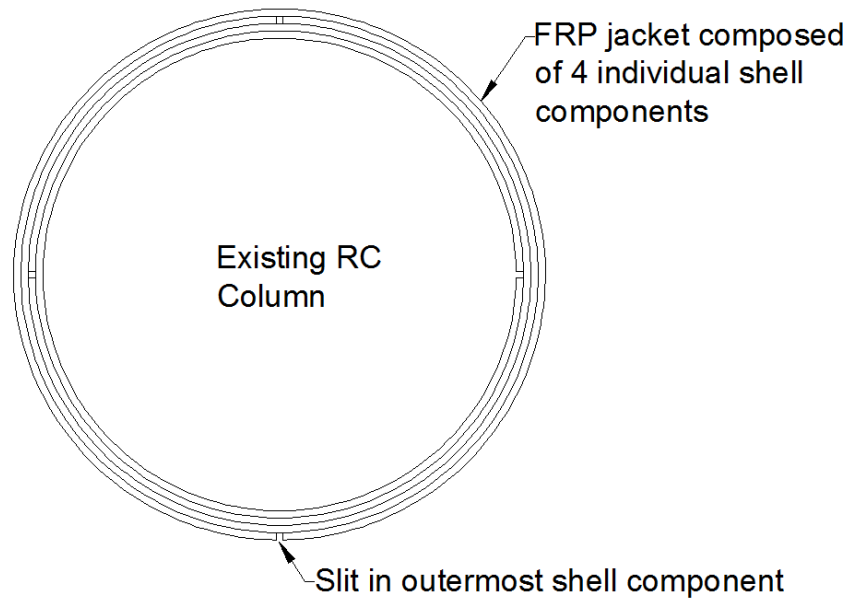
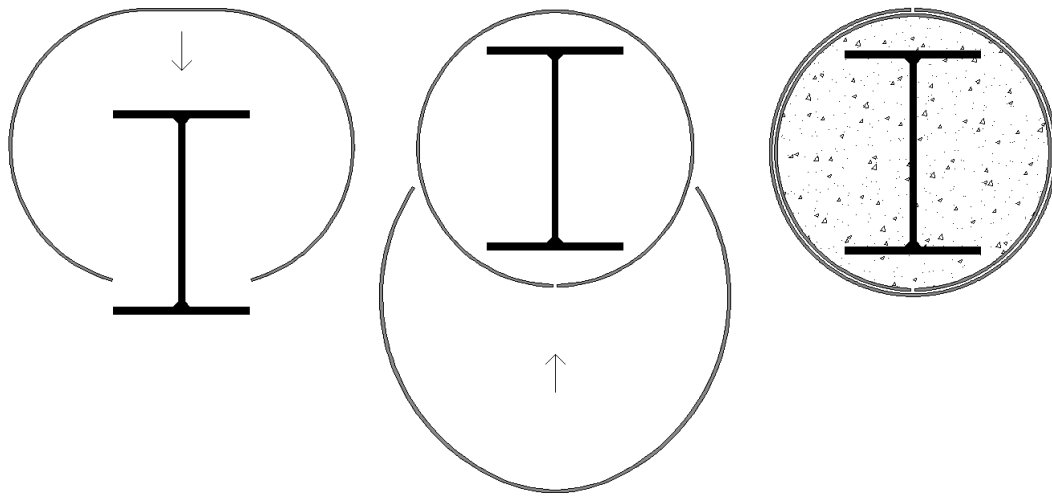


Figure 1.2: Snap-Tite FRP Jacketing System



(a) Place the first slotted tube element around the in situ steel W section

(b) Epoxy an additional slotted tube element around the first

(c) Fill the void with concrete

Figure 1.3: Proposed Slotted Tube System by Liu et al. (2005)

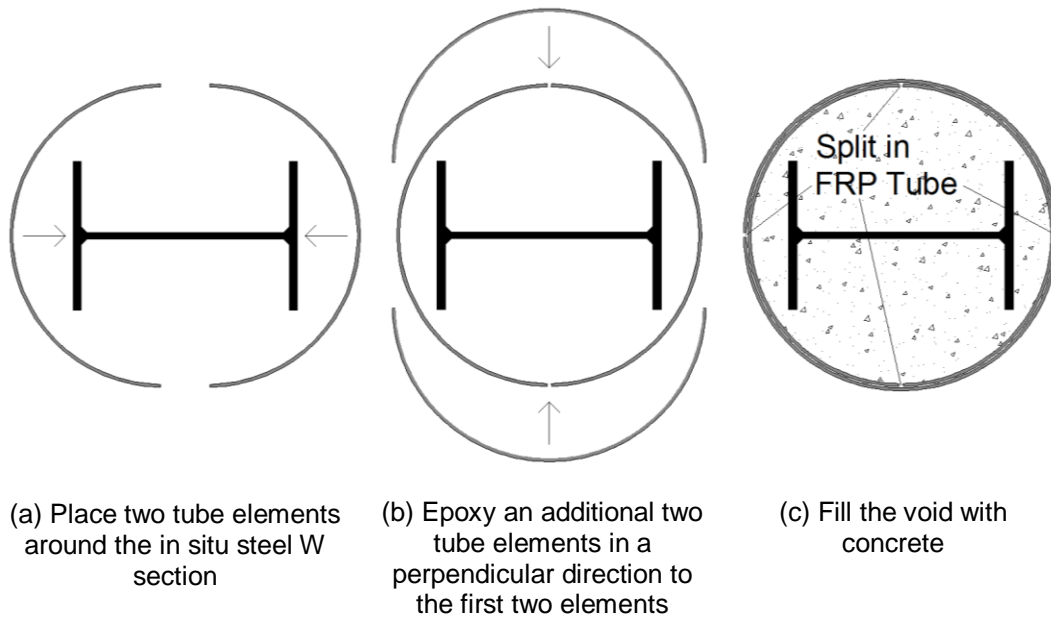


Figure 1.4: Proposed Onion Skin Jacket System by Liu et al. (2005) and Karimi et al. (2010)

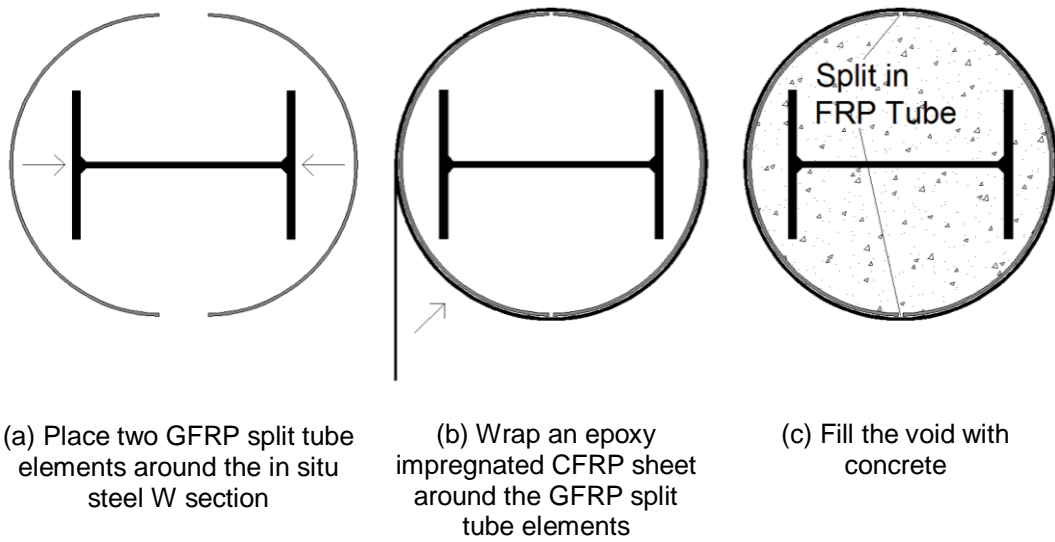


Figure 1.5: Proposed CFRP-Wrapped Split-GFRP-Confined Concrete-Steel Composite System

Chapter 2 - Experimental Program

2.1 Introduction

An experimental program was designed to investigate three main issues related to confinement of steel columns. The first issue directly investigates the inclusion of a steel W section within confined concrete. The response of confined concrete has been studied and modelled extensively by others. In addition, Liu et al. (2005) and Karimi et al. (2010) both investigated the response of composite columns comprised of a steel W section encased in confined concrete but did not compare it to that of confined concrete without an encased steel section. The current study investigates the direct effect of adding a W section to a confined concrete column. This is accomplished by testing and contrasting confined concrete with and without a steel W section. The second objective of the study is to investigate a practical application technique to apply the system in a retrofit scenario in situ on an existing W section column. Liu et al. (2005) and Karimi et al. (2010) both proposed application techniques, but due to simplicity of construction they both employed solid, premanufactured tubes in their studies. The current study investigates the effects of a suitable application technique. The third objective of the study is to investigate the effect of using concrete with shrinkage reducing admixture in concrete confined by CFRP. Various studies use different techniques to explore the effect of shrinkage reducing admixture and reach varying

conclusions. This study directly investigates the effects of using concrete with shrinkage reducing admixture in a confined concrete application.

2.2 Testing Matrix

Results from a total of eighteen stub column tests are presented in this study. Three specimens were tested for each of the six column types investigated. The first three specimens tested were steel W150x14 section columns. They were used as control specimens in order to evaluate the performance of the proposed retrofit technique. These specimens, denoted as C1, are shown in Figure 2.1 (a). The data for these specimens has been obtained from research work by Karimi et al. (2010). The remaining fifteen column tests were tested as part of this study at the Applied Dynamics Laboratory at McMaster University. Column type C2, shown in Figure 2.1 (b), is a CFRP-Confined Concrete column. This column type was tested to evaluate the response of a confined concrete column without the presence of a steel section. The specimens consist of a concrete core surrounded by a CFRP tube. The CFRP tube comprises two and a half wraps in order to provide 2 plies of CFRP with an overlap of half the column circumference to resist debonding. Column type C3, also shown in Figure 2.1 (b), is CFRP-Confined Shrinkage Reducing Admixture (SRA) Concrete column. It has the same physical properties as column type C2, except the concrete for column type C3 includes shrinkage reducing admixture. This column type is tested to evaluate the effect of

shrinkage reducing admixture on confined concrete. Column type C4, shown in Figure 2.1 (c) is a CFRP-Confined Concrete-Steel Composite column. This column type has a steel section at the center, which is encased by concrete that is confined by a CFRP tube. The CFRP tube has two and a half plies of CFRP which provides two plies of confinement and a half a circumference length of overlap to resist debonding. Column type C5, is CFRP-Confined SRA Concrete-Steel Composite column and is also shown in Figure 2.1 (c). It has the same physical properties as column type C4, except the concrete for column type C5 includes shrinkage reducing admixture. This column type was tested to evaluate the effect of shrinkage reducing admixture on confined concrete-steel composite columns. The final column type, C6, is a CFRP-Wrapped Split-GFRP-Confined Concrete-Steel Composite column. This column type has a steel section at the center, which is encased by concrete that is surrounded by a hybrid FRP tube. This tube is comprised of a two ply, GFRP tube that is split in two pieces along the length. These two pieces are wrapped with two and a half plies of CFRP to form a hybrid FRP tube shown in Figure 2.1 (d). All 18 column test specimens were 500 mm in length. The testing matrix is summarized in Table 2.1.

2.3 Composite Column Components

2.3.1 Steel Section

2.3.1.1 *Material Properties*

The steel section selected was a W150x14 and its properties are shown in Table 2.2. According to CAN/CSA S16-09 from the Canadian Institute of Steel Construction (2008), the W150x14 section will experience cross-sectional yielding prior to local buckling. This is the same section used by Karimi et al. (2009) and the properties obtained from coupon tests indicate a yield strength of 411 MPa and an ultimate strength of 526. In the FRP-concrete-steel composite columns, the area of the steel section represented 5.12% of the gross concrete area.

2.3.1.2 *Preparation*

The steel specimens were cut to 500 mm lengths using a gravity feed band saw. The ends were subsequently ground flush and square with a grinder.

2.3.2 FRP Tube

2.3.2.1 *Datasheet Material Properties*

The CFRP used is Tyfo SCH-41S, which is comprised of Tyfo S Epoxy and Tyfo SCH-41S reinforcing fabric. Tyfo SCH-41S is a custom weave, unidirectional carbon fabric with aramid cross fibers. The carbon is

orientated in the 0° direction with the aramid fibers at 90° as shown in Figure 2.2. The GFRP used is Tyfo SEH-51A, which is comprised of Tyfo S Epoxy and Tyfo SEH-51A reinforcing fabric. Tyfo SEH-51A is a custom weave, unidirectional glass fabric with glass cross fibers. The primary glass fibers are orientated in the 0° direction with additional cross glass fibers at 90° . The properties for the composite laminates are provided on the data sheets from Fyfe (Fyfe Co. LLC, 2010; Fyfe Co. LLC, 2010) and are summarized in Table 2.3.

2.3.2.2 *Coupon Test Material Properties*

A 2 ply sheet of CFRP laminate was fabricated in the laboratory. The two part Tyfo S Epoxy was mixed according to the manufacturer's directions and then rolled into the Tyfo SCH-41S reinforcing fabric. Two plies of epoxy impregnated fabric were placed on top of each other, each orientated in the same direction. They were placed between two flat surfaces to cure. Once the laminate sheet had cured, eight flat coupon specimens were cut from it. Each coupon measured 36 mm wide by 360 mm long and had a nominal thickness of 2 mm. The nominal thickness was used for the calculation of material properties as is commonly done for wet-layup FRP (Lam & Teng, 2004). Four coupons were cut from the sheet in the primary fiber direction and four were cut in the secondary fiber direction.

These coupons were tested according to ASTM D3039/D3039M (2008), ASTM D7565/D7565M (2010), and ACI 440.3R (2004) requirements. The coupons were rectangular with a gauge length of 200 mm. The loading device had hydraulic grips and therefore the coupons did not have tabs on the ends for gripping. Tabs are not required in the aforementioned standards if failure does not occur prematurely at the grip location. None of the tested coupons failed in the vicinity of either grip. The tests used Digital Image Correlation (DIC) on a 2D Aramis System to provide accurate strain values during testing. The longitudinal strain and the transverse strain were measured for each coupon in order to calculate Poisson's ratio (ν) for the CFRP laminate. The ultimate tensile strength, tensile modulus, elongation at break, and Poisson's ratio were found for each coupon. The results are presented in Table 2.4 as mean values with corresponding coefficients of variation. The stress-strain material response curves are shown in Figure 2.3 (a) and (b) for the primary and secondary fiber directions, respectively. The primary fiber direction response displayed a slight reduction in stiffness at approximately 85% of the ultimate strain due to the onset of progressive failure. The secondary fiber direction response displayed a distinct loss of stiffness around 4500 $\mu\epsilon$. It is postulated that this is due to the loss of stiffness from the epoxy matrix due to cracking and stiffness being provided solely from the aramid fibers. The tensile moduli of the first and second portions of the curve are

6.8 and 2.5 GPa, respectively. Photographs of two failed coupons are shown in Figure 2.4.

Poisson's ratio is calculated with the formulae for small deflections as,

$$v_{ps} = -\frac{\varepsilon_s}{\varepsilon_p} \quad (2.1)$$

where ε_p and ε_s are the strains in the primary and secondary fiber directions, respectively, and v_{ps} is Poisson's ratio that corresponds to a contraction in the secondary fiber direction due to an extension in the primary fiber direction. This expression was evaluated from the coupon tests of the primary fiber direction. Due to the relatively large difference in stiffness in the primary and secondary directions, Poisson's ratio for CFRP corresponding to a contraction in the primary direction due to an extension in the secondary fiber direction, v_{sp} , was a small value. As such, it was difficult to determine its value accurately from the strain measurements due to the slight natural variation in the strain measurements. Therefore, the relationship for an orthotropic material was used to calculate this value as,

$$v_{sp} = \frac{v_{ps}}{E_p} E_s \quad (2.2)$$

where E_p and E_s are the Young's modulus values in the primary and secondary fiber directions, respectively.

The values for the properties in the primary fiber direction were found to be in good agreement with the manufacturer specified material properties. The ultimate tensile strength was 3.0% lower, the tensile modulus was 1.2% lower, and the elongation at break was 5.6% greater than the values specified on the manufacturer supplied datasheet. The ultimate tensile strength in the secondary direction was found to be 49.3% greater than the value listed on the datasheet. The remaining properties were not given on the material datasheet.

The primary and secondary fiber directions were orientated in the hoop and axial directions, respectively. This allowed the primary fiber direction to provide hoop confinement to the concrete columns. These axes were denoted h and a , for hoop and axial, respectively. These direction definitions are shown on a column specimen in Figure 2.5.

2.3.2.3 *Tube Construction*

The following process was employed to fabricate

the FRP tubes: 1) Cardboard forms were cut to approximately 500 mm lengths and fitted with round wooden spacer disks to ensure the cardboard forms maintained their shape. The cardboard forms were then wrapped with shrink-wrap to facilitate their removal from the finished product. 2) FRP sheets were cut to the correct length to ensure two and a half wraps. 3) The two-part, Tyfo S epoxy was mixed at a volume ratio of

100:42 as specified. It was blended at a low speed with a mixing attachment on a hand drill until it had a uniform consistency. 4) FRP sheets were rolled rigorously with a roller until they were impregnated with the epoxy. The sheets were flipped over multiple times and rolled from both sides until they became pliable and had a soft feel. Figure 2.6 (a) shows this process. 5) FRP sheets were then wrapped around the cardboard forms. Plastic wrap was wrapped around the wet tubes to hold the FRP in place during the curing process. The wrapped specimens can be seen in Figure 2.6 (b). 6) The tubes were placed in a horizontal position to cure so that the epoxy would not flow to one end of the tube during the curing process. 7) Once the epoxy cured, the tubes were cut to length. 8) After cutting, the wooden disks and the cardboard forms were removed as shown in Figure 2.6 (c). A finished FRP tube is shown in Figure 2.6 (d). The constructed FRP tubes had a mean interior diameter of 207.4 mm with a coefficient of variation of 0.35%

A total of twelve CRFP and three GFRP tubes were constructed using the procedure described above. Once the GFRP tubes were completed they were each cut in half along their length to form two pieces as shown in Figure 2.7 (a). To improve constructability, the two pieces were then placed around a cardboard form as shown in Figure 2.7 (b). CFRP was wrapped around the split GFRP tube (which acted as a stay in place form) two and a half times in order to provide 2 plies of CFRP with an overlap of

half the column circumference to resist debonding. The wrap was started in the middle of one of the GFRP split tube pieces, 90 degrees around the circumference from the split as shown in Figure 2.7 (c). This process created the cross-section shown in Figure 2.8. The weakest part of this cross-section is shown at the bottom of the figure as having 2 plies of CFRP. This weak point is only the width of the gap in the GFRP tube, which was 5 mm. The fifteen tubes are shown in Figure 2.9 prior to the placing of concrete.

2.3.2.4 *Tube Properties*

Two samples of tube were tested in compression to evaluate the compressive stiffness of the CFRP tube. They were cut to a length of 200 mm to avoid buckling effects during testing. The ends of the tube were held in place with Hydro-Stone against thick steel end plates during testing. Four axial strain gauges on the specimen were used to measure axial strain and are shown in Figure 2.10 (a). Four string pots were placed between the two steel end plates to measure axial displacement. A photograph of the end plates and the string pots is presented in Figure 2.10 (b). Following peak capacity, the CFRP cracked internally and the plies slipped past each other. This caused cracking and bulging of the epoxy matrix as shown in Figure 2.11. It should be noted that the test was stopped once an axial strain of $30,000 \mu\epsilon$ was reached; the tube remained stable throughout testing. The load versus strain response curves for both

tube samples are presented in Figure 2.12. The tube had a mean ultimate capacity of 79.6 kN with a coefficient of variation of 1.8%. The cross-section of the tube had an ultimate compressive strength of 28.5 MPa and a compressive modulus of 6.3 GPa. A study by the Ford Motor Company (1982) on the compression of graphite prepreg (carbon fiber) tubes reported the failure mechanism to be interpenetration. The Ford Motor Company also found that on the load-displacement response curve, collapse began at a high load and sustained a decreasing load under additional displacement. The results of the current study are in agreement with these findings.

2.3.3 Concrete

2.3.3.1 *Mix Design*

The concrete mix design can be found in Table 2.5. Tetraguard AS20 Shrinkage-Reducing Admixture from BASF was used as the shrinkage reducing admixture. Tetraguard AS20 admixture works by reducing the capillary tension of pore water, which is a primary cause of drying shrinkage. In the current study, 2.05% Tetraguard AS20 admixture by mass of cement was used, which can reduce drying shrinkage by as much as 80% at 28 days (BASF, 2010). The material datasheet reports that it reduces drying shrinkage cracking and micro cracking and that compressive strength loss is minimal.

2.3.3.2 *Material Strength*

The results from concrete cylinder tests at 28 days and at 85 days, which was the time of column testing, can be found in Table 2.6 for normal and shrinkage reducing admixture concrete. For normal concrete, the average compressive strength of cylinder tests at 28 days was 24.4 MPa with a coefficient of variation of 3.3%. The average compressive strength of concrete cylinders tested at the time of column testing was 26.2 MPa with a coefficient of variation of 1.6% which is a 7% increase in concrete strength compared to the strength at 28 days. For the shrinkage reducing admixture concrete the average compressive strength of cylinders tested at 28 days was 21.1 MPa with a coefficient of variation of 1.4%. The average compressive strength of concrete cylinders tested at the time of column testing was 24.3 MPa with a coefficient of variation of 3.6% which is a 15% increase in concrete strength compared to the strength at 28 days.

2.4 Composite Column Construction

The specimens that contained steel sections were fitted with wooden spacers, which held the steel section in the center of the tube while the concrete was being placed to minimize eccentricity in the composite columns. One of these wooden spacers is shown in Figure 2.13. The steel section was not consistently oriented with respect to the FRP overlap joint for the CFRP-Confined Concrete-Steel Composite and CFRP-Confined

SRA Concrete-Steel Composite specimens. However, the steel section in the CFRP-Wrapped Split-GFRP-Confined Concrete-Steel Composite specimens had a consistent orientation as shown in Figure 2.8.

The concrete constituents were weighed out according to the mix design shown in Table 2.5 and subsequently mixed on site. The concrete was then placed in the FRP tubes. The concrete was rodded with a steel rod and consolidated with a handheld concrete vibrator as it was placed to ensure complete elimination of air pockets from the composite columns. After the concrete cured, the wooden spacer disks were removed and the ends of the specimens were finished with Hydro-Stone to ensure uniform loading of the specimen cross-section.

2.5 Test Setup and Instrumentation

2.5.1 Specimen Preparation

Axial load was applied to the column through end caps in order to ensure application of uniform loading on the cross section. The end caps consisted of a steel ring welded to thick steel end plates. Care was taken to ensure complete contact between the steel section and the plate. To center the column in the end cap, a small metal dowel was fixed to the center of the steel section in the composite column. This dowel was fit into a hole at the center of the end cap as shown in Figure 2.14 (a). Once the column was centered in the end cap and flush against the steel end plate,

the area around the column was filled with Hydro-Stone to hold it in place during testing. A schematic of an installed end cap is shown in Figure 2.14 (b) and a photograph is shown in Figure 2.14 (c).

2.5.2 Specimen Instrumentation

Measurements were taken in both the axial and the hoop directions. A total of four string pot displacement transducers were used to measure axial displacement between the end caps on each specimen. The string pots were fastened at the four corners of the end caps. In addition, four strain gauges were located equidistance around the circumference at the mid-height of each specimen to measure axial strain. An additional four strain gauges, oriented in the hoop direction, were symmetrically located around the circumference at the mid-height of each specimen to measure hoop strain. The specimen instrumentation can be seen in Figure 2.15.

2.5.3 Test Setup

The specimens were loaded axially in a self-reacting frame. The bottom support for the specimen was fixed and the top support was hinged. The columns were loaded with a 5,000 kN actuator and the load was measured with a dual bridge load cell with similar capacity. The test setup can be seen in Figure 2.16. The loading is displacement-controlled and applied at a rate of 0.75 mm/min.

2.6 Test Results

2.6.1 Load-Displacement Response

The axial load versus axial strain response curve was obtained from both the strain gauges and the string pots. The axial strain for each specimen response curve was initially obtained from the axially orientated strain gauges. At high strain values, several strain gauges debonded from the specimen. As a result, in this portion of the response curves the string pot measurements were used to determine strain. The string pot measurements were divided by the length of the specimen to obtain strain values. Lam and Teng (2003) suggest a bilinear curve with a parabola for the first portion and a linear section for the second portion of the response of confined concrete. The parabolic portion describes the gradual development of confinement as axial load increases until the confinement has fully developed and the response becomes linear. For consistency, the transition between strain gauge measurements and string pot measurements was taken as the point between the beginning parabolic portion of the curve and the linear ascending branch. The strain gauge measurements were taken as the average of the four axially orientated strain gauges. In a similar manner, the string pot measurements were taken as the average of the four string pots. The hoop strain was taken as the average of the four hoop strain gauge readings. The axial load versus

axial strain response curves are presented in Figure 2.17 for all fifteen specimens from column types C2, C3, C4, C5, and C6.

Figure 2.18 (a) through (f) present axial load versus axial displacement response curves including error bars indicating standard deviation for all six specimen types individually. In the initial parabolic portion of the curve all column types exhibit a low standard deviation. The standard deviation values for the column type C2, CFRP-Confined Concrete Column, and column type C4, CFRP-Confined Concrete-Steel Composite Column, are found to show the greatest deviation in the linear portion of the curve. The standard deviation values for column type C3, CFRP-Confined SRA Concrete Column, and column type C5, CFRP-Confined SRA Concrete-Steel Composite Column, are found to increase in the linear portion of the curve but to a less degree than column types C2 and C4. The standard deviation of column type C6, CFRP-Wrapped Split-GFRP-Concrete Composite Column, is found to remain low in the linear portion of the curve.

Figure 2.19 (a) compares the average axial load versus axial strain response curves for all column types. Figure 2.19 (b) compares the average axial load versus hoop strain response curves for column types C2, C3, C4, C5, and C6. The curves in Figure 2.19 represent the mean of

the three specimens of each column type and include error bars indicating one standard deviation.

2.6.2 Failure Modes

2.6.2.1 *Steel Section Failure*

The column type covered by this type of failure is C1: Steel Section. Failure of the steel section was initiated by yielding of the cross-section. Subsequently, local buckling of the flanges and web followed. A photograph of a failed specimen is shown in Figure 2.20. These steel sections were previously tested and reported on by Karimi et al. (2010).

2.6.2.2 *CFRP Confined Concrete Failure*

The column types covered by this type of failure include C2: CFRP-Confined Concrete and C3: CFRP-Confined SRA Concrete. For the confined concrete specimens, failure was due to FRP rupture. The FRP ruptured in the two ply region of the CFRP jacket for all specimens. The FRP ruptured along vertical lines, allowing the concrete in this vicinity to dilate extensively. The concrete in the region where the rupture occurred was pulverized and spalled off. Concrete that remained intact after failure formed two separate cones, one in each end cap. Photographs of two of the failed specimens of column type C2 are shown in Figure 2.21 (a) and (b). A schematic of the characteristic failure is shown in Figure 2.21 (c). Two of the failed specimens of column type C3 are shown in Figure 2.22

(a) and (b). A close up photograph of the pulverized and spalled off concrete is shown in Figure 2.22 (c).

2.6.2.3 *CFRP-Confined Concrete-Steel Composite Failure*

The column types covered by this type of failure include C4: CFRP-Confined Concrete-Steel Composite and C5: CFRP-Confined SRA Concrete-Steel Composite. The steel section in column types C4 and C5 was not orientated consistently with respect to the overlap in the CFRP tube. Figure 2.23 shows the orientation of the rupture and the steel section in the CFRP tube for all column type C4 and C5 specimens. The rupture occurred in the half of the tube which had two plies regardless of the orientation of the steel section for five of the six specimens from column types C4 and C5.

Failure is initiated by rupture of the CFRP jacket in the 2 ply region. The confined concrete in the immediate vicinity of the rupture cracks and dilates rapidly due to the loss of confinement. The dilating concrete loses the majority of its strength as it begins to spall off. The loss of strength near the rupture forces the column to bend in the direction of the rupture and dilated concrete. As a result of the bending, the compressive flanges on the steel section buckle. The concrete in the rectangle between the flanges and the web is still highly confined and the concrete on the outside of the flanges begins to lose confinement and dilate forcing the flanges to

buckle outwards. The buckling is most pronounced on the flanges nearest the rupture least pronounced on the flanges opposite the rupture location.

It is postulated that the orientation of rupture with respect to the steel section was driven by inducing slight unintended bending into the specimens. This is expected to occur due to small eccentricities in the test set up, small errors in the concentric placement of the steel section in the CFRP tube during construction, inaccuracies in placing the end plates perfectly parallel, and imperfections in ensuring the complete contact of the steel section with the end plates. The compressive side of the specimen under this slight bending is subjected to higher axial compression than the opposing side of the specimen. It was observed that eventual rupture of the FRP jacket occurred on the compressive side of the specimen which experienced higher levels of compression. Depending on the direction of bending, each specimen can be characterized as bending predominately about either the strong or weak axis of the steel section. Specimens that exhibited bending about the strong axis were better able to resist the additional compressive forces and failed at higher axial strains and loads than the specimens that bent about the weak axis.

It can be seen from Figure 2.23 that column type C4 specimens 1 and 2 and column type C5 specimens 1 and 2 can be characterized as bending about the strong axis whereas column type C4 specimen 3 and column

type C5 specimen 3 can be characterized as bending about the weak axis. In Figure 2.17 (a), C4-3 and C5-3 are seen to have failed prematurely compared to the other specimens of their types.

The test for column type C4 specimen 1 was stopped at 2,200 kN due to safety concerns. The specimen was unloaded and not disturbed while proper safety precautions were erected around the test set-up. The specimen was then reloaded until failure occurred. The resulting load – displacement curve for this specimen was assembled from the two test responses.

It should also be noted that the CFRP jacket for column type C4 specimen 2 failed 15 mm from the FRP overlap as shown in Figure 2.24. Lam and Teng (2004) reported several CFRP-confined concrete specimens had a maximum hoop strain at or near the beginning interface of the fiber sheet. They suggest this may be due to the jacket bending as a shell as a result of the thickness change. As can be seen in Figure 2.17 (a), C4-2 failed prematurely compared to the C4-1 specimen. The premature failure is attributed to increased hoop strain values occurring near the CFRP overlap which led to premature FRP rupture at this location. This is supported by the fact that the specimen was much more intact after failure than the other two C4 specimens.

In five of the six specimens of column types C4 and C5 there was no debonding failure and the FRP overlap joint stayed intact. However, half a circumference of the CFRP jacket for column type C5 specimen 1 debonded, starting at the FRP overlap. When the debonded portion of the jacket was removed from the specimen, it was observed that CFRP rupture had occurred underneath the debonded portion. The CFRP rupture occurred in the 3 ply region of the jacket as shown in Figure 2.23, however rupture occurred under the debonded portion therefore failure only ruptured through two plies of CFRP. The response of this specimen was not significantly different from the response of the other two specimens of this column type therefore no special consideration will be given to this failure mechanism.

Photographs of the failed specimens of column type C4 and C5 are shown in Figure 2.25 and Figure 2.26, respectively.

2.6.2.4 Split Tube Confined Concrete Composite Failure

The column type covered by the failure mechanism in this section is column type C6: CFRP-Wrapped Split-GFRP-Confined Concrete-Steel Composite. The CFRP-Wrapped Split-GFRP-Confined Concrete-Steel Composite specimens failed due to FRP rupture. All three specimens failed at the weak point in the cross-section, which was shown in Figure 2.8 as the gap in the GFRP tube that was wrapped with only two plies of

CFRP. Guided by this weak point in the cross-section, the FRP jacket ruptured completely from top to bottom along a straight line. Photographs of the three failed specimens are shown in Figure 2.27. The ruptured FRP jacket of one of the C6 specimens is presented in Figure 2.28 (a). Following the FRP rupture, the concrete spalled off and the flanges of the steel section buckle. The buckled steel section is shown in Figure 2.28 (b) and (c). It should be noted that due to the consistent orientation of the steel section in the FRP tube, the flanges were always located in the region with an additional 2 plies of GFRP.

2.6.3 Ultimate Experimental Measures

The experimental results are given in Table 2.7. The metrics include ultimate load, ultimate axial strain, and mean ultimate hoop strain. These values are representative of the three specimens of each column type and are presented as a mean value and a coefficient of variation (C.O.V.). FRP rupture occurred at a greater ultimate hoop strain than the mean ultimate hoop strain listed in Table 2.7. Figure 2.29 compares the maximum ultimate hoop strain to the mean ultimate hoop strain for all specimen types.

2.6.4 Hoop Strain

2.6.4.1 *Ultimate Hoop Strain*

The largest hoop strain at failure was found with column type C3: CFRP-Confined SRA Concrete columns and had a mean value of 9513 $\mu\epsilon$. The primary fiber coupon tests had an average ultimate strain of 12,678 $\mu\epsilon$ and the datasheet reported an ultimate elongation of 12,000 $\mu\epsilon$. The significant reduction in the FRP ultimate strain on confined concrete columns has been well documented in recent literature and several explanations have been provided. An investigative study by Lam & Teng (2004) suggests three factors contribute to this reduction: 1) curvature of the FRP jacket; 2) deformation non-uniformity of cracked concrete; and 3) the overlapping zone in the FRP jacket. The curvature causes a direct decrease in the ultimate strain. The non-uniformity of cracked concrete and the overlapping zone in the FRP jacket cause considerable variation in the hoop strain distribution. The three factors combine to form an average ultimate hoop strain that is much lower than that obtained from the coupon tests.

2.6.4.2 *Hoop Strain Distribution*

The distribution of hoop strain around the circumference was established from the four strain gauges located around the circumference of the columns at mid-height. The distribution was plotted for the hoop strains at

ultimate load. These plots are shown in Figure 2.30 for all fifteen specimens that contained FRP jackets.

Lam & Teng (2004) demonstrated that although the hoop strain varies considerably, the confining pressure around the circumference is much more consistent. The majority of the variability in the hoop strain distribution arises from the overlap region being thicker which results in lower strain values. However, the confining pressure is developed by tension in the FRP jacket which is dependent on the elastic modulus, the thickness, and the ultimate strain of the jacket. Thus, although the strain is lower in the overlap region, the thickness is greater, which results in fairly consistent confining pressure (Lam & Teng, 2004). The remaining variability in the confining pressure is due to the non-uniformity of the concrete deformation which causes local effects in the FRP jacket. This effect is magnified by the buckling of the steel flanges.

2.6.5 Enhancement Factors

2.6.5.1 *Composite Action Index*

A strength enhancement index was introduced by Yang et al. (2008) to compare the load carrying capacity of the composite specimen to the sum of the individual components. This index was also applied as a composite action index (C.A.I.) by Karimi et al. (2010) and is defined as,

$$C.A.I. = \frac{P_{ult.}}{A_s F_y + A_c f'_c} \quad (2.3)$$

where A_c is the cross-sectional area of concrete, A_s is the cross-sectional area of steel, P_{ult} is the ultimate capacity of the specimen, F_y is the yield strength of the steel section, and f'_c is the compressive strength of unconfined concrete as measured by cylinder tests.

2.6.5.2 Confinement Ratio

Lam & Teng (2003) introduced a confinement ratio (C.R.) that was representative of the actual state of stress in the FRP confinement at failure. The confinement ratio is given by,

$$C.R. = \frac{f_l}{f'_c} \quad (2.4)$$

where f_l is the maximum confining pressure and is defined as,

$$f_l = \frac{2E_h t \varepsilon_{h,rupt}}{d} \quad (2.5)$$

where E_h is Young's modulus of the FRP tube in the hoop direction, t is the thickness of the FRP tube, d is the inner diameter of the FRP tube, and $\varepsilon_{h,rupt}$ is the maximum hoop strain at FRP rupture.

2.6.5.3 *Effective Confined Concrete Strength*

The composite action, as evaluated by C.A.I., was assumed to be mostly due to the confinement action of the concrete. Assuming an elastic-perfectly plastic stress-strain curve for the steel section, the estimated effective confined concrete compressive strength, f'_{cc} , can be calculated by,

$$f'_{cc} = \frac{P_{ult.} - A_s F_y}{A_c} \quad (2.6)$$

2.6.5.4 *Energy Dissipation Capacity*

Karimi et al. (2012) used the energy dissipation capacity (E_d) of the specimens as a metric for composite columns. The energy dissipation capacity of a column is connected to the area under the load-displacement curve. Karimi et al. (2012) simplified the calculation of E_d by idealizing the response as an elastic-perfectly plastic curve as shown in Figure 2.31. The value of E_d is then calculated as,

$$E_d = \left[\frac{1}{2} \delta_y + (\delta_u - \delta_y) \right] P_{ult.} \quad (2.7)$$

where δ_y and δ_u are the axial yielding displacement and the ultimate axial displacement, respectively. The axial yielding displacement is calculated by dividing the axial displacement corresponding to 75 percent of the ultimate load by 0.75. In addition, this area was found through numerical

integration of the load-displacement curves to provide an E_d value for the different specimen types. A plot showing the mean energy dissipation capacity values for the different specimen types is shown in Figure 2.32 for both calculation methods and includes error bars representing one standard deviation. The two methods had comparable results.

The four above outlined enhancement factors ($C.A.I.$, $C.R.$, f'_{cc} , and E_d) have been computed for all six column types and are presented in Table 2.8.

2.6.6 Confinement Effects

The shape of the response curve for confined concrete is dependent on the maximum confining pressure. The expression for the maximum confining pressure is given in Equation (2.5). Lam & Teng (2003) outlined three levels of confinement based on the characteristics of the response curve. The first is characterized by a monotonically increasing bi-linear curve and is called highly confined. For this type of confinement the ultimate strain and the ultimate load are realized simultaneously at failure. They outline low confinement as having a post peak descending branch with ultimate failure reached at a value below the unconfined concrete strength. This level of confinement is considered insufficient to be applied as confined concrete. Average confinement is again characterized by a post peak descending branch where the maximum strength is reached

before failure. However, this type maintains a strength above the unconfined concrete strength until failure. Furthermore, Lam & Teng (2003) suggest a minimum confinement ratio of $C.R. \geq 0.07$ as criteria for FRP-confined concrete to be classified as sufficiently confined. The values of C.R. for the specimens in this study range from 0.46 to 0.72 and as such are above the minimum required value. In addition, all of the specimens exhibit monotonically increasing bi-linear curves which classifies them as highly confined.

2.7 Experimental Findings

2.7.1 Effect of Adding a Steel Section to Confined Concrete

The effect of adding a steel section to confined concrete is demonstrated by comparing column type C2: CFRP-confined concrete to column type C4: CFRP-confined Concrete Steel Composite. A plot comparing the response of these two column types is shown in Figure 2.33. The stiffness of column type C4 is greater than the column type C2 in the initial portion of the response. In this region the steel is acting in its elastic regime and adding additional stiffness to the confined concrete. The second linear portion begins around 1.5 mm of axial displacement for both column types. In this region the stiffness of each curve is almost identical. The steel section is in its plastic regime in this portion of the response and is not adding any additional stiffness to the composite column. The

difference between the two curves in this portion was found to have an average value of 704 kN with a coefficient of variation of 1.7% which is very close to the experimentally determined ultimate capacity of the steel section, which was reported as 722 kN.

Column type C4 only reached 72.2% of the ultimate axial strain of column type C2. Both column types failed due to the rupture of the CFRP jacket. However, the rupture of the CFRP jacket in column type C4 was accelerated by stress concentrations in the confined concrete near the tips of the W section flanges. The inclusion of the steel W section in column type C4 resulted in a lower axial displacement and a lower confined concrete strength compared to column type C2.

2.7.2 Split Tube Effects

The effect of the split tube can be demonstrated by a comparison of column type C4: CFRP-Confined Concrete-Steel composite column and column type C6: CFRP-Wrapped Split-GFRP-Confined Concrete-Steel Composite column. A plot comparing the response of these two column types is shown in Figure 2.34. It can be seen that while both column types display little difference in the beginning region of the curve, column type C6 displays much less deviation from the mean along the linear ascending branch than column type C4. These results indicate that repeatable behavior can be obtained over the entire response range using the CFRP-

Wrapped Split-GFRP-Confined Concrete-Steel Composite column technique. The stiffness of each column type is nearly identical for the initial portion of the response. The yield point of column type C6 is slightly higher and the second portion of the response is slightly stiffer than column type C4. Although column type C4 only reached 72.2% of the ultimate axial strain of column type C2, column type C6 reached 107% of the axial strain of column type C2. Column type C4 failed at a lower axial displacement than column types C2 and C6 due to stress concentrations in the confined concrete core near the tips of the W section flanges. Column type C6 had the optimal orientation of the steel section in the FRP jacket such that the stress concentrations caused by the flanges occurred in the region of the jacket that included an additional two plies of GFRP.

Column type C6 has an ultimate load capacity that is 29% greater with a coefficient of variation that is 36% lower than column type C4. Column type C6 also demonstrates a 48% increase in ultimate axial strain and a 19% increase in maximum ultimate hoop strain over column type C4. The increases in ultimate load capacity and ultimate axial strain also lead to an 83% increase in energy dissipation capacities. The CFRP-Wrapped Split-GFRP-Confined Concrete-Steel Composite column, type C6, has a composite action index that is 29% greater than CFRP-Confined Concrete-Steel composite column, type C4. The confinement ratio for

column type C6 is also 19% greater than type C4 due to an increased maximum confining pressure.

It is postulated that the GFRP split tube configuration, used in column type C6 and shown in Figure 2.8, forces failure to occur at a very localized location, which results in increased ultimate capacity, compared to the column type C4 which did not utilize a GFRP split tube system. Harries & Carey (2003) suggested the cumulative probability of weakness in FRP jackets due to their larger size than tensile coupons as a reason for the discrepancy between in situ strain capacities and coupon test strain capacities. In a similar manner, the split tube specimens force failure at the 2 ply CFRP weak point on the cross-section as shown in Figure 2.8. This single location for failure on the cross-section leads to less cumulative probability of weakness in the FRP jacket.

2.7.3 Shrinkage Reducing Admixture Effects

The effects of the shrinkage reducing admixture can be recognized by comparing column type C2: CFRP-Confined Concrete column with column type C3: CFRP-Confined SRA Concrete column. Figure 2.35 (a) compares the responses of column types C2 and C3. The response is normalized by the unconfined concrete strength of each concrete type and includes error bars representing one standard deviation. The two responses fall within the error bars of each other and are not statistically

different. The effect of the shrinkage reducing admixture is seen to be negligible on the confined concrete response.

The effects of the shrinkage reducing admixture can also be realized by comparing column type C4: CFRP-Confined Concrete-Steel Composite column with column type C5: CFRP-Confined SRA Concrete-Steel Composite column. Figure 2.35 (b) compares the responses of column types C4 and C5. The effect of the steel is assumed as elastic-perfectly plastic and subtracted from the response in order to compare the response of the confined concrete. The concrete response is then normalized by the unconfined concrete strength of each concrete type. These curves do not include error bars since they are calculated curves and the error from the original column types is not directly applicable. The largest difference in normalized effective confined concrete strength for any given strain is 6.7%. The COV of the ultimate load for column type C4 and C5 are 4.4% and 1.2%, respectively. The curves are not significantly different from each other indicating that the effect of the shrinkage reducing admixture is negligible on the confined concrete response.

Figure 2.36 compares the ratio of confined concrete strength to unconfined concrete strength versus strain for column types C2, C3, C4, and C5. Again, it is clear from this comparison that the shrinkage reducing

admixture does not have a clear effect on the response of confined concrete.

Karimi et al. (2010) found a 20% increase in compressive strength for a specimen that included shrinkage reducing admixture. In their study, the specimen without shrinkage reducing admixture displayed a post peak descending branch and was classified as having average confinement. The specimen with shrinkage reducing admixture displayed a monotonically increasing response and was classified as highly confined. They suggested that the shrinkage reducing admixture pushed the confinement level from average to highly confined and this helped the specimen realize a 20% increase in compressive strength. The results of the current study found shrinkage reducing admixture to have a negligible effect on the confined concrete strength. However, the specimens in this study were all highly confined and it is suggested that perhaps this limited the amount of increase in compressive strength that could be realized.

The lack of finding any distinguishable results agrees with other literature. El Chabib et al. (2005) tested concrete confined in GFRP tubes. They compared concrete with ordinary Portland cement to concrete with expansive cement that also included a commercial shrinkage-reducing admixture. They reported no significant change in concrete strength or ductility under uniaxial compression. Harries et al. (2003) used a small

gap created by plastic wrap to investigate the effect of bonded versus unbonded FRP jackets on the column response. They reported that the gap did not significantly affect the overall efficiency of the FRP jacket. Yang et al. (2008) greased the inside of a confining tube in an effort to simulate the loss of contact due to concrete shrinkage. They found less than 5% difference in the ultimate load and little variation in the response of the greased or ungreased specimens. These findings may well confirm that the shrinkage of concrete inside FRP tubes is negligible. Naguib and Mirmiran (2001) reported that the sealing of concrete by placing it in an FRP tube will prevent moisture exchange with the ambient air which will eliminate drying creep. Their shrinkage tests on concrete-filled FRP tubes (CFFT) demonstrated that shrinkage deformations were low compared to that of exposed concrete. Furthermore, push out tests by Li et al. (2005) on CFFT specimens indicated a 0.42 MPa bond between the concrete core and the FRP jacket. This bond works to resist shrinkage during the curing process.

2.8 Conclusions

An experimental program was designed and performed in order to investigate the effect of adding a steel W section to confined concrete, the effect of using a split tube system, and the effect of using concrete with shrinkage reducing admixture. A total of 18 stub column tests representing six unique column types were considered. The column types included

steel W sections; CFRP-confined concrete; CFRP-confined concrete which included shrinkage reducing admixture; CFRP-confined concrete-steel composite; CFRP-confined shrinkage reducing admixture concrete-steel composite; and CFRP-wrapped split-GFRP-confined concrete-steel composite. Based on comparisons between column types the following conclusions can be drawn:

1. The response of confined concrete that includes a steel W section is similar to the response of confined concrete plus the elastic-perfectly plastic steel contribution.
2. Confined concrete that includes a steel W section fails prematurely due to the stress concentrations in the confined concrete that arise from the buckling flanges.
3. The novel CFRP-wrapped split-GFRP system forces failure to occur along a predetermined line thus reducing the cumulative probability of failure which leads to an increased ultimate capacity.
4. The use of shrinkage reducing admixture in confined concrete has an indistinguishable effect on the confined concrete strength.

Table 2.1: Testing Matrix

Column Type Description	ID.	Quantity	Steel	Confined Concrete	Concrete Type	Plies of GFRP	Plies of CFRP
Steel Section	C1	3	Yes	No	--	--	--
CFRP-Confined Concrete	C2	3	No	Yes	Normal	--	2
CFRP-Confined SRA Concrete	C3	3	No	Yes	SRA	--	2
CFRP-Confined Concrete-Steel Composite	C4	3	Yes	Yes	Normal	--	2
CFRP-Confined SRA Concrete-Steel Composite	C5	3	Yes	Yes	SRA	--	2
CFRP-Wrapped Split-GFRP-Confined Concrete-Steel Composite	C6	3	Yes	Yes	Normal	2	2

Table 2.2: Steel Section W150x14 Properties

Designation	Area (mm ²)	I_x 10 ⁶ (mm ⁴)	I_y 10 ⁶ (mm ⁴)	Depth (mm)	Flange Width (mm)	Flange Thickness (mm)	Web Thickness (mm)
W150x14	1730	6.87	0.918	150	100	5.50	4.30

Table 2.3: FRP Composite Laminate Properties from Data Sheets

	Fabric	Laminate Thickness (mm)	Primary Fiber Direction			Secondary Fiber Direction
			Ultimate Tensile Strength (MPa)	Tensile Modulus (GPa)	Elongation at Break ($\mu\epsilon$)	Ultimate Tensile Strength (MPa)
CFRP	SCH-41S	1.0	876	72.4	12,000	40.6
GFRP	SHE-51A	1.3	575	26.1	22,000	20.7

Table 2.4: Coupon Test Material Properties

	Ultimate Tensile Strength		Tensile Modulus		Elongation at Break		Poisson's ratio
	(MPa)	C.O.V. (%)	(GPa)	C.O.V. (%)	($\mu\epsilon$)	C.O.V. (%)	
Primary Fiber Direction, p	849.9	0.51	71.5	4.51	12,678	5.83	$\nu_{ps} = 0.263$
Secondary Fiber Direction, s	60.6	10.00	6.8	14.98	19,026	10.45	$\nu_{sp} = 0.025$

Table 2.5: Concrete Mix Design

Mix Design	Normal Concrete (kg / m ³ of concrete)	Shrinkage Reducing Admixture Concrete (kg / m ³ of concrete)
Water	229	222
Cement	341	341
Fine Aggregate	683	683
Course Aggregate	986	986
Admixture	0	7
w/c Ratio	0.672	0.672
Density	2239	2239

Table 2.6: Concrete Cylinder Test Results

Concrete Type	Test Date (days)	Compressive Stress (MPa)	C.O.V. (%)
Normal Concrete	28 day	24.4	3.3
Normal Concrete	85 day	26.2	1.6
Shrinkage Reducing Admixture Concrete	28 day	21.1	1.4
Shrinkage Reducing Admixture Concrete	85 day	24.3	3.6

Table 2.7: Experimental Results

	Ultimate Load		Ultimate Axial Strain		Mean Ultimate Hoop Strain	
	Mean (kN)	C.O.V. (%)	Mean ($\mu\epsilon$)	C.O.V. (%)	Mean ($\mu\epsilon$)	C.O.V. (%)
C1	722	0.3%	--	--	--	--
C2	2,437	3.2%	25,141	8.0%	8,823	4.3%
C3	2,402	3.0%	25,333	10.1%	9,513	11.4%
C4	2,812	4.4%	18,148	14.5%	6,509	19.3%
C5	2,941	1.2%	28,906	10.1%	9,213	8.2%
C6	3,621	2.8%	26,858	9.0%	8,197	4.6%

Table 2.8: Enhancement Factors

	C.A.I.	$f_{i,a}$ (MPa)	C.R.	f_{cc} (MPa)	f'_{cc}/f'_{co}	Ed (kJ)
C1	1.02	--	--	--	--	1.06
C2	2.75	15.39	0.587	72.1	2.75	21.59
C3	2.93	17.43	0.717	71.1	2.93	21.36
C4	1.81	11.94	0.456	65.5	2.50	19.83
C5	1.97	15.55	0.640	69.6	2.86	32.78
C6	2.33	14.24	0.544	90.8	3.47	36.19

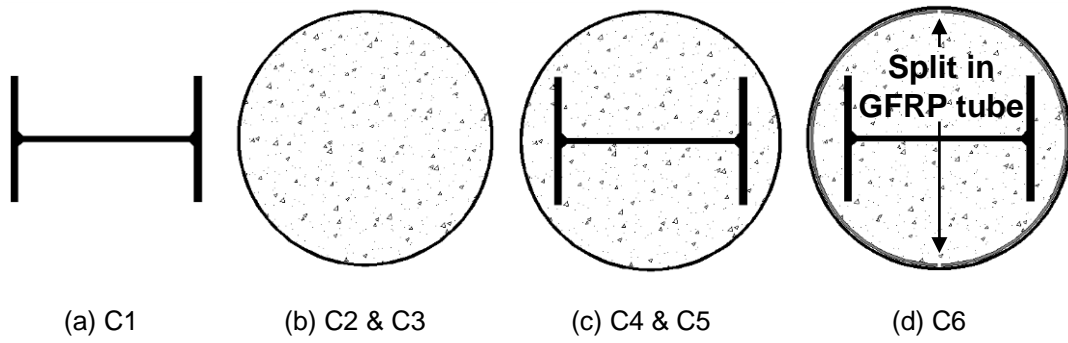


Figure 2.1: Column Types

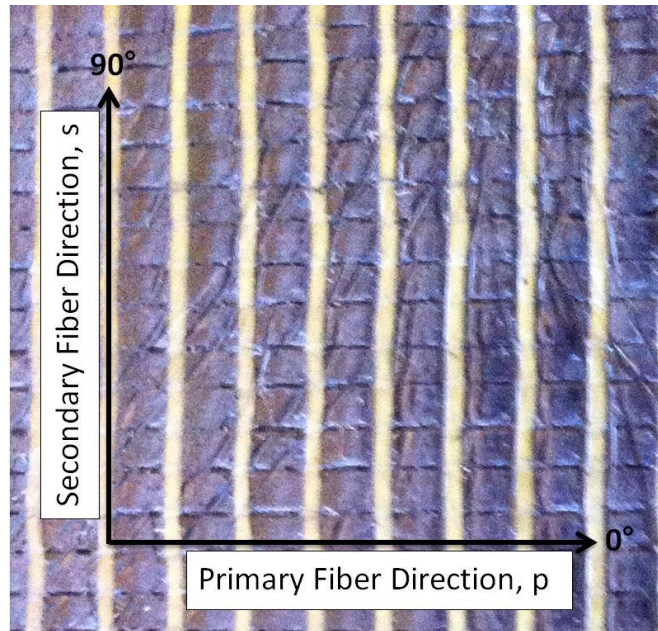
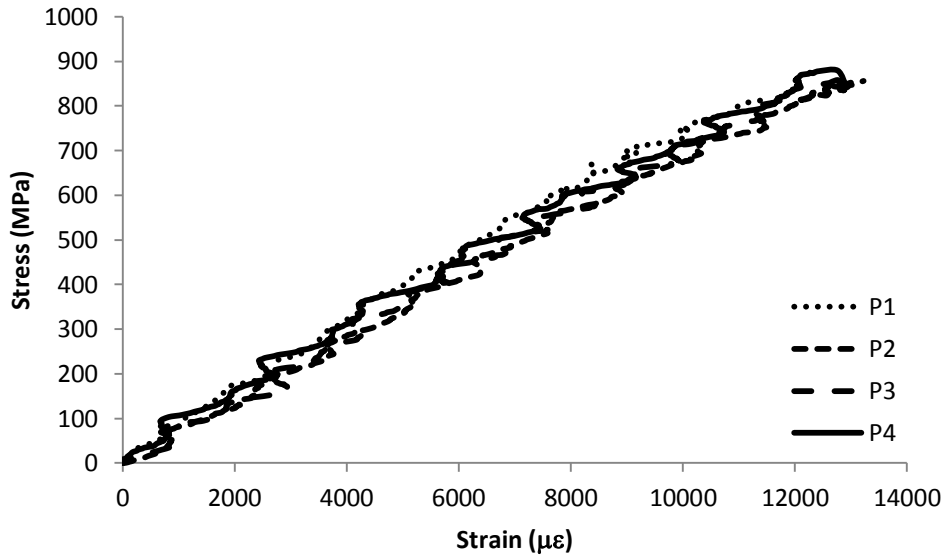
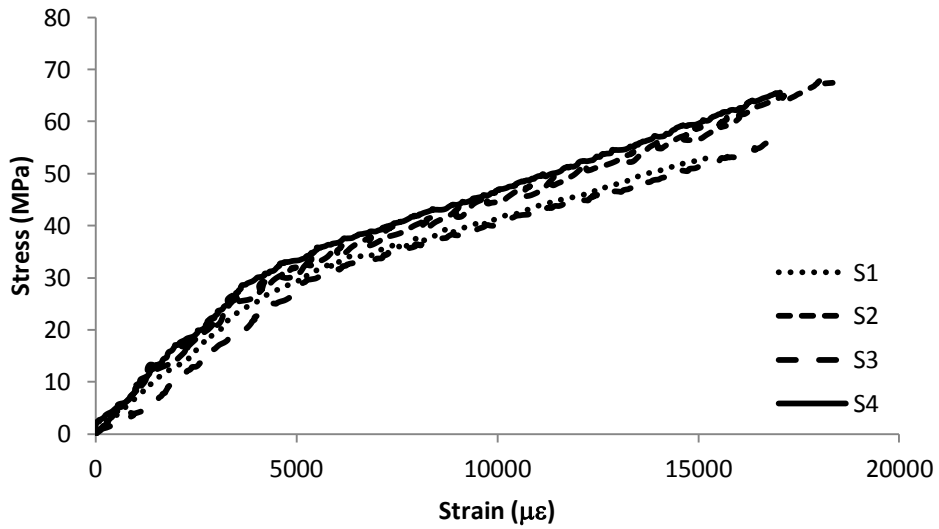


Figure 2.2: CFRP Fiber Directions

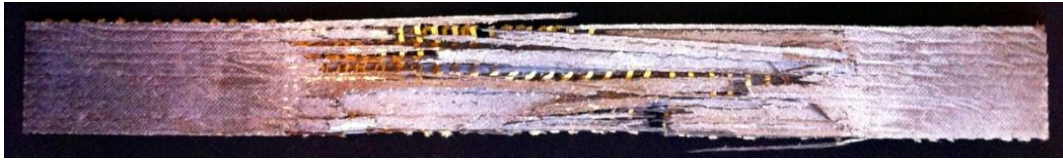


(a) Primary Fiber Direction



(b) Secondary Fiber Direction

Figure 2.3: CFRP Coupon Tensile Response Curves



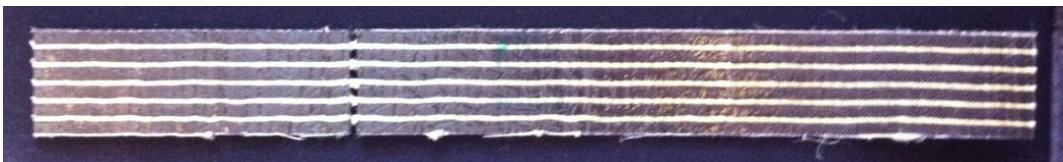
(a) Primary Direction: Front



(b) Primary Direction: Back



(c) Secondary Direction: Front



(d) Secondary Direction: Back

Figure 2.4: Failed CFRP Coupons

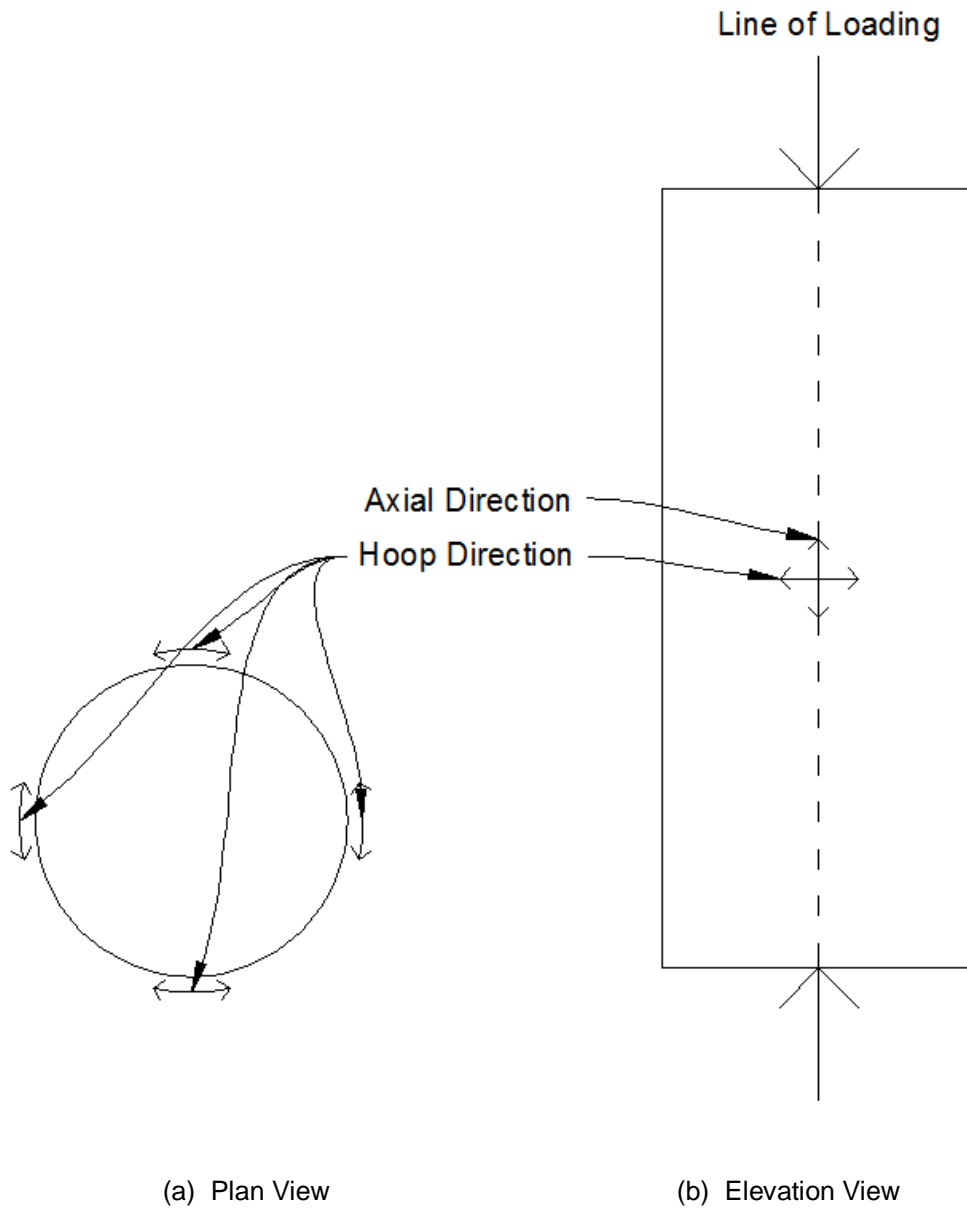


Figure 2.5: Direction Definitions



(a) Impregnating the fabric with epoxy



(b) Curing Specimen



(c) Removing the cardboard form



(d) Completed FRP Tube

Figure 2.6: FRP Tube Construction Process

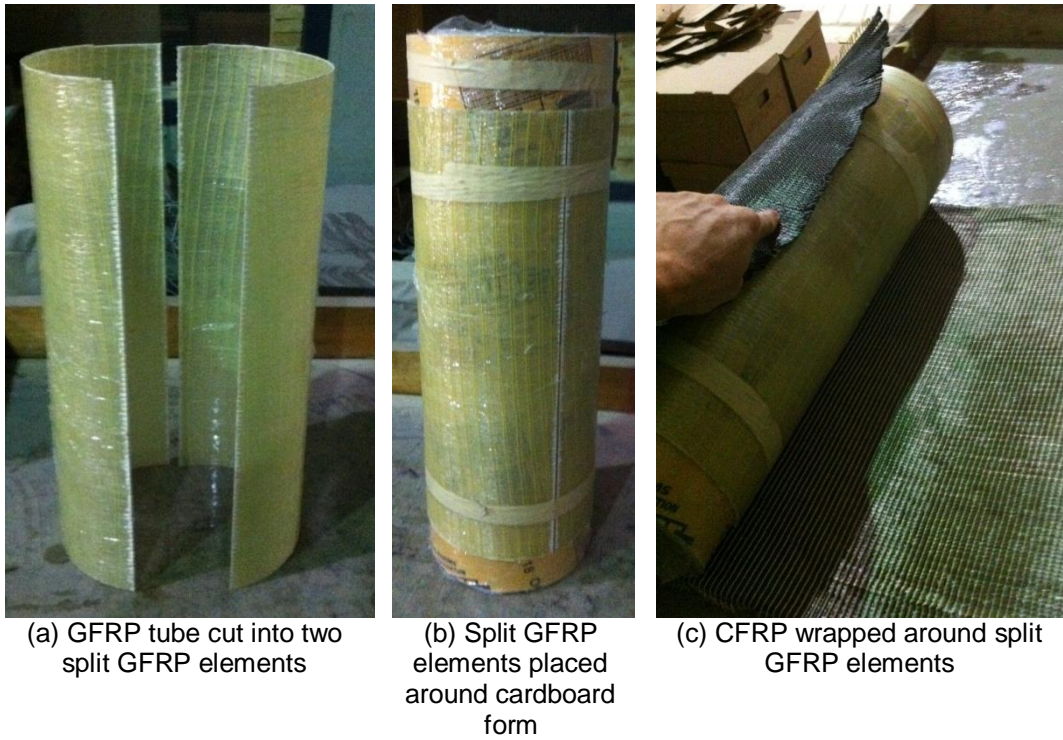


Figure 2.7: Column Type C6 Split Tube Construction Process

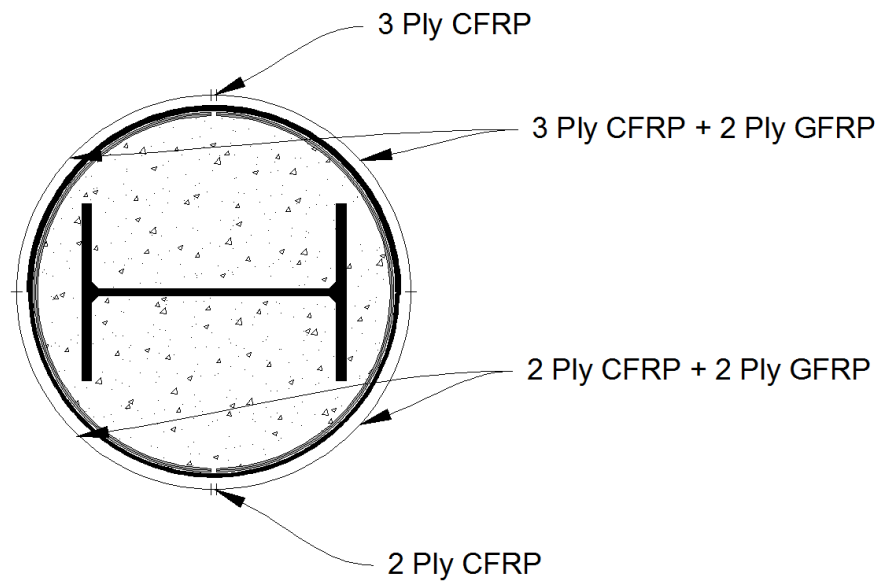


Figure 2.8: CFRP-Wrapped Split-GFRP-Confined Concrete-Steel Composite Specimen Cross-Section



C6

C4

C2

C5

C3

Figure 2.9: FRP Tubes Prior to Placing Concrete

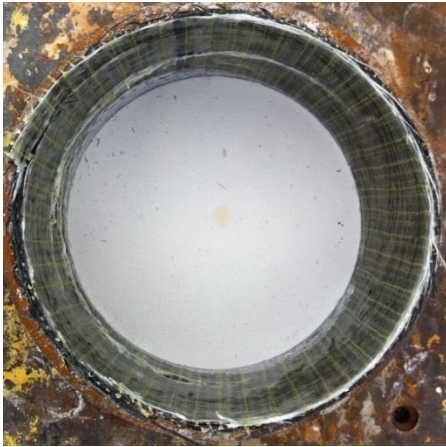


(a) Strain Gauges



(b) String Pots

Figure 2.10: Tube Instrumentation



(a) Failed Cross-section



(b) Failure Location

Figure 2.11: Failed CFRP Tube

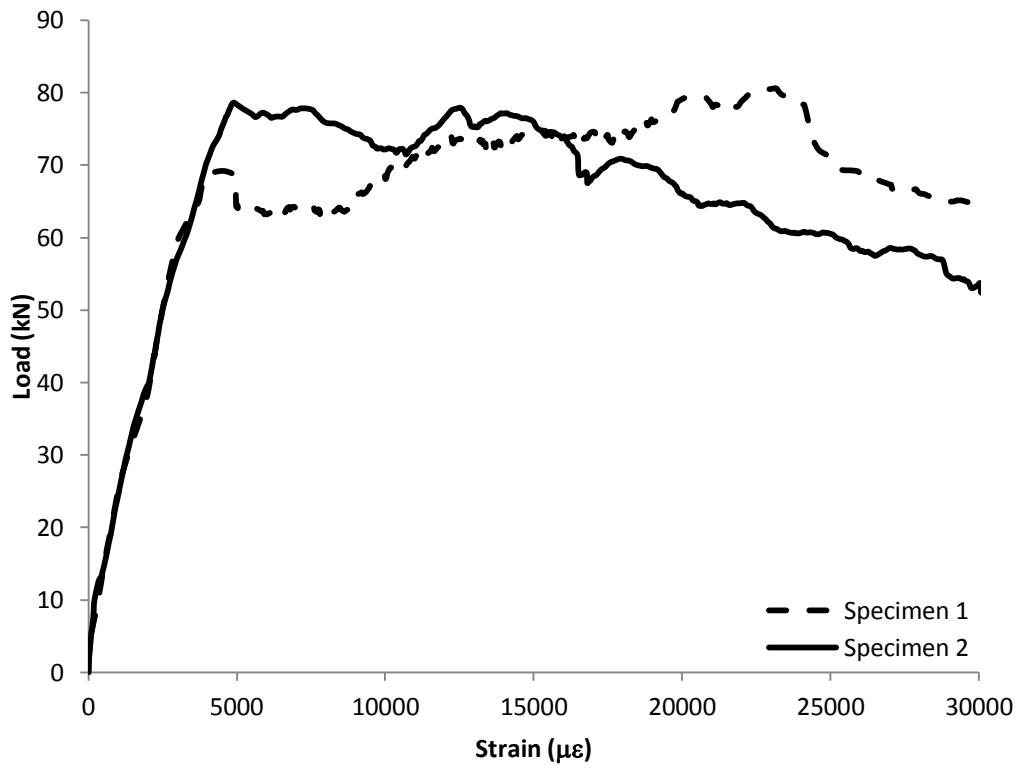


Figure 2.12: CFRP Tube Response Curves

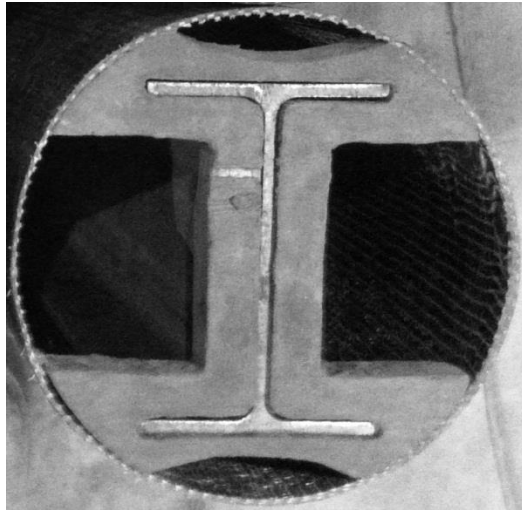
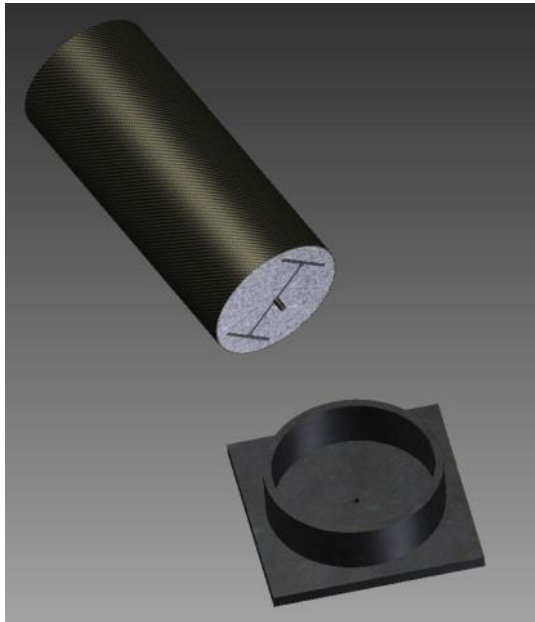


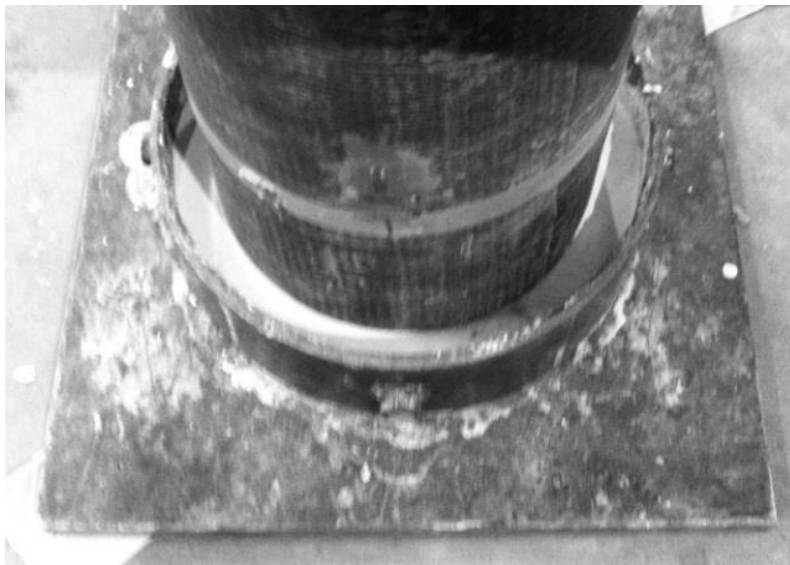
Figure 2.13: Wooden Spacer



(a) Centering Dowel System

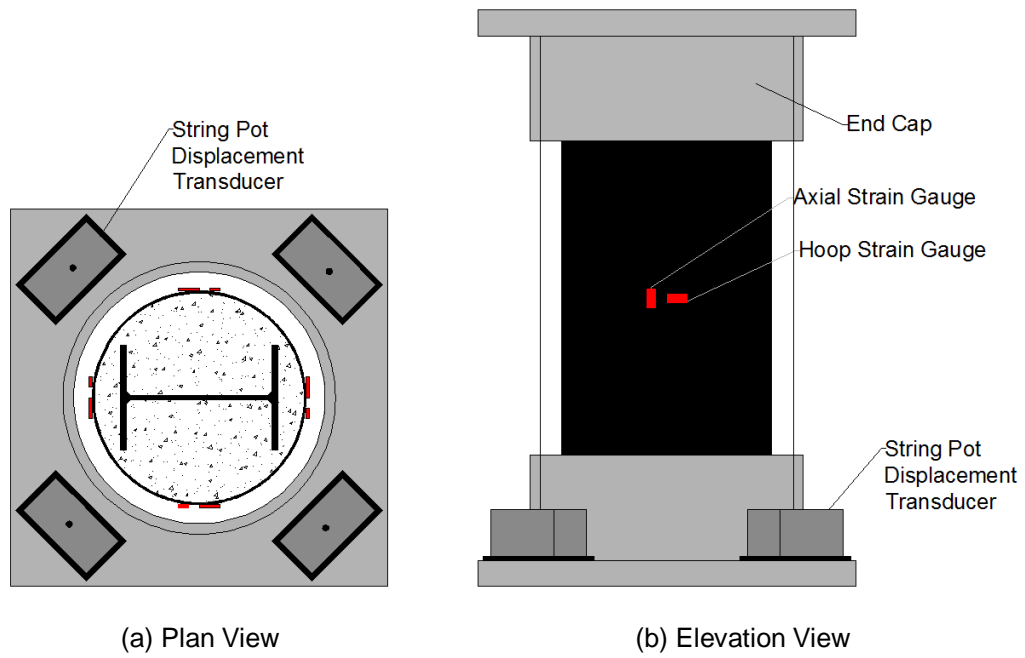


(b) End Cap Schematic



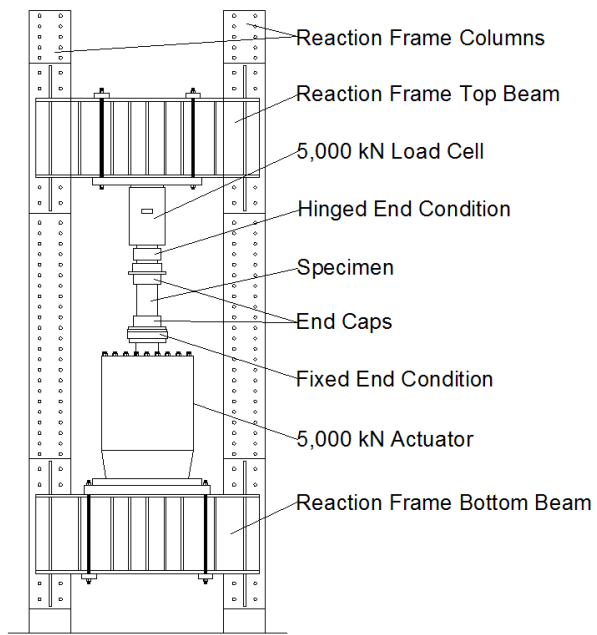
(c) End Cap Photograph

Figure 2.14: Specimen Preparation



(c) Photograph

Figure 2.15: Instrumentation



(a) Schematic



(b) Photograph

Figure 2.16: Test Setup

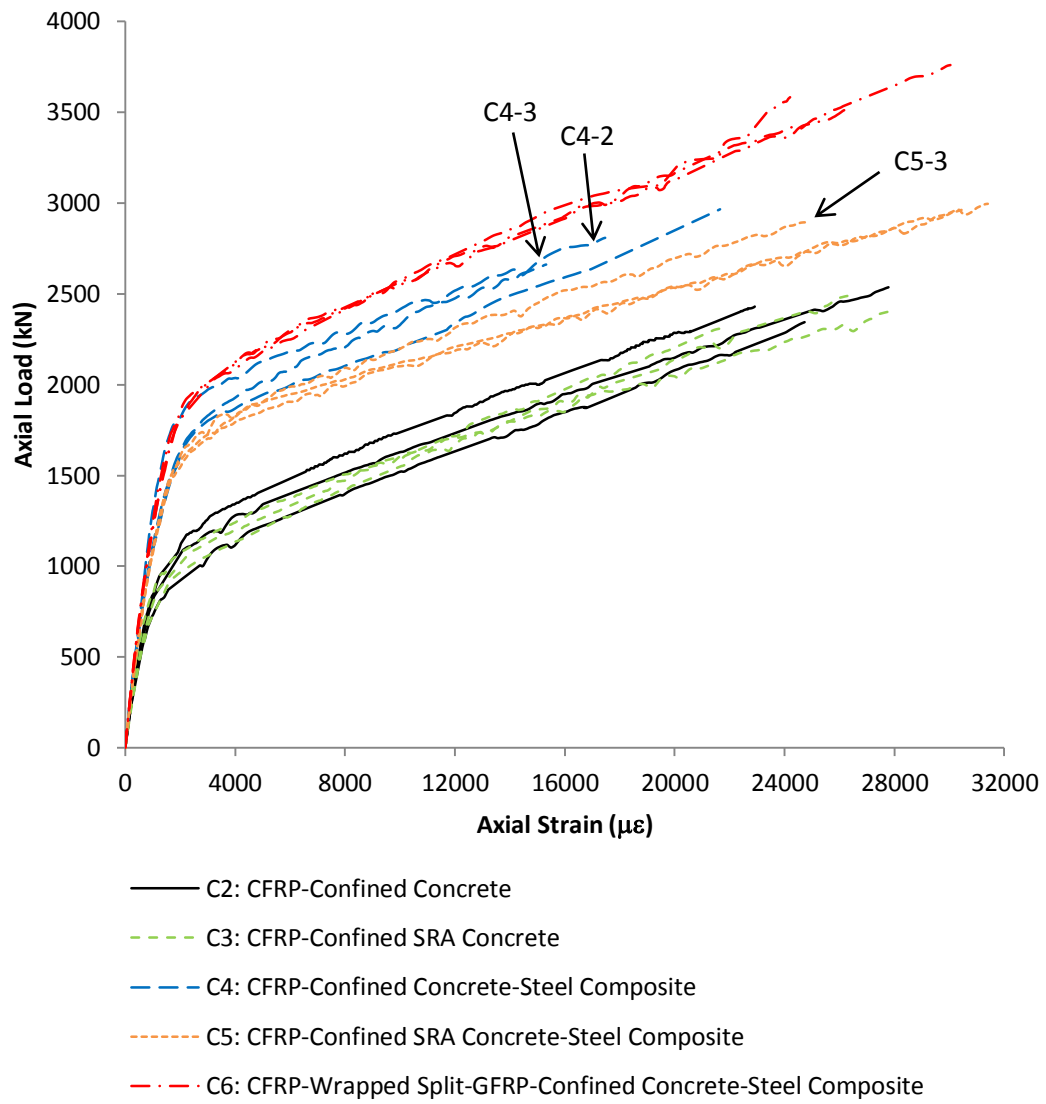
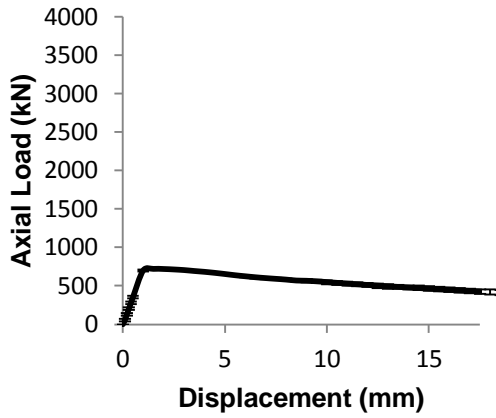
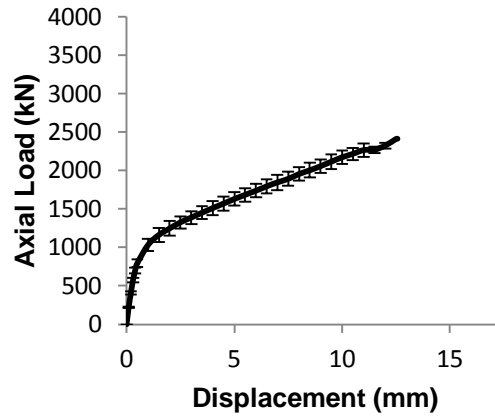


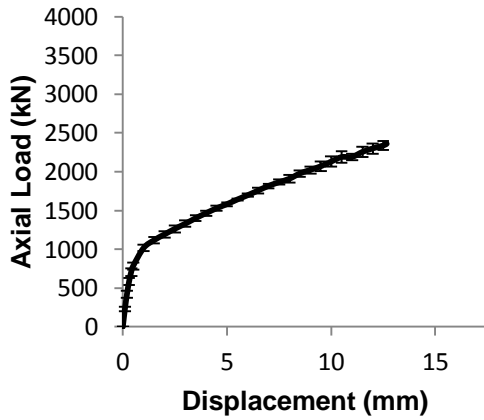
Figure 2.17: Axial Load vs. Axial Strain Column Specimen Response



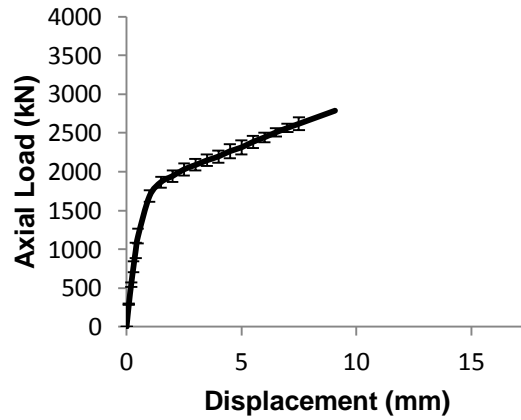
(a) C1: Steel Section



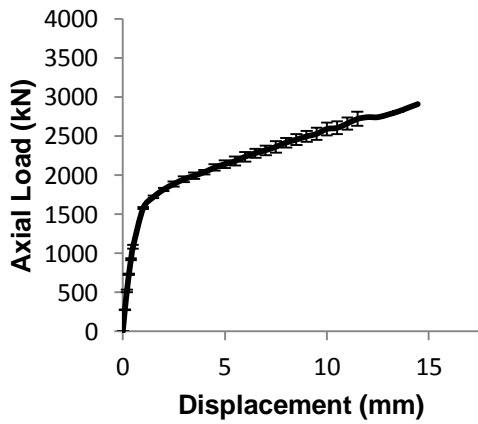
(b) C2: CFRP-Confined Concrete Composite



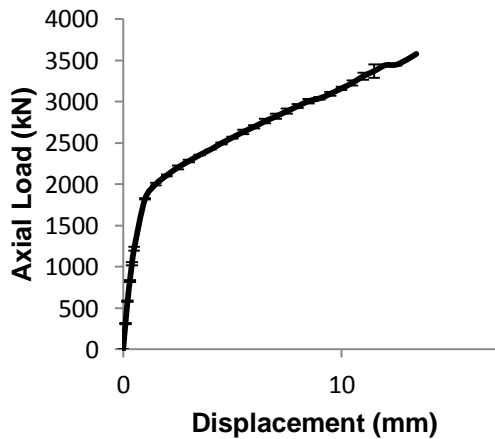
(c) C3: CFRP-Confined SRA Concrete Composite



(d) C4: CFRP-Confined Concrete-Steel Composite

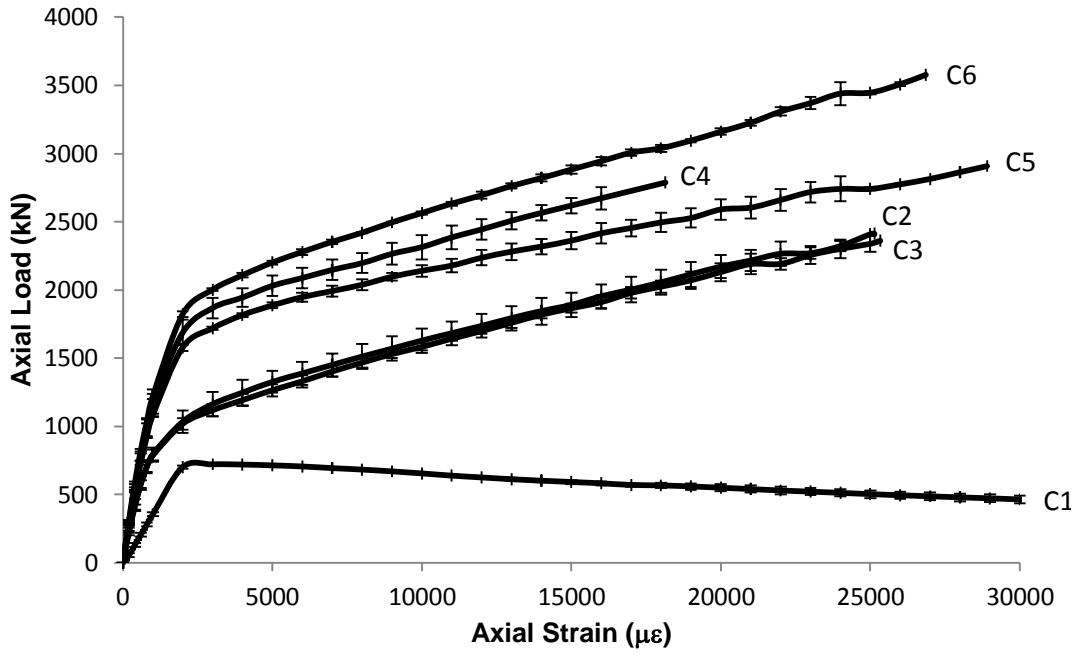


(e) C5: CFRP-Confined SRA Concrete-Steel Composite

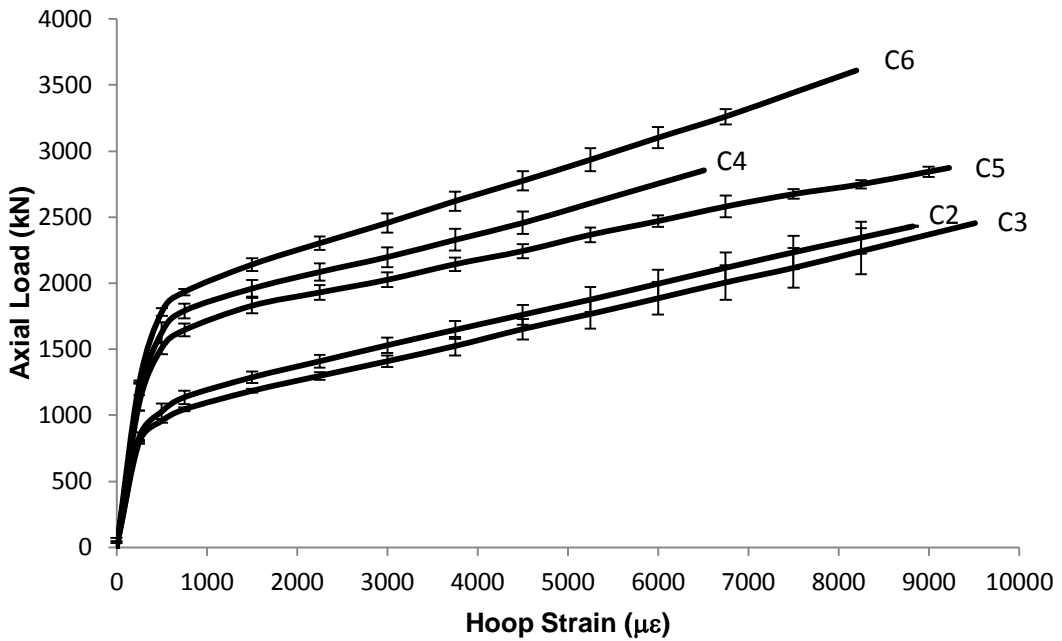


(f) C6: CFRP-Wrapped Split-GFRP-Confined Concrete-Steel Composite

Figure 2.18: Axial Load vs. Axial Displacement Column Type Response



(a) Axial Load vs. Axial Strain Response



(b) Axial Load vs. Hoop Strain Response

Figure 2.19: Comparison of Column Type Load – Strain Response



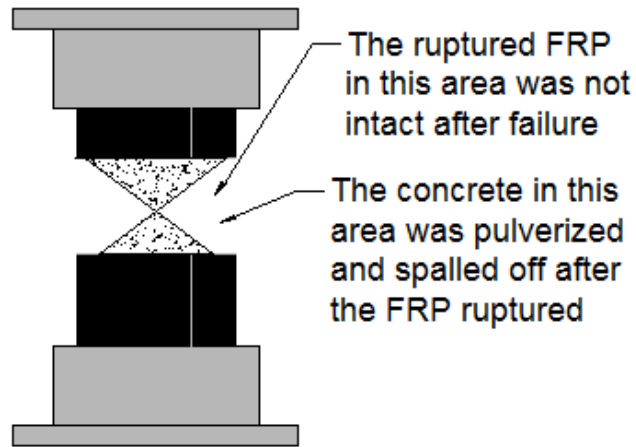
Figure 2.20: C1 – Steel Section Failed Specimen (From Karimi et al. (2010))



(a) C2-1



(b) C2-2



(c) Post Failure Schematic

Figure 2.21: CFRP-Confined Concrete Failed Specimens



(a) C3-1



(b) C3-2



(c) C3-2 Close Up

Figure 2.22: CFRP-Confined Shrinkage Reducing Admixture Concrete Failed Specimens

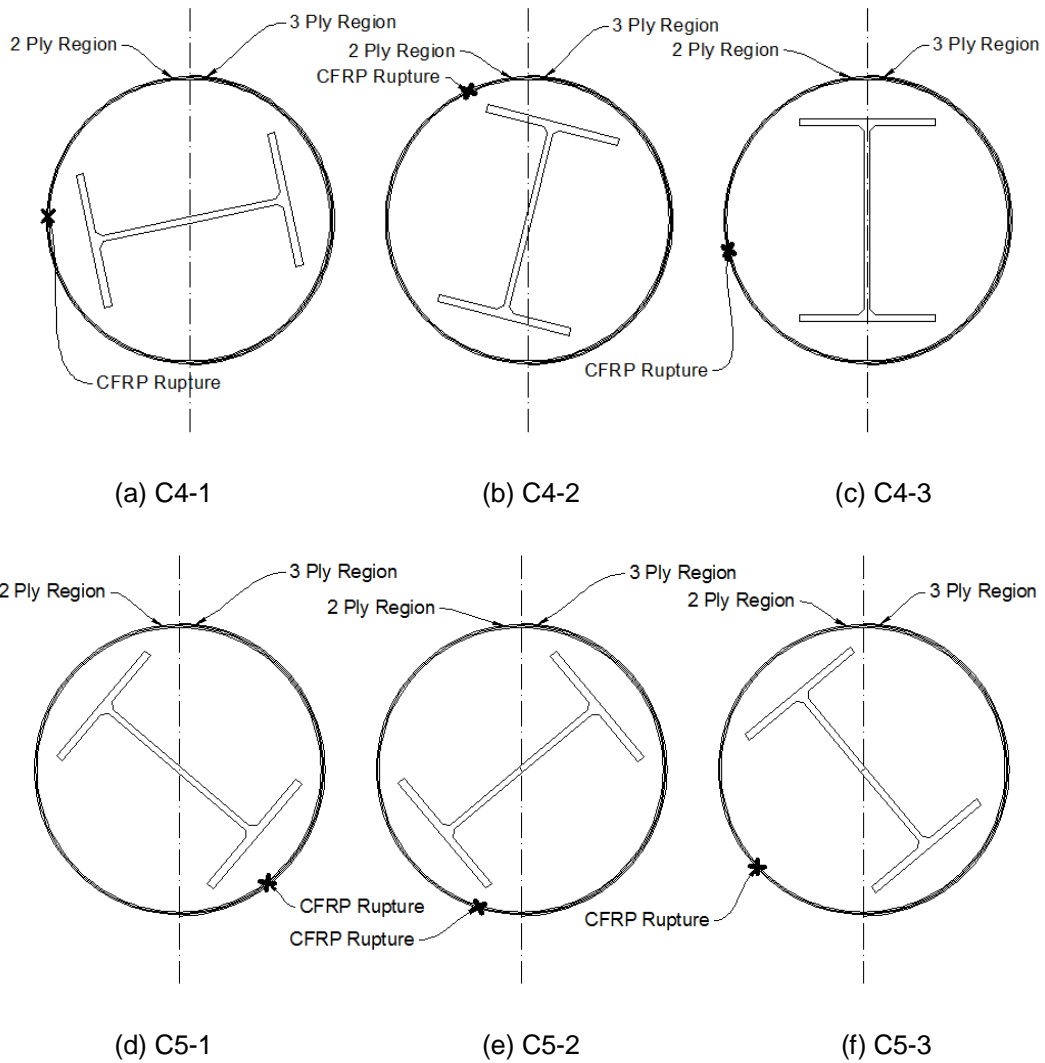


Figure 2.23: Steel, Rupture, and Overlap Location Orientation



Figure 2.24: C4-2 CFRP Rupture Location



(a) C4-1



(b) C4-2



(c) C4-3

Figure 2.25: CFRP-Confined Concrete-Steel Composite Failed Specimens



(a) C5-1



(b) C5-2



(c) C5-3

Figure 2.26: CFRP-Confined Shrinkage Reducing Admixture Concrete-Steel Composite Failed Specimens



(a) C6-1



(b) C6-2



(c) C6-3

Figure 2.27: CFRP-Wrapped Split-GFRP-Confined Concrete-Steel Composite Failed Specimens



(a) Ruptured FRP Jacket



(b) Flange Buckling – Front View



(c) Flange Buckling – Side View

Figure 2.28: CFRP-Wrapped Split-GFRP-Confined Concrete-Steel Composite Failed Specimen Components

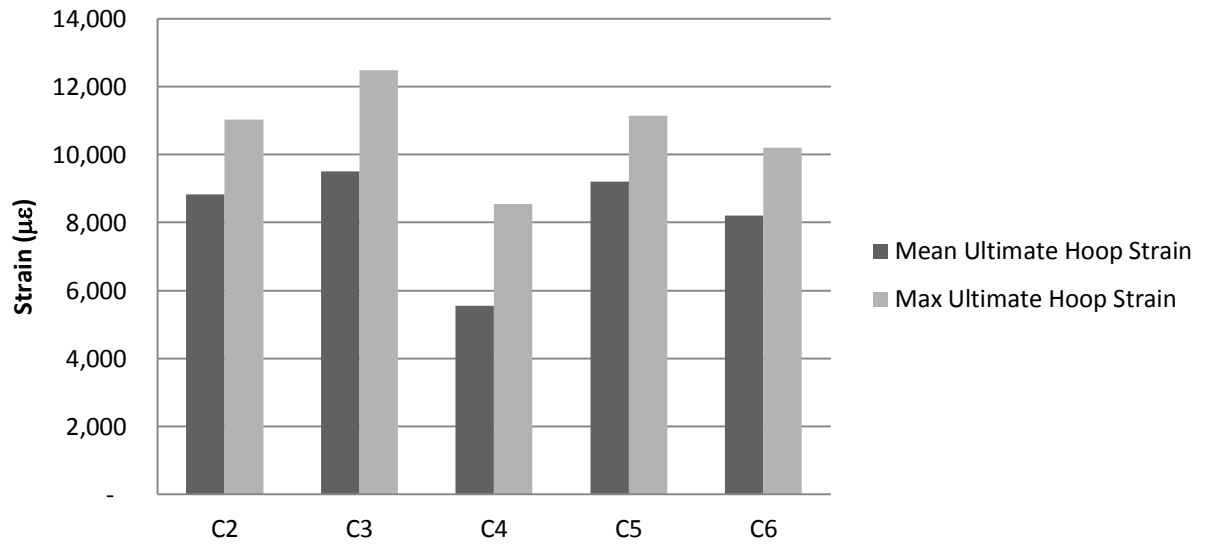


Figure 2.29: Ultimate Hoop Strain

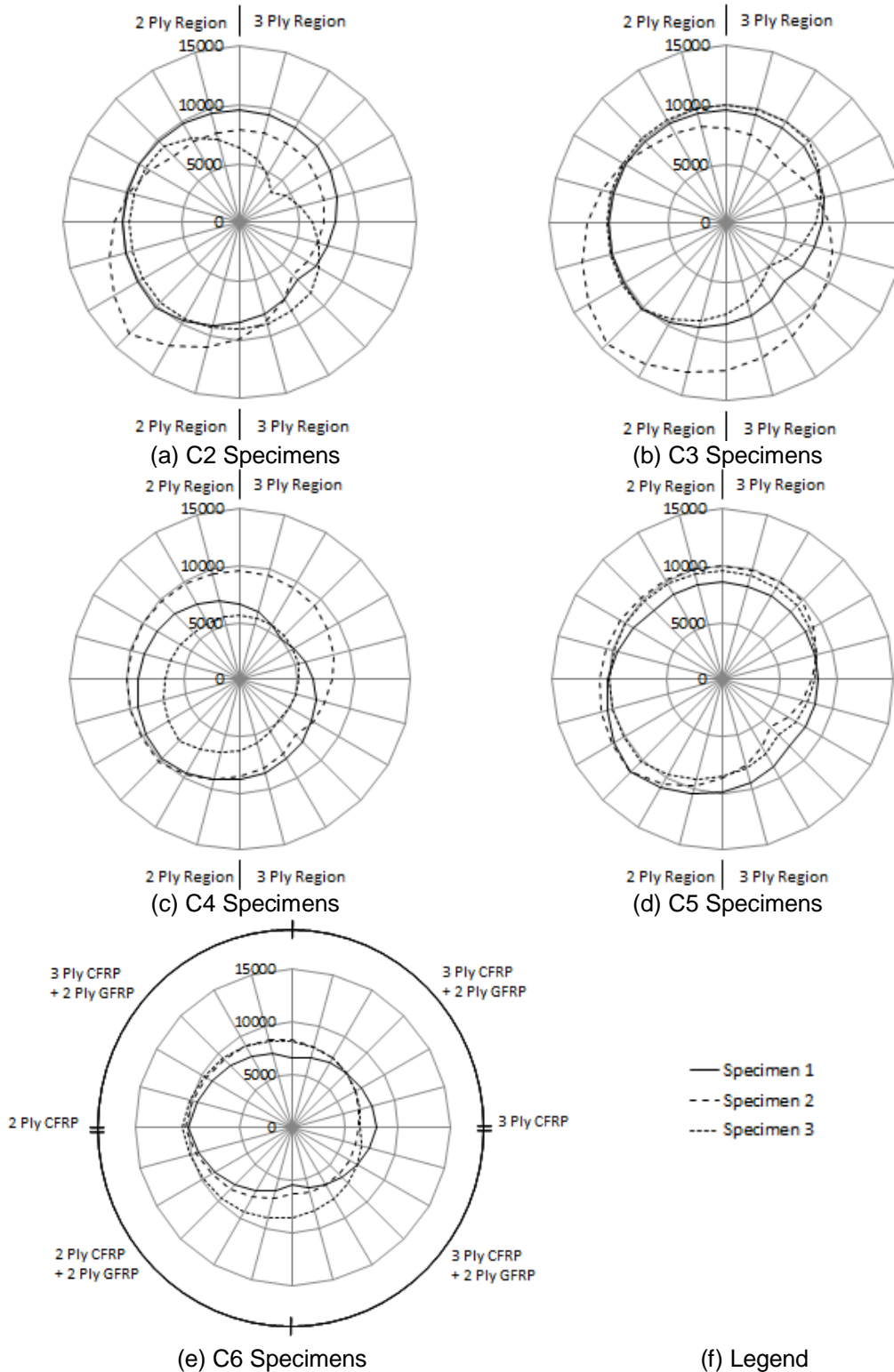


Figure 2.30: Hoop Strain Distribution around Circumference at Ultimate Capacity

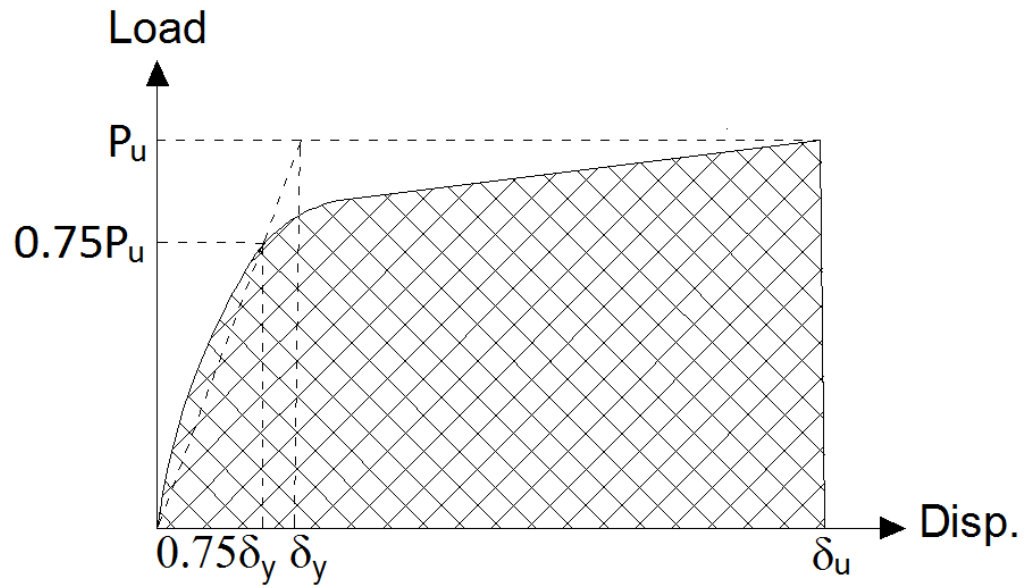


Figure 2.31: Definition of Energy Dissipation Capacity Idealization

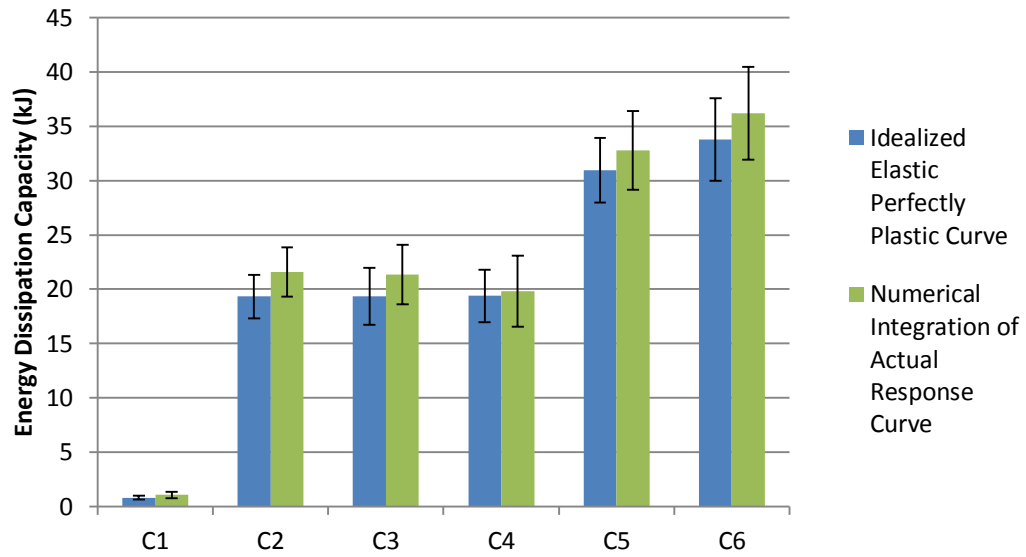


Figure 2.32: Energy Dissipation Capacity

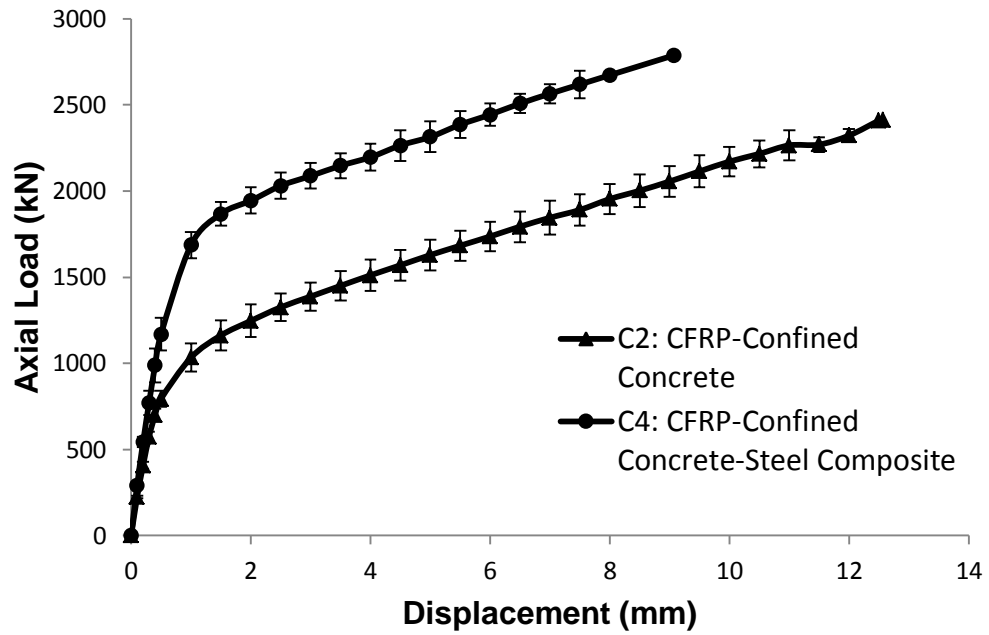


Figure 2.33: Effect of Adding Steel W Section to CFRP Confined Concrete

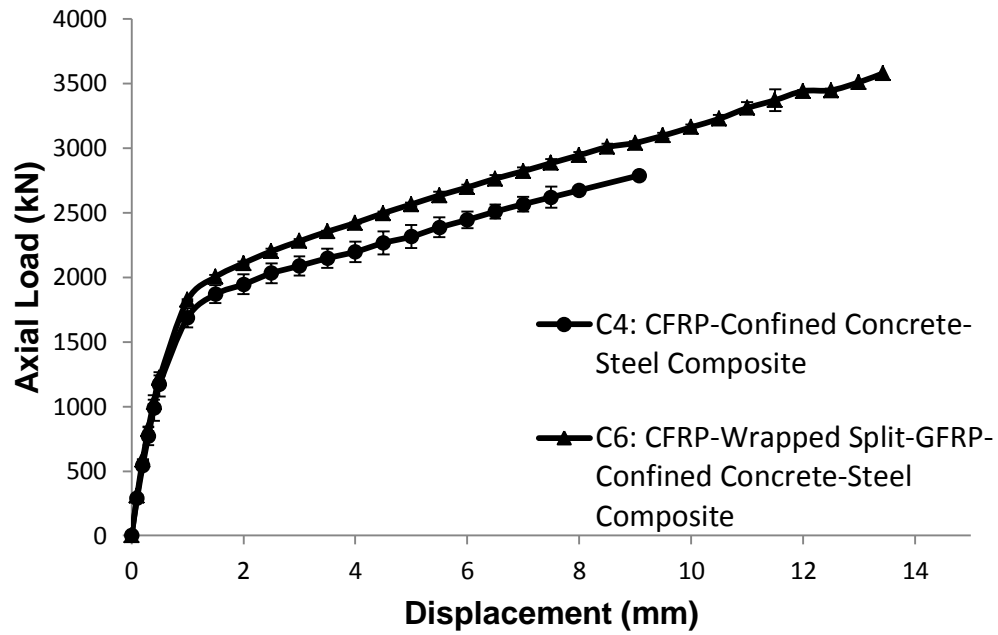
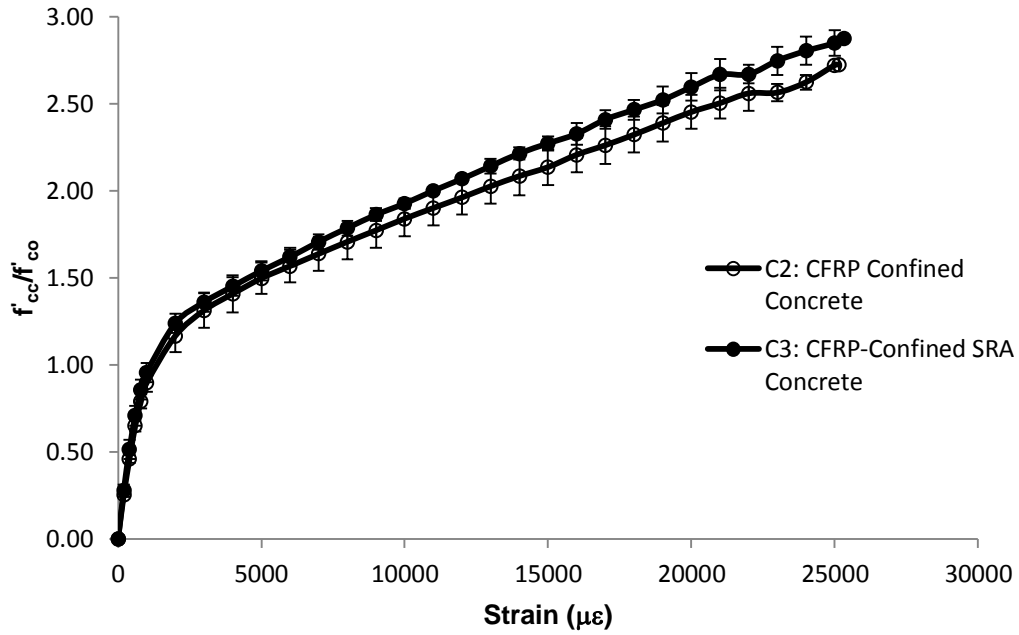
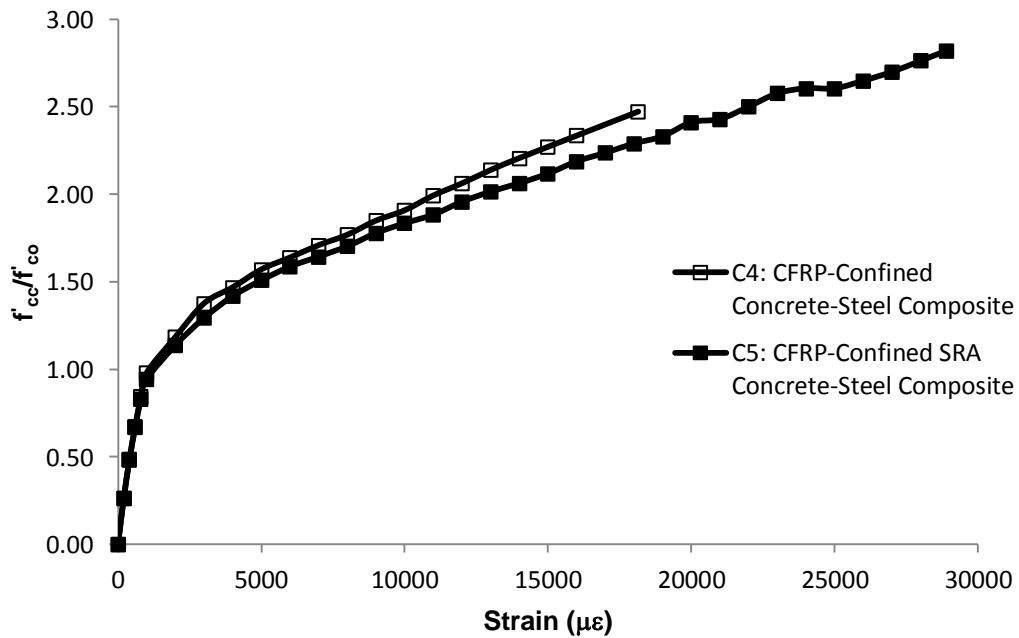


Figure 2.34: Split Tube Effects



(a) CFRP Confined Concrete Comparison



(b) CFRP Confined Concrete-Steel Composite Comparison

Figure 2.35: Shrinkage Reducing Admixture Effects on Confined Concrete

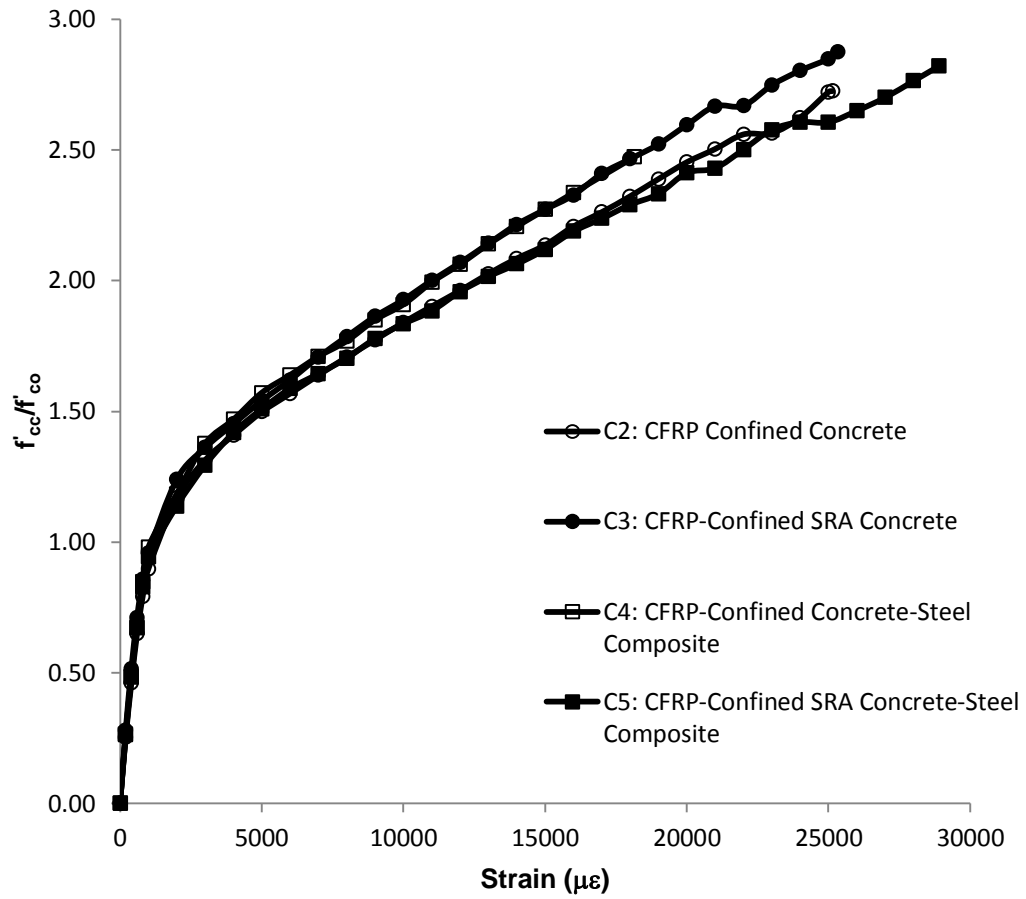


Figure 2.36: Shrinkage Reducing Admixture Effects Compared

Chapter 3 - Modelling

3.1 Introduction

The various axial load versus axial displacement response curves for the three different composite column types tested in this study are investigated. The primary objective of this chapter is to investigate various models which can be used to predict the response of the composite columns. The load versus displacement response of the composite columns is obtained by summing the contributions from the different components. Only the column types containing normal concrete are considered in this chapter. These include column types C2, C4, and C6 as shown in Figure 3.1. First, column type C2: CFRP-Confined Concrete is modelled. Next, the model is extended to include the effects of the steel section in column type C4: CFRP-Confined Concrete-Steel Composite. Finally, the model is applied to column type C6: CFRP-Wrapped Split-GFRP-Confined Concrete-Steel Composite.

A number of models have been suggested from investigations into the response of confined concrete. These models can be divided into two categories: design-orientated models and analysis-orientated models. Design-orientated models are encapsulated in closed form equations that provide a relatively simple and conservative estimate of the confined concrete response. Analysis-orientated models consider the response of

the concrete, the FRP jacket, and the interaction between the two. They are not closed form and require an iterative incremental approach. However, they are more capable of accurately describing the confined concrete response. Both design-orientated and analysis-orientated models are investigated in this study.

3.2 Composite Column Response

The composite column response for the columns tested in this study is due to contributions from the steel and the confined concrete. The column strength is determined using strain compatibility as described by the expression,

$$P(\varepsilon) = A_c f_c(\varepsilon) + A_s f_s(\varepsilon) \quad (3.1)$$

where ε is the axial strain of the column and $P(\varepsilon)$, $f_c(\varepsilon)$, and $f_s(\varepsilon)$ are the column capacity, concrete stress, and steel stress as functions of axial strain, respectively. A_c and A_s are the cross-sectional area of concrete and steel, respectively.

3.3 Steel Section Response

The steel response is assumed as elastic-perfectly plastic. The yield point is taken as 411 MPa as determined by coupon tests. This compares well with the average yield stress value of 417 MPa determined from steel section compressive tests. The results from column type C1: Steel Section

column tests in Chapter 2 show the post peak gradual loss of capacity with increasing strain due to local buckling. This effect is minimized in the composite columns due to the encasing action of the concrete on the steel flanges, which works to delay local buckling. This increase in load carrying capacity at high strains is attributed to the composite action.

3.4 Concrete Parameters

The concrete is found to have an unconfined compressive strength, f'_c , of 26.2 MPa at 85 days. This corresponds to the time of column testing. The unconfined concrete was only tested for compressive strength, therefore the elastic modulus and strain at peak compressive stress are estimated using appropriate formulae. Clause 8.6.2.2 of CSA Standard A23.3-04: Design of Concrete Structures (CSA, 2004) gives the unconfined concrete elastic modulus, E_c , as,

$$E_c = (3300\sqrt{f'_c} + 6900\left(\frac{\gamma_c}{2300}\right)^{1.5}) \quad (3.2)$$

where f'_c is the unconfined concrete strength and γ_c is the density of concrete.

De Nicolo et al. (1994) determined a more accurate expression for the strain of unconfined concrete at peak compressive stress, ε_{co} , than the widely assumed constant value of 2,000 $\mu\varepsilon$. The expression is given as,

$$\varepsilon_{co} = 0.00076 + \left[\left(\frac{0.626f'_c}{f^*} - 4.33 \right) 10^{-7} \right]^{0.5} \quad (3.3)$$

where $f^* = 1$ MPa and f'_c is expressed in MPa.

Using these expressions, the elastic modulus is estimated to be 23,519 MPa and the strain at peak unconfined concrete stress as 1,859 $\mu\varepsilon$. These values are used as required throughout this chapter.

3.5 Biaxial State of Stress

Push-out tests on GFRP-confined concrete performed by Li et al. (2005) found the interfacial bonding between the concrete core and the GFRP jacket to be 0.42 MPa. They suggest that although the interfacial bonding strength is not high, it will still transfer axial load from the concrete core to the FRP jacket. It is expected that a CFRP jacket will have a similar interfacial bonding strength and therefore the FRP jackets in the current study are assumed to have been loaded in the axial direction. The FRP in the current study was also loaded axially by the Hydro-Stone, which was used to cast the ends of the column specimens in the end caps.

As a result, the CFRP tube is assumed to be in a biaxial state of stress in the confined concrete columns. A small element of the CFRP tube is considered in Figure 3.2. The element is in tension in the hoop direction and in compression in the axial direction of the column. The hoop and

axial directions are denoted by h and a, respectively. The relatively thin tube section is considered as a plane stress element. The constitutive relationship for a plane stress, orthotropic material is given as,

$$\begin{Bmatrix} \varepsilon_h \\ \varepsilon_a \\ \gamma_{ah} \end{Bmatrix} = \begin{bmatrix} \frac{1}{E_h} & \frac{-\nu_{ah}}{E_a} & 0 \\ \frac{-\nu_{ha}}{E_h} & \frac{1}{E_a} & 0 \\ 0 & 0 & \frac{1}{G} \end{bmatrix} \begin{Bmatrix} \sigma_h \\ \sigma_a \\ \tau_{ah} \end{Bmatrix} \quad (3.4)$$

where E_h is Young's modulus in the hoop direction, ε_h is the strain in the hoop direction, σ_h is the stress in the hoop direction, E_a is Young's modulus in the axial direction, ε_a is the strain in the axial direction, σ_a is the stress in the axial direction, ν_{ah} is Poisson's ratio corresponding to a contraction in the hoop direction due to an extension in the axial direction, ν_{ha} is Poisson's ratio corresponding to a contraction in the axial direction due to an extension in the hoop direction, G is the shear modulus, γ_{ah} is the shear strain, and τ_{ah} is the shear stress. As shown in Figure 3.2, the element is oriented such that there is no shear stress, therefore the relationship simplifies to,

$$\begin{Bmatrix} \varepsilon_h \\ \varepsilon_a \end{Bmatrix} = \begin{bmatrix} \frac{1}{E_h} & \frac{-\nu_{ah}}{E_a} \\ \frac{-\nu_{ha}}{E_h} & \frac{1}{E_a} \end{bmatrix} \begin{Bmatrix} \sigma_h \\ \sigma_a \end{Bmatrix} \quad (3.5)$$

This relationship can be expressed as,

$$\sigma_h = \frac{E_h}{1 - \nu_{ah}\nu_{ha}}(\varepsilon_h + \nu_{ah}\varepsilon_a) \quad (3.6)$$

$$\sigma_a = \frac{E_a}{1 - \nu_{ah}\nu_{ha}}(\varepsilon_a + \nu_{ha}\varepsilon_h) \quad (3.7)$$

Poisson's ratio, ν_{ah} , controls the contribution of the axial strain to the hoop stress as shown in Equation (3.6). If Poisson's ratio is zero, Equation (3.6) simplifies to a uniaxial stress-strain relationship. The value of ν_{ah} was calculated in Chapter 2 as 0.025, which is a small value and limits the effect of the axial strain on the hoop stress. Since ε_h is positive and ε_a is negative, it can be determined from Equation (3.6) that a decrease in axial strain or an increase in hoop strain results in an increase in hoop stress. The axial strain works to reduce the hoop stress, which means that ignoring the biaxial state of stress and using a uniaxial state of stress will result in a lower predicted capacity value. As a result, it is conservative to use a uniaxial model.

The complete stress-strain relationship for the secondary direction of the CFRP, which was orientated in the axial direction on the columns, is shown in Figure 3.3. Tensile stresses are shown as positive and compressive as negative. The tensile curve was taken from coupon tests and the compressive curve was taken from the tube compression tests, both of which were presented in Chapter 2. In both tension and compression, the elastic limit is approximately 4,500 $\mu\varepsilon$. The ultimate axial

strain of the FRP on the column specimens at failure was significantly higher than the elastic limit of $4,500 \mu\epsilon$. The model used in Equations (3.4) - (3.7) for the biaxial state of stress is based on Hooke's law, which is only applicable within the elastic limit. Thus Equations (3.6) and (3.7) are not valid at failure strain values. Furthermore, Poisson's ratio was calculated from the elastic modulus, which is not applicable at failure strain levels.

As the strain values at failure exceed the elastic limits of the secondary direction of the CFRP, the biaxial state of stress analysis is not considered to be applicable. Due to the lack of stiffness in the axial direction of the tube, and thus a small Poisson's ratio, ν_{ah} , the assumption of a unidirectional state of stress analysis is considered acceptable. This is in agreement with Naguib and Mirmiran (2001) who reported that the FRP jacket is only subjected to a biaxial state of stresses if the fiber architecture is designed with considerable axial stiffness.

3.6 Uniaxial State of Stress

The CFRP used in the construction of the FRP tubes was a unidirectional fabric orientated in the hoop direction. Thus unidirectional models that utilize the properties of the FRP in the hoop direction and neglect any contribution of the FRP to the axial response of the composite column are investigated.

3.7 Design-Orientated Model

The original design-orientated model by Lam and Teng (2003) was selected as it is widely used as a result of its relative simplicity and accurate predictions. This model was later revised by Teng et. al. (2009) after additional testing. The two models have the same framework but have different definitions for the ultimate concrete strength and the ultimate axial strain. Both revisions are considered in this study.

3.7.1 Design-Orientated Model Framework

The stress-strain model by Lam and Teng (2003) involves a response curve with a parabola for the first portion and a straight line for the second portion of the curve as shown in Figure 3.4. The parabola reflects the gradual effects of confinement as the axial stress increases. The basic assumptions of the model are that: 1) The first portion of the stress-strain curve is parabolic and the second portion is linear. 2) The initial slope of the parabolic section at zero strain is taken as the stiffness of the unconfined concrete. 3) There is no change in slope between the first and second parts of the curve ensuring a smooth transition. 4) The parabolic, non-linear portion of the curve is affected by the presence of the FRP jacket. 5) The linear portion ends at failure where both the ultimate axial strain and the compressive strength of the confined concrete are reached. 6) The linear portion of the curve intersects the axial stress axis at a stress equal to the unconfined concrete strength.

The confined concrete stress-strain response curve is then given by a piece-wise expression,

$$f_c(\varepsilon) = \begin{cases} E_c \varepsilon - \frac{(E_c - E_2)^2}{4f'_c} \varepsilon^2 & (0 \leq \varepsilon \leq \varepsilon_t) \\ f'_c + E_2 \varepsilon & (\varepsilon_t \leq \varepsilon \leq \varepsilon_{cc}) \end{cases} \quad (3.8)$$

where ε_t is the transition strain between the initial parabolic portion and the second straight linear portion of the curve. The transition strain is given by,

$$\varepsilon_t = \frac{2f'_c}{(E_c - E_2)} \quad (3.9)$$

The slope of the ascending linear branch, E_2 , is given by,

$$E_2 = \frac{f'_{cc} - f'_c}{\varepsilon_{cc}} \quad (3.10)$$

where ε_{cc} is the ultimate axial strain of confined concrete.

The expression for the response depends on the unconfined concrete strength; the unconfined concrete elastic modulus; the ultimate confined concrete strength; and the ultimate axial strain. For any application, the unconfined concrete strength will be known and the unconfined concrete elastic modulus can be calculated by an empirical formula as is done in this study. What is unknown is the ultimate state at failure; specifically the

confined concrete strength and the ultimate axial strain of confined concrete. One of the benefits of the Lam and Teng (2003) model framework is that it can readily incorporate the use of experimental or predicted values for the confined concrete strength and the ultimate axial strain.

3.7.2 Modelling of Column Type C2: CFRP-Confined Concrete

The determination of the confined concrete stress-strain state at failure is a challenge for a predictive model. This section compares the ultimate axial strain and confined concrete strength determined from the experiment program, the original model by Lam and Teng (2003), and the revised model by Teng et al. (2009). The experimental values used are those from column type C2: CFRP-confined concrete. The properties of this column type will also be used in the predictive value determinations. The specimens included two and a half wraps of CFRP, however, the extra half a wrap which was used to resist debonding will be ignored and the CFRP jacket will be considered as 2 ply CFRP.

3.7.2.1 *Experimental Values*

The experimental ultimate axial strain was 25,141 $\mu\epsilon$ with a coefficient of variation of 8.0%. The confined compressive strength of concrete was 71.4 MPa with a coefficient of variation of 3.2%.

3.7.2.2 *Lam and Teng (2003)*

Lam and Teng (2003) first note that hoop strain in the FRP jacket at rupture, $\varepsilon_{h,rupt}$, is substantially lower than the ultimate strain of FRP coupon tests, ε_{frp} . They suggest using a percentage of the ultimate strain of the FRP coupon tests as,

$$\varepsilon_{h,rupt} = \Omega_{frp} \varepsilon_{frp} \quad (3.11)$$

where Ω_{frp} is the FRP efficiency factor, which is a ratio of hoop rupture strain in the FRP jacket to FRP material ultimate tensile strain as determined from coupon tests. The study by Lam and Teng (2003) gathered a database of 52 CFRP specimens to determine an average value of $\Omega_{frp} = 58.6\%$ with a coefficient of variation of 26.1%.

Column type C2 had an ultimate hoop strain of 8,547 $\mu\varepsilon$, which was calculated as the average over all four strain gauges around the circumference of the column. This corresponds to a value of $\Omega_{frp} = 67.4\%$, which is within 0.58 standard deviations of the mean value reported by Lam and Teng (2003).

A later study by Lam and Teng (2004) demonstrated that using the average strains from the non-overlap region provided a better representation of the actual state of strain in the jacket as the hoop strain is always lower in the overlap region due to the increased thickness. This

later study by Lam and Teng (2004) reported a value of $\Omega_{frp} = 58.1\%$ when the strains were averaged over the whole circumference, which is very close to the value of $\Omega_{frp} = 58.6\%$ reported earlier. However, when the hoop strains from the overlap region were excluded, the ratio increased to $\Omega_{frp} = 63.7\%$ with a coefficient of variation of 9.1%.

Column type C2 had an average ultimate hoop strain of 10,019 $\mu\epsilon$ when the hoop strain measurements from the overlap region were excluded from the average. This corresponds to a value of $\Omega_{frp} = 79.0\%$. This is 2.64 standard deviations higher than the results of the study by Lam and Teng (2004). The value found in the current study of $\Omega_{frp} = 79.0\%$ is used for the remainder of the modelling as it is found to give better results than the suggested value from Lam and Teng (2003). It is recognized that a predictive model needs to estimate this ratio itself in order to be applicable. Much work is currently being done in this area by others to better understand the factors contributing to this ratio. The value from Lam and Teng (2004) was based on only nine specimens. A larger database with hoop strain values averaged from the non-overlap region is necessary to create a more representative statistical value.

One half of the confined concrete cross-section is shown in Figure 3.5 with the confinement pressure and the hoop tension pressure identified. The

model by Lam and Teng (2003) defines the maximum confining pressure, f_l , as,

$$f_l = \frac{2E_h t \varepsilon_{h,rupt}}{d} \quad (3.12)$$

where E_h is Young's modulus in the hoop direction, t is the FRP tube thickness, and d is the inner diameter of the FRP tube. This relationship can easily be worked out by integrating the confining pressure around the half circumference and summing the forces in the vertical direction in Figure 3.5.

The confinement ratio (C.R.) is defined as,

$$C.R. = \frac{f_l}{f'_c} \quad (3.13)$$

and is used in the expressions for ultimate strain and confined concrete strength.

The compressive strength of confined concrete, f'_{cc} , is given by,

$$\frac{f'_{cc}}{f'_c} = 1 + k_1 \frac{f_l}{f'_c} \quad (3.14)$$

where k_1 is the confinement effectiveness ratio. Lam and Teng (2003) suggest a value of $k_1 = 3.3$ based on a best fit of the database they used.

The ultimate axial strain is given by,

$$\frac{\varepsilon_{cc}}{\varepsilon_{co}} = c + k_2 \left(\frac{f_l}{f'_c} \right) \left(\frac{\varepsilon_{h,rup}}{\varepsilon_{co}} \right)^{0.45} \quad (3.15)$$

where c is the normalized ultimate strain of unconfined concrete and k_2 is the strain enhancement coefficient. Lam and Teng (2003) recommend that the value of c be taken as 1.75 so that if no confinement is present, the ultimate strain becomes 0.0035 if ε_{co} is taken as the typical value of 0.002. Lam and Teng (2003) suggest a value of $k_2 = 12$ based on a best fit of the database they used. Using these expressions, the ultimate axial strain is 28,354 $\mu\varepsilon$ and the confined compressive strength of concrete is 71.8 MPa. The confined concrete strength is 0.5% greater than the experimentally determined strength and the predicted ultimate axial strain is 12.7% larger than the experimental ultimate axial strain.

3.7.2.3 *Teng et al. (2009)*

Teng et al. (2009) recognized that the model by Lam and Teng (2003) overestimated the ultimate axial strain for FRP jackets with a large amount of FRP. They introduced revised expressions for the ultimate axial strain and the confined concrete strength that would fit within the model framework for the stress-strain response. First the confinement ratio is divided into two components, which include the confinement stiffness ratio,

$$\rho_K = \frac{2E_h t}{\left(\frac{f'_c}{\varepsilon_{co}}\right) d} \quad (3.16)$$

and the strain ratio,

$$\rho_\varepsilon = \frac{\varepsilon_{h,rupt}}{\varepsilon_{co}} \quad (3.17)$$

such that,

$$C.R. = \frac{f_l}{f'_c} = \rho_K \rho_\varepsilon \quad (3.18)$$

The confinement stiffness ratio is a measure of the stiffness of the FRP confining material relative to that of the concrete core. The strain ratio is a measure of the strain capacity of the FRP confining material relative to that of the concrete core.

The revised expression for the confined concrete strength is given as,

$$\frac{f'_{cc}}{f'_c} = 1 + 3.5(\rho_K - 0.01)\rho_\varepsilon \quad (3.19)$$

and the revised expression for ultimate axial strain is,

$$\frac{\varepsilon_{cc}}{\varepsilon_{co}} = 1.75 + 6.5\rho_K^{0.8}\rho_\varepsilon^{1.45} \quad (3.20)$$

The coefficients in these expressions were fit using regression analysis to the database used in the study by Lam and Teng (2003). Using these two revised expressions, the ultimate axial strain can be calculated for column type C2 as 24,897 $\mu\epsilon$ and the confined compressive strength of concrete as 69.6 MPa. The value for the confined concrete strength is 2.5% lower than the experimentally determined strength and the predicted ultimate strain is 1.0% lower than the experimental ultimate strain. The value for the ultimate axial strain from Teng et al. (2009) matches the experimental result better than the original Lam and Teng (2003) model.

3.7.2.4 Response Comparison

The load versus axial strain curves resulting from the different ultimate axial strains and confined concrete strengths are shown in Figure 3.6. This plot compares the experimental response to the curves from Lam and Teng's (2003) original model and the Teng et al. (2009) revised model. The original model response curve is within 2.18 standard deviations of the experimental response curve. The revised model is within 1.53 standard deviations of the experimental response curve. The revised model can be seen to fit the experimental results better than the original model and nearly fits within the lower standard deviation bars of the experimental curve for much of the response. The revised model by Teng

et al. (2009) will be used for column types C4 and C6 as it provides a much better fit to the experimental response for column type C2.

3.7.3 Modelling of Column Type C4: CFRP-Confined Concrete-Steel Composite

Column type C4: CFRP-Confined Concrete-Steel Composite had an average ultimate hoop strain of $7,707\mu\varepsilon$ which corresponds to an FRP efficiency factor of $\Omega_{frp} = 60.8\%$. This factor is used in the model by Teng et al. (2009) to provide the response of the confined concrete in column type C4. The complete column response is calculated using Equation (3.1) by summing the contribution of the confined concrete and the encased steel. The plot in Figure 3.7 compares the assumed elastic-perfectly plastic steel response, the Teng et al. (2009) confined concrete response, the Teng et al. (2009) confined concrete + elastic-perfectly plastic steel response, and the experimental response curve of column type C4. The concrete and steel responses are each taken as the material response acting over the appropriate material cross-sectional area from column type C4. It can be observed from Figure 3.7 that the response given by the Teng et al. (2009) confined concrete + elastic-perfectly plastic steel response is lower than the experimental response. However, it is found to predict the response of the composite column within 3 standard deviations.

3.7.4 Modelling of Column Type C6: CFRP-Wrapped Split-GFRP-Confined Concrete-Steel Composite

The FRP jacket for column type C6: CFRP-Wrapped Split-GFRP-Confined Concrete-Steel Composite column is not uniform. It includes an inner two plies of GFRP which is split across the cross-section into two halves. It also has an outer two and a half plies of continuous CFRP. The jacket stiffness changes at different locations around the circumference of the cross-section due to these changes in composition around the jacket cross-section.

The confining pressure, σ_l , as a function of hoop strain, ε_h , can be calculated as,

$$\sigma_l(\varepsilon_h) = \frac{2E_h t \varepsilon_h}{d} \quad (3.21)$$

Equation (3.21) can be used to find the confining pressure at the strain gauge locations around the circumference. The measured hoop strain distribution is not uniform around the circumference due to the changes in jacket stiffness as was shown in Chapter 2 by Figure 2.30 (e). However, the confining pressure, which depends on jacket stiffness and hoop strain, is quite consistent around the circumference of the cross-section as is shown in Figure 3.8. The consistent confining pressure is in reasonable agreement with the confining pressure provided at the location with 2 plies

of CFRP. This implies that the split tube jacket used in column type C6 can be modelled by considering the jacket stiffness and ultimate hoop strain from the 2 ply CFRP location in the cross-section.

Owing to the cross-section of column type C6, the only strain gauge with 2 plies of CFRP was the gauge near the split in the GFRP tube which was wrapped with 2 plies of CFRP. The average of the strains recorded at this location was $10,202 \mu\epsilon$, which corresponds to an FRP efficiency factor of $\Omega_{frp} = 80.5\%$. The plot in Figure 3.9 compares the unconfined concrete response, the assumed elastic-perfectly plastic steel response, the Teng et al. (2009) confined concrete response, the Teng et al. (2009) confined concrete + elastic-perfectly plastic steel response, and the experimental response curve of column type C6. The concrete and steel response curves are each taken as the material response acting over the appropriate material cross-sectional area from column type C6. As can be observed from Figure 3.9, there is significant deviation between the Teng et al. (2009) confined concrete + elastic-perfectly plastic steel response curve and the experimental response curve. The model does not reach the same ultimate axial strain and the entire model response is below the experimental response. However, if the FRP efficiency factor is increased to $\Omega_{frp} = 83.9\%$ the axial strain matches the experimental value. This minor difference can be attributed to the strain gauge at the 2 ply GFRP split region being located slightly off the split and thus recording a lower strain

value. However, even if the FRP efficiency factor is increased, the model response is still significantly less than the experimental response curve for this column type. In addition, the stiffness of the linear second portion of the response is observed to be 13% lower in the model response compared to the experimental response. It is postulated that the response predicted by the model is overly conservative since it ignores the contribution of the split GFRP tube elements.

3.7.4.1 Increased Jacket Stiffness Effects

Although the confining pressure is consistent around the circumference of the column, the jacket stiffness varies considerably. It was reported by Fam and Rizkalla (2001) that the confinement effectiveness of an FRP jacket increases with increased jacket stiffness. They found that the ultimate axial strain does not change significantly but the confined concrete strength and the stiffness of the second linear portion of the response curve both increase with greater jacket stiffness. In the current modelling of column type C6, the model response curve underestimates the experimental curve for the entire response. This is in part due to the fact that the Teng et al. (2009) model only considers the stiffness from the 2 plies of CFRP and neglects the effects of the GFRP split tube. Including the effect of the GFRP will increase the confinement stiffness ratio, which will lead to a higher confined concrete strength and increased stiffness in the second portion of the response curve.

The design-orientated model cannot incorporate the additional jacket stiffness in a straight forward manner due to the simplistic nature of the model. As a result, a more detailed analysis-orientated model is required to implement the increased jacket stiffness effects.

3.7.5 Comparison of All Design-Orientated Model Responses

A comparison of the experimental and design-orientated model response curves for column types C2, C4, and C6 is presented in Figure 3.10. The model for column type C2 can be seen to nearly fit within the lower standard deviation bars of the experimental curve. The model for column type C4 underestimates the experimental response. The model for column type C6 greatly underestimates the response for the entire curve due to the increased jacket stiffness being ignored as discussed in the previous section.

3.8 Analysis-Orientated Model

An active confinement model is described in literature as a confinement model in which the concrete core is confined by a constant and uniform confining pressure exerted by the confining material. The most popular active confinement model is that by Mander et. al. (1988) which was introduced for reinforced concrete subjected to uniaxial compressive loading. The model assumes the confining pressure offered by the

transverse reinforcement is constant and equal to the yield strength of the reinforcing bars.

In contrast, a passive confinement model is described in literature as a confinement model in which the confining pressure exerted by the confining material on the concrete core is dependent on the lateral expansion of the concrete core. The lateral expansion of the concrete core starts at zero and increases as additional load is applied. Likewise, the confining pressure starts at zero and increases until the maximum confining pressure of the confining material is reached. A passive confinement model requires several relationships: 1) The relationship between the axial strain of the concrete core and the hoop strain of the confining material. 2) The relationship for the confining material between hoop strain and confining pressure. 3) The effect of the confining pressure on the relationship between axial stress and axial strain of the concrete core. The first relationship is an integral part of every passive confinement model and varies between different models. The second relationship can be worked out by statics and is consistent among different models. The majority of analysis-orientated models develop the third relationship by using multiple active confinement models, each at different confining pressures.

The passive confinement model response curve is then constructed through an incremental iterative process with the following steps. 1) The hoop strain is selected. 2) The confining pressure is found for this particular hoop strain. 3) The axial strain of the concrete core is determined for this particular hoop strain. 4) The axial concrete stress is determined for this axial concrete strain using an active confinement model at the confining pressure determined in the second step of this process. The particular location of the axial concrete stress – axial concrete strain from the active confinement model curve is also a point on the passive confinement model curve. The hoop strain is then incremented and the procedure is repeated to form a family of active confinement model curves each at a unique confining pressure. The passive confinement model curve is then generated by passing through the family of active confinement model curves as shown in Figure 3.11 using the properties of column type C2.

There are several analysis-orientated models available in the literature. A recent study by Marques and Chastre, (2012) which compared the performance of nine FRP-confined concrete models, reported that the model by Chastre and Silva (2010) gave the best predictions overall. However, this model with the suggested parameters was not found to be a good fit for the experimental response curves in the current study. A recent MSc thesis by Hu (2011) reviewed eight analysis-orientated models

and reported that the model by Teng et al. (2007) provided the most accurate predictions of peak axial stress and the best lateral to axial strain relationship. They also indicated that the model by Teng et al. (2007) allows for easy modification of the confining materials which is beneficial in order to include the effects of column type C6: CFRP-Wrapped Split-GFRP-Confined Concrete-Steel Composite column. The analysis-orientated model by Teng et al. (2007), as revised by Jiang and Teng (2007), is selected for this study. It should be noted that they are the authors of the design-orientated model that was employed in the previous design-orientated model section.

3.8.1 Analysis-Orientated Model Framework

The model depends on the relationship between axial strain, ε_c , and hoop strain, ε_h . This relationship is given as,

$$\frac{\varepsilon_c}{\varepsilon_{co}} = A \left(1 + \frac{16E_h t \varepsilon_h}{d f'_c} \right) \left\{ \left[1 + B \left(\frac{\varepsilon_h}{\varepsilon_{co}} \right) \right]^C - e^{-D \left(\frac{\varepsilon_h}{\varepsilon_{co}} \right)} \right\} \quad (3.22)$$

where the constants A, B, C, and D are 0.85, 0.75, 0.7 and 7, respectively

The confining pressure provided by the FRP jacket for a particular hoop strain is,

$$\sigma_l(\varepsilon_h) = \frac{2E_h t \varepsilon_h}{d} \quad (3.23)$$

where σ_l is the confining pressure due to hoop strain ε_h .

The peak axial stress in the active confinement model, f_{cc}^* , is given as,

$$\frac{f_{cc}^*}{f'_c} = 1 + k_1 \frac{\sigma_l}{f'_c} \quad (3.24)$$

where $k_1 = 3.5$. Jiang and Teng (2009) note that although this value was determined from FRP-confined concrete, it provides accurate predictions for the active confinement model. The axial strain at peak axial stress in the active confinement model, ε_{cc}^* , is given by,

$$\frac{\varepsilon_{cc}^*}{\varepsilon_{co}} = 1 + 17.5 \left(\frac{\sigma_l}{f'_c} \right)^\alpha \quad (3.25)$$

The original analysis-orientated model by Teng et al. (2007) had a value of $\alpha = 1.0$ which was replaced with a value of $\alpha = 1.2$ in the revised model by Jiang and Teng (2007). The updated value of $\alpha = 1.2$ from the revised model is utilized in the current study for the analysis-orientated model.

The relationship between axial stress, f_c , and axial strain, ε_c , for the active confinement model concrete is given as,

$$\frac{f_c}{f_{cc}^*} = \frac{(\varepsilon_c/\varepsilon_{cc}^*)^r}{r - 1 + (\varepsilon_c/\varepsilon_{cc}^*)^r} \quad (3.26)$$

where the constant r accounts for the brittleness of concrete and is defined as,

$$r = \frac{E_c}{E_c - f'_{cc} / \varepsilon_{cc}^*} \quad (3.27)$$

A hoop strain value, ε_h , can be specified from which the axial strain, ε_c , and the confining pressure, σ_l , can be found with Equations (3.22) and (3.23), respectively. Then the axial stress can be found from Equation (3.26) by using the definitions for f'_{cc} and ε_{cc}^* from Equations (3.24) and (3.25), respectively. This procedure is presented in a flowchart in Figure 3.12.

A range of hoop strains can be specified to give the complete stress-axial strain and stress-hoop strain response curves. The final hoop strain can be specified as the FRP jacket rupture hoop strain to provide the ultimate point on the stress-strain response curves.

3.8.2 Modelling of Column Type C2: CFRP-Confined Concrete

Column type C2 was modelled with a 2 ply CFRP jacket. The experimental hoop strain measurements were only considered from the two strain gauges located outside the FRP overlap region. The strain in the overlap region was lower due to increased jacket stiffness and the model response does not accurately fit this data. Figure 3.13 presents the experimental axial-hoop strain relationship compared to that given by Equation (3.22). The equation accurately describes this relationship. The FRP efficiency factor determined from the non-overlap region of the jacket

was $\Omega_{frp} = 79.0\%$ and this value is used to determine the ultimate hoop strain for the model. The experimental versus the model response for column type C2 is shown in Figure 3.14. The model is in excellent agreement with the experimental response for both axial and hoop strain.

3.8.3 Modelling of Column Type C4: CFRP-Confined Concrete-Steel Composite

The confined concrete response for column type C4 was modelled with a 2 ply CFRP jacket. The complete column response is calculated in Equation (3.1) by summing the contribution of the confined concrete and the encased steel. The experimental hoop strain measurements were only considered from the two strain gauges located outside the FRP overlap region. Figure 3.15 presents the experimental axial-hoop strain relationship compared to that given by Equation (3.22). The equation accurately describes this relationship. The FRP efficiency factor determined from the non-overlap region of the jacket was $\Omega_{frp} = 60.8\%$ and this value is used to determine the ultimate hoop strain for the model response. The experimental versus the model response for column type C4 is shown in Figure 3.16. The model is in excellent agreement with the experimental response for both axial and hoop strain.

3.8.4 Modelling of Column Type C6: CFRP-Wrapped Split-GFRP-Confined Concrete-Steel Composite

The confined concrete response for column type C6 was first modelled with a 2 ply CFRP jacket to represent the strength of the weakest point on the cross-section of the FRP jacket. The complete column response is calculated in Equation (3.1) by summing the contribution of the confined concrete and the encased steel. The experimental hoop strain measurements were only considered from the one strain gauge located near the split in the GFRP tube, which was wrapped with 2 plies of CFRP. Figure 3.17 presents the experimental axial-hoop strain relationship compared to that given by Equation (3.22). The equation accurately describes this relationship. The FRP efficiency factor determined from the 2 ply CFRP region of the jacket was $\Omega_{frp} = 80.5\%$ and this value is used to determine the ultimate hoop strain for the model response. The experimental response versus the model response for column type C6 is shown in Figure 3.18. The analytical model significantly underestimates the entire load versus strain response curve.

Figure 3.19 (a) presents a comparison of the experimental axial-hoop strain relationships for column types C2, C4, and C6 with hoop strains averaged from the 2 ply CFRP regions around the jacket. All three column types have similar relationships which were shown to match the modelled relationships closely in Figure 3.13, Figure 3.15, and Figure 3.17. Figure

3.19 (b) presents a comparison of the experimental axial-hoop strain relationships for column types C2, C4, and C6 with hoop strains averaged from all strain gauges around the jacket. It can be noted from this figure that the relationship for column types C2 and C4 are in close agreement and that for any significant axial strain value, the hoop strain value for column type C6 is below that of column types C2 and C4. This demonstrates the additional stiffness of the CFRP-Wrapped Split-GFRP jacket. The added stiffness is not being considered in the analytical model, which is expected to lead to a difference between the model and experimental response curves for column type C6 as was observed in Figure 3.18.

3.8.4.1 Modified Model to Include Increased Stiffness of Hybrid Jacket

The added stiffness of the CFRP-Wrapped Split-GFRP jacket is accounted for by considering two locations on the FRP jacket. One location is the split in the GFRP tube where the FRP jacket consists of 2 plies of CFRP. This location is referred to as the 2 ply CFRP location. The other location is at a distance away from the split in the GFRP tube where the FRP jacket is comprised of 2 plies of CFRP plus 2 plies of GFRP. This location is referred to as the hybrid jacket location. The two locations are shown in Figure 3.20.

The jacket stiffness appears in the expression for the confining pressure, Equation (3.23), as E_{ht} . The definition is updated to include the jacket stiffness contribution from the 2 plies of GFRP in the hybrid jacket location and is expressed as $E_{CFRP}t_{CFRP} + E_{GFRP}t_{GFRP}$. This results in a 47.5% increase in jacket stiffness. The jacket stiffness also appears in the relationship between axial and hoop strain as given in Equation (3.22). Figure 3.21 presents a comparison of the experimental and modelled axial-hoop strain relationships for the jackets comprised of 2 ply CFRP and 2 ply CFRP + 2 ply GFRP. It is clear that the model can be extended to accurately describe the axial-hoop strain relationship for the column specimen considering the increased stiffness from the GFRP. It is also clear that the hoop strain for the hybrid jacket location is always less than the hoop strain for the 2 ply CFRP location for any particular axial strain. A relationship between the hoop stress of the hybrid jacket location and the 2 ply CFRP location is required in order to describe the complete response of the split tube jacket specimens.

For the same axial strain, the hoop strain of the hybrid jacket location is less than that of the 2 ply CFRP location, at all levels of axial strain. A factor, β , is proposed to account for the lower hoop strain at rupture due to the increased jacket stiffness. This factor is expressed as,

$$\beta = \varepsilon_{h,rupt,Hybrid} / \varepsilon_{h,rupt,CFRP} = \Omega_{Hybrid} / \Omega_{CFRP} \quad (3.28)$$

where Ω_{Hybrid} and Ω_{CFRP} are the FRP efficiency factors for the hybrid jacket location and the 2 ply CFRP location, respectively, and $\varepsilon_{h,rupt,CFRP}$ and $\varepsilon_{h,rupt,Hybrid}$ are the maximum hoop strains at rupture for the 2 ply CFRP location and the hybrid jacket location, respectively. This factor is determined from experimental hoop strain measurements as $\beta = 77.4\%$ for the hybrid jacket location comprised of 2 plies of CFRP plus 2 plies of GFRP compared to the 2 ply CFRP location.

3.8.4.1.1 *Confining Pressure Approach to Determine β factor*

A theoretical approach is used to predict an appropriate value for β . It is assumed that the confining pressure is consistent around the hybrid FRP jacket. The confining pressure distribution around the hybrid jacket was shown in Figure 3.8 to be consistent even though the jacket cross-section changed considerably. Using this assumption and equating the confining pressure at the 2 ply CFRP location to the confining pressure at the hybrid location, a relationship for β can be derived as follows,

$$\beta = \frac{E_{CFRP} t_{CFRP}}{E_{CFRP} t_{CFRP} + E_{GFRP} t_{GFRP}} \quad (3.29)$$

This expression gives a value of $\beta = 67.5\%$ which is lower than the experimentally determined value of $\beta = 77.4\%$. Although the confining

pressure is fairly uniform around the jacket, there are some discrepancies that can lead to the poor prediction of the β factor. In addition, this approach assumes that the strain is consistent across the thickness of the jacket which may not necessarily be the case. This technique was not found to provide an adequate means to predict the β factor.

3.8.4.1.2 Proposed Approach to Determine β Factor

The relationship between axial and hoop strain, given by Equation (3.22), was found in Figure 3.21 to fit the experimental strain measurement relationship closely for both the 2 ply CFRP location and the hybrid location comprised of 2 ply CFRP and 2 ply GFRP. If this expression is equated for the two jacket locations at a particular axial strain, the hybrid jacket will have a lower hoop strain than the 2 ply CFRP jacket. Equating these two expressions at the ultimate axial strain value leads to the proposed relationship,

$$\begin{aligned}
 & \left(1 + \frac{16E_{CFRP}t_{CFRP}\varepsilon_{h,rupt,CFRP}}{d f'_c} \right) \\
 & \left\{ \left[1 + B \left(\frac{\varepsilon_{h,rupt,CFRP}}{\varepsilon_{co}} \right) \right]^C - e^{-D \left(\frac{\varepsilon_{h,rupt,CFRP}}{\varepsilon_{co}} \right)} \right\} \\
 & = \left(1 + \frac{16E_{Hybrid}t_{Hybrid}\beta\varepsilon_{h,rupt,CFRP}}{d f'_c} \right) \tag{3.30} \\
 & \left\{ \left[1 + B \left(\frac{\beta\varepsilon_{h,rupt,CFRP}}{\varepsilon_{co}} \right) \right]^C - e^{-D \left(\frac{\beta\varepsilon_{h,rupt,CFRP}}{\varepsilon_{co}} \right)} \right\}
 \end{aligned}$$

This expression can be solved for the β factor after substituting in all of the known parameters for a particular CFRP-wrapped split-GFRP jacket. Figure 3.22 shows the influence of the number of plies of GFRP on the factor β based on the proposed expression. The β factor is 100% when there are no plies of GFRP and decreases with an increase in the number of plies of GFRP.

This relationship can be utilized to find the β factor for the 2 ply CFRP location and the hybrid location comprised of 2 plies of CFRP and 2 plies of GFRP as $\beta = 78.2\%$. This is 1.0% higher than the experimentally determined factor, which is suitably close and as such this relationship is utilized to determine the β factor for the analysis-orientated modelling.

This relationship inherently ensures that the same ultimate axial strain is reached regardless of the increased stiffness of the jacket since the

relationship is developed by equating the ultimate axial strain. Figure 3.19 (a) indicates that the axial-hoop strain relationship at the 2 ply CFRP location is in agreement for column types C2, C4, and C6. Since failure consistently occurs in the 2 ply CFRP location on column type C6, the ultimate axial strain is not affected by the increased stiffness provided by the 2 GFRP plies. The hybrid locations of the tube will reach the hoop strain dictated by the β factor simultaneous with the 2 ply CFRP location reaching the CFRP hoop rupture strain. This is consistent with the fact that an increase in the number of GFRP plies does not affect the ultimate strain of the weak point in the cross-section. This can be seen from the 2 ply CFRP location in column type C6 reaching an FRP efficiency factor of $\Omega_{frp} = 80.5\%$ which is only 1.9% higher than the FRP efficiency factor of $\Omega_{frp} = 79.0\%$ reached by the 2 ply CFRP jacket in column type C2.

3.8.4.1.3 Incorporating the Influence of Jacket Stiffness into the Analysis Orientated Model

The FRP efficiency factor determined from the hybrid location comprised of 2 plies of CFRP and 2 plies of GFRP was experimentally determined as $\Omega_{Hybrid} = 61.8\%$. Using the calculated factor of $\beta = 78.2\%$ and the experimentally determined FRP efficiency factor of the 2 ply CFRP location of $\Omega_{CFRP} = 80.5\%$, the predicted FRP efficiency factor is $\Omega_{Hybrid} = 63.0\%$ which is 1.8% greater than the experimentally determined value. The experimental versus analysis-orientated model response curve is

shown in Figure 3.23 for an FRP efficiency factor of $\Omega_{\text{Hybrid}} = 63.0\%$. The experimental and analysis-orientated model hoop strains are both taken from the hybrid location. The analysis-orientated model underestimates the entire response, however the results are in better agreement than when the model neglects the influence of increased jacket stiffness.

3.8.5 Comparison of All Analysis-Orientated Model Responses

A comparison of the experimental and analysis-orientated model responses for column types C2, C4, and C6 is presented in Figure 3.24. The model for column type C2 fits well within the standard deviation bars of the experimental curve. The model for column type C4 also fits within the standard deviation bars of the experimental response curve for much of the response. The model for column type C6 underestimates the response for the entire curve.

3.9 Conclusion

The load-strain responses of column types C2, C4, and C6 are investigated through the use of four predictive models. Two design-orientated models are examined: the first is a popular model by Lam and Teng (2003) and the second is a revised version of this model by Teng et al. (2009). The revised model provides a better definition for ultimate axial strain for heavily confined FRP jackets, which results in an improved fit to the experimental response compared to the original model. The revised

design-orientated model is able to predict the response adequately for column types C2 and C4. However, it significantly under predicts the response of column type C6 due to the increased thickness of the CFRP-wrapped split-GFRP jacket. Summing the contributions of the composite column components using strain compatibility is found to accurately predict the response of column type C4.

Two analysis-orientated models are also examined in order to implement the effects of the increased jacket stiffness of column type C6. They include a model by Teng et al. (2007) and a revision to this model by Jiang and Teng (2007). The revised model includes an updated expression for ultimate axial strain in the active confinement model. Overall the analysis-orientated model provides a much better fit to the experimental response of the column types. However, it also under predicts the response of column type C6 when the model assumes the jacket as 2 plies of CFRP. It is recognized that the hybrid jacket stiffness can be utilized in the model if an appropriate reduction to the FRP efficiency factor is made. A factor is proposed to account for the lower FRP efficiency factor and a technique to determine this factor is also introduced. The analysis-orientated model is updated to account for the additional stiffness in the split tube jacket. The modified model demonstrates significant improvement in predicting the response of column type C6 over the model which ignores the additional GFRP plies in the split tube jacket.

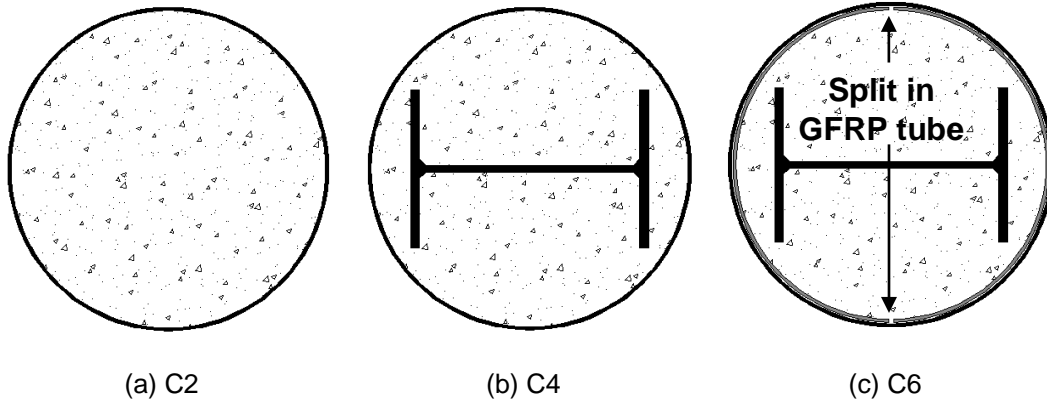


Figure 3.1: Column Types

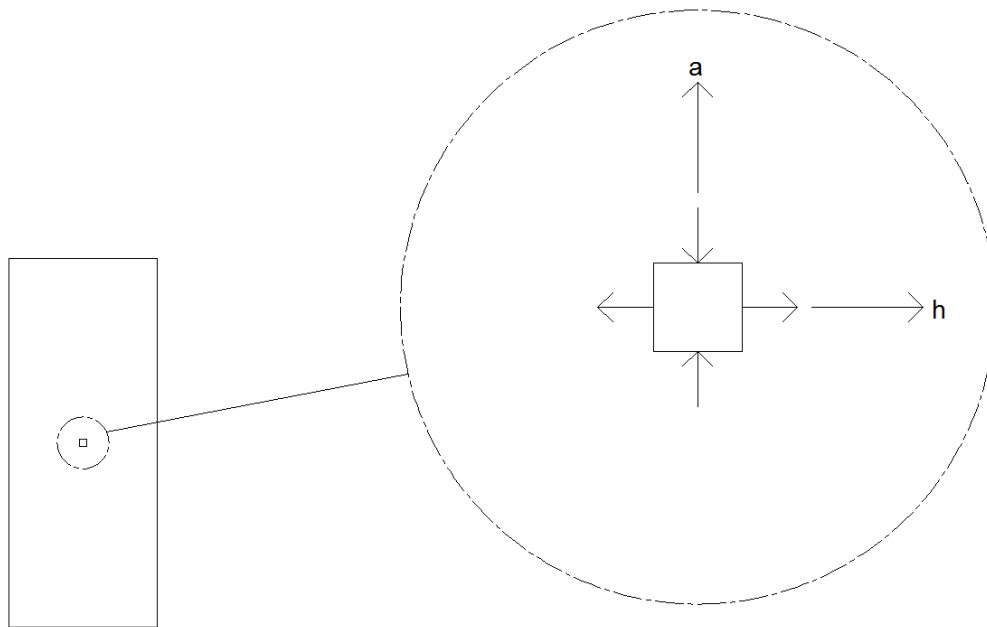


Figure 3.2: Biaxial State of Stress in CFRP Jacket

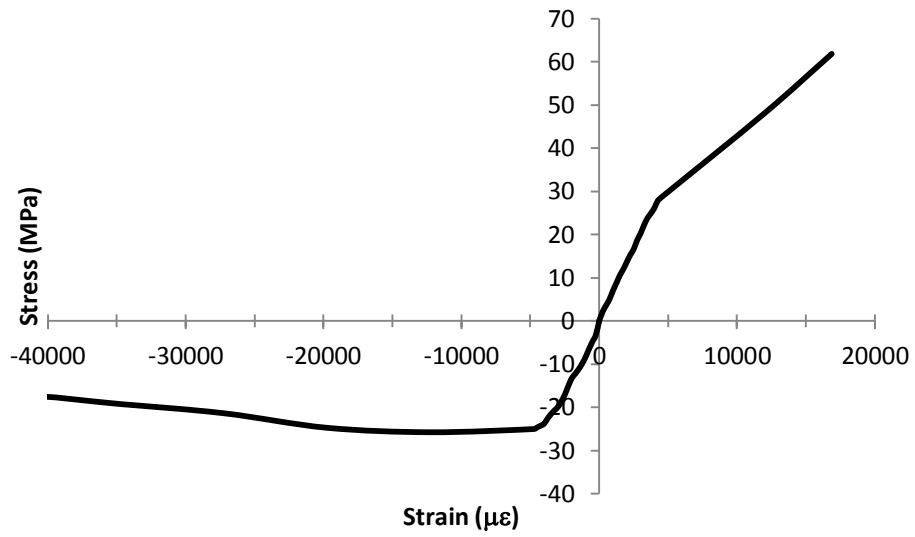


Figure 3.3: CFRP Secondary Direction Material Response Curve

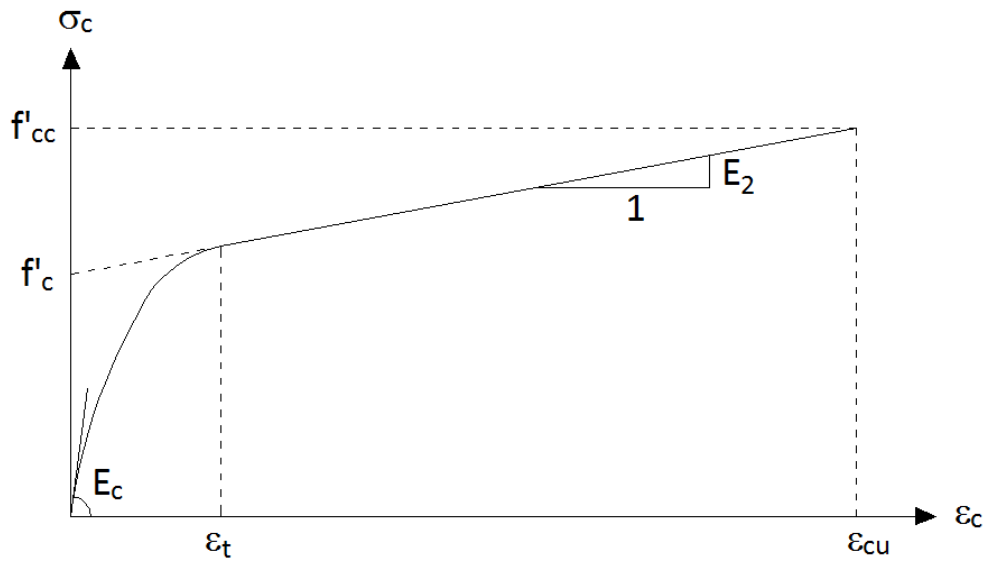


Figure 3.4: Model Framework

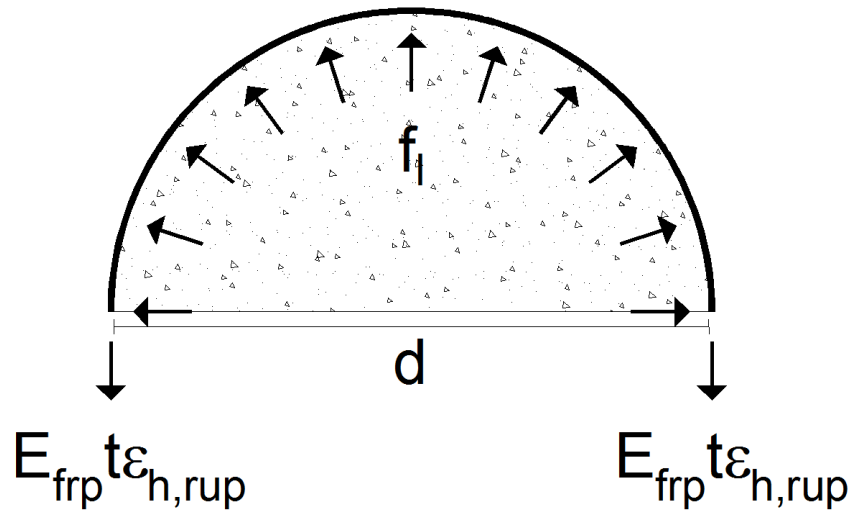


Figure 3.5: Confining Action

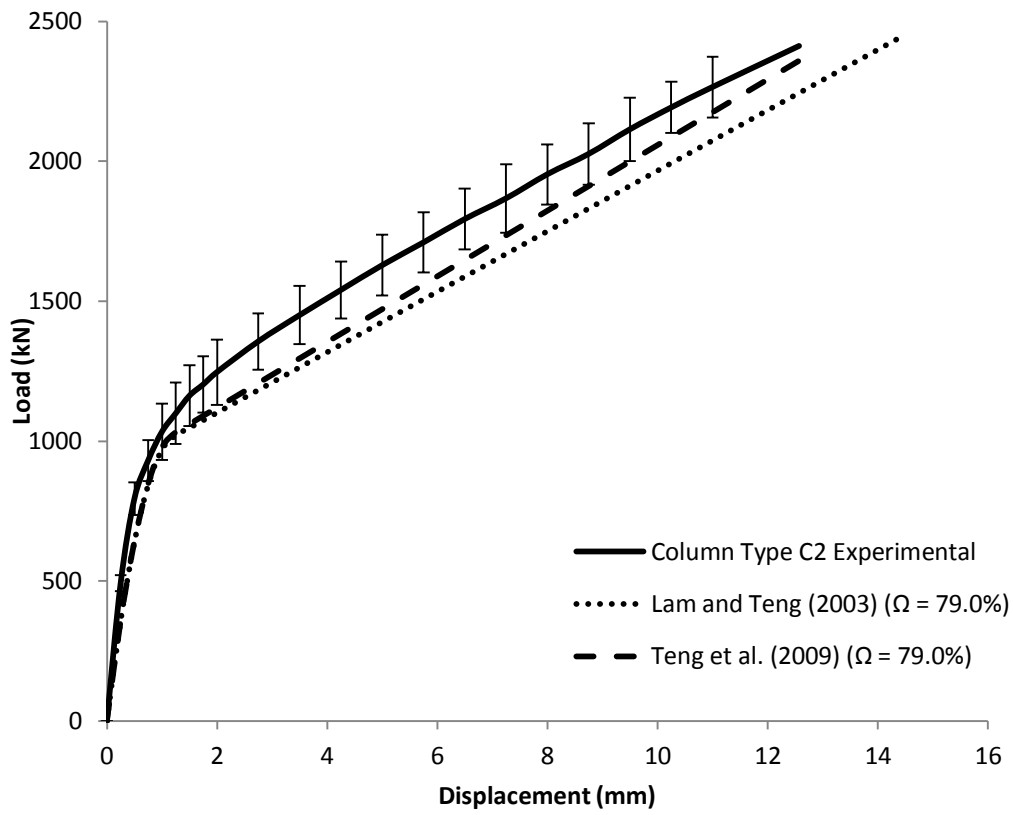


Figure 3.6: Design-Orientated Model for Column Type C2

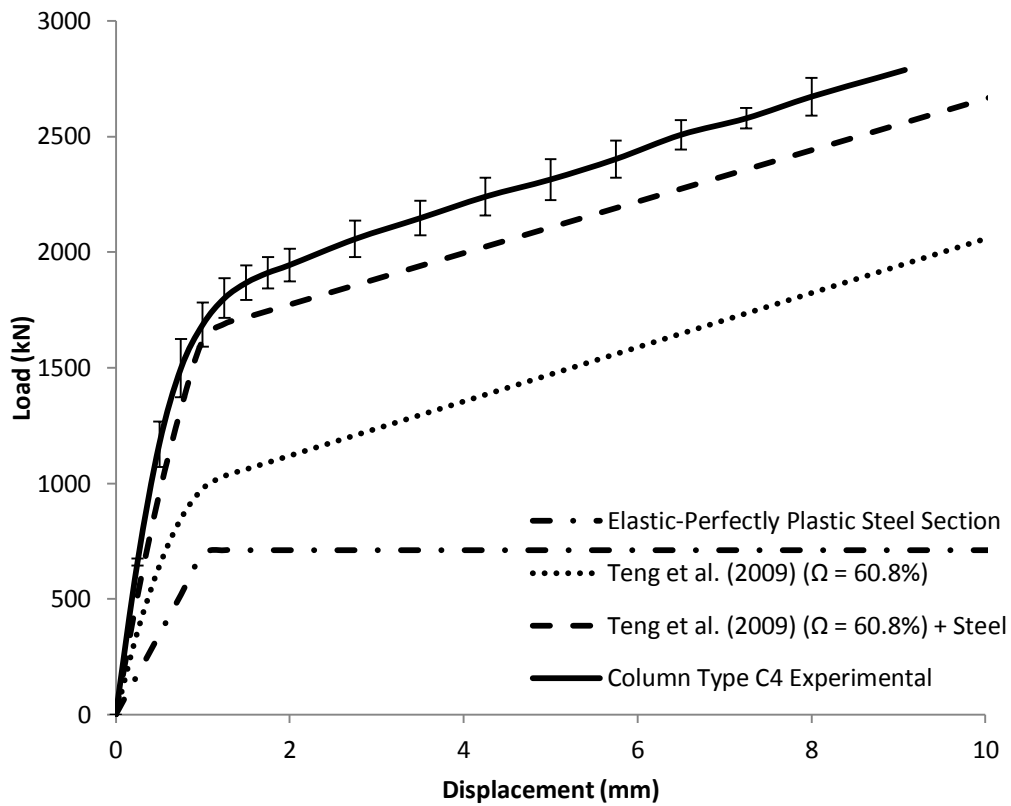
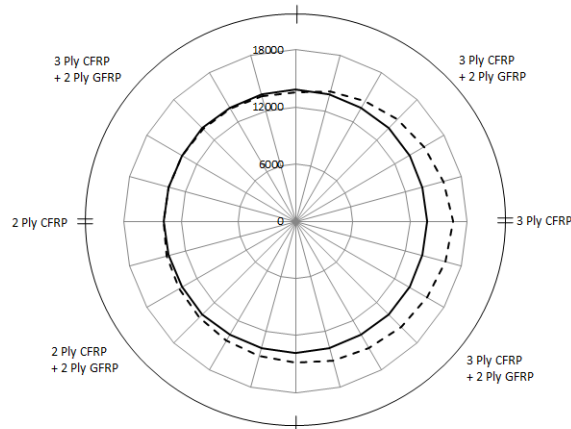
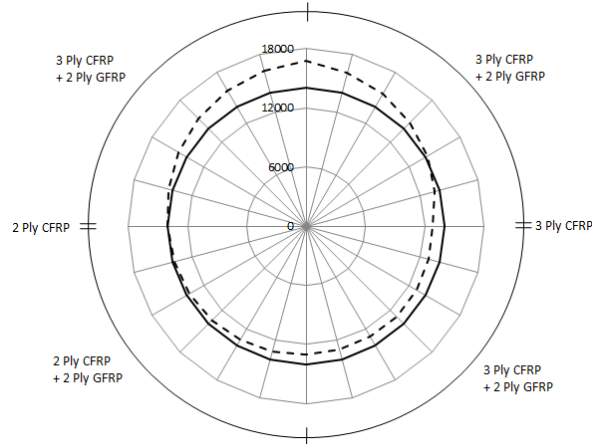


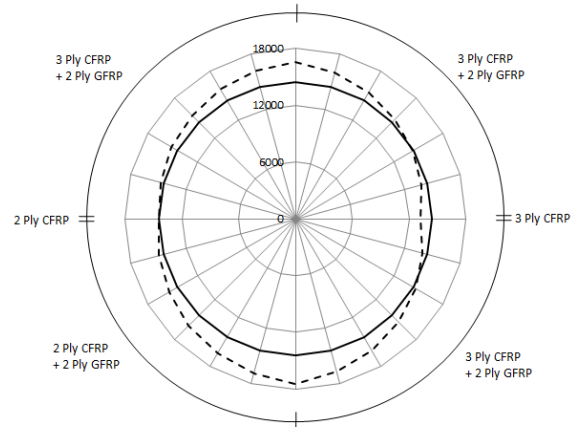
Figure 3.7: Design-Orientated Model for Column Type C4



(a) C6-1



(b) C6-2



(c) C6-3

- Confining Pressure Calculated at Each Strain Gauge
- Confining Pressure Determined from Strain Gauge at 2 Ply CFRP Location

(d) Legend

Figure 3.8: Confining Pressure Distribution around Circumference

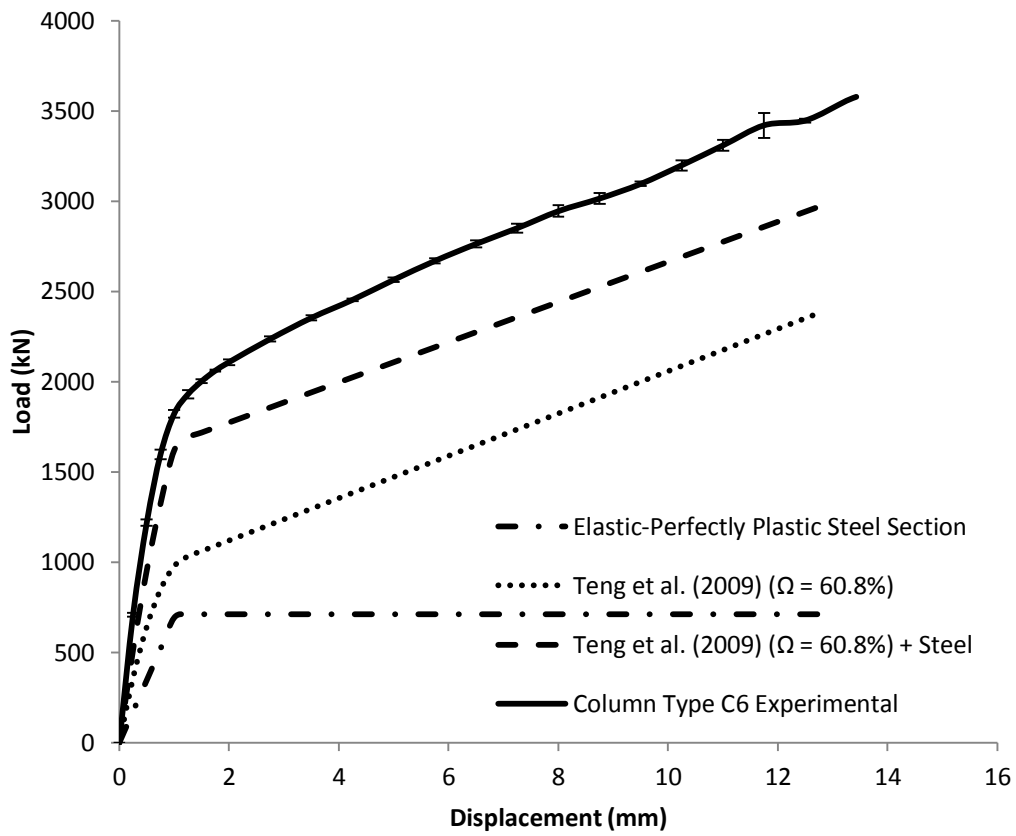


Figure 3.9: Design-Orientated Model for Column Type C6

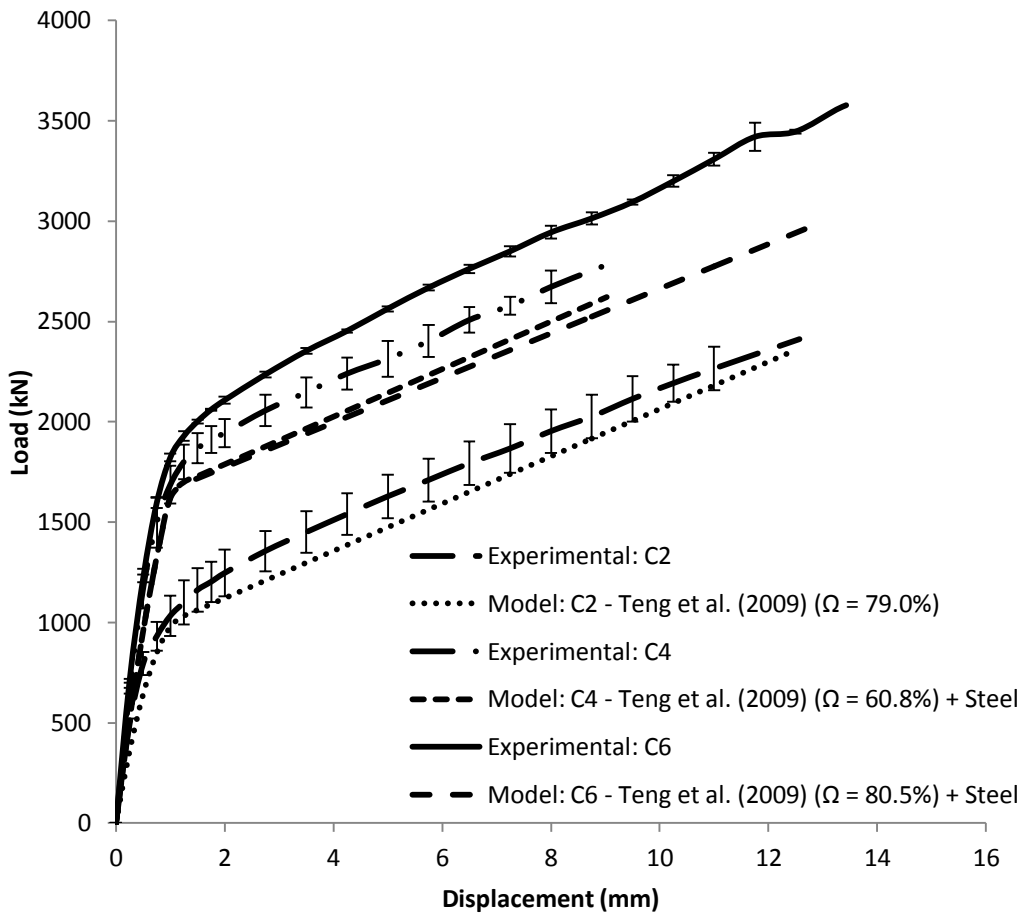


Figure 3.10: Design-Orientated Model Comparison Plot

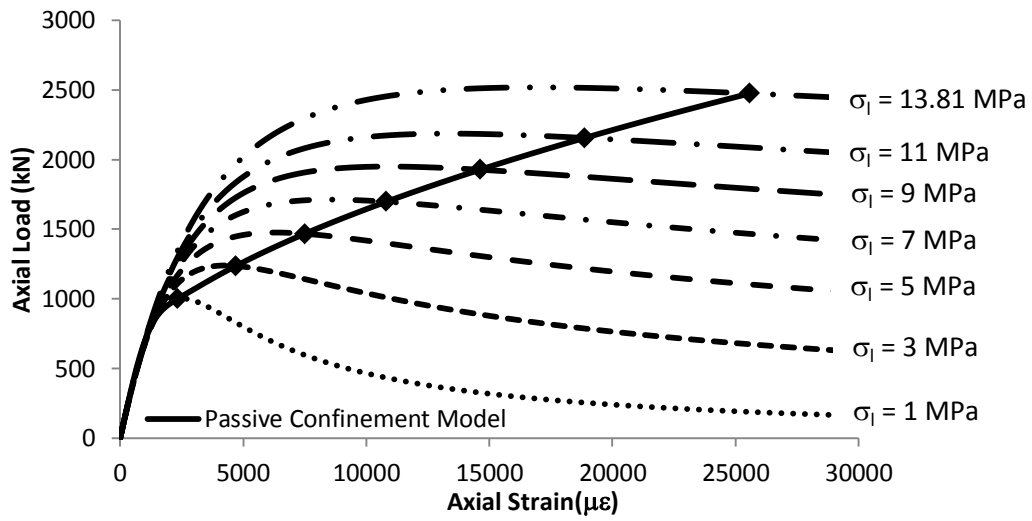


Figure 3.11: Generation of a Passive Confinement Model from a Family of Active Confinement Models with the Properties of Column Type C2

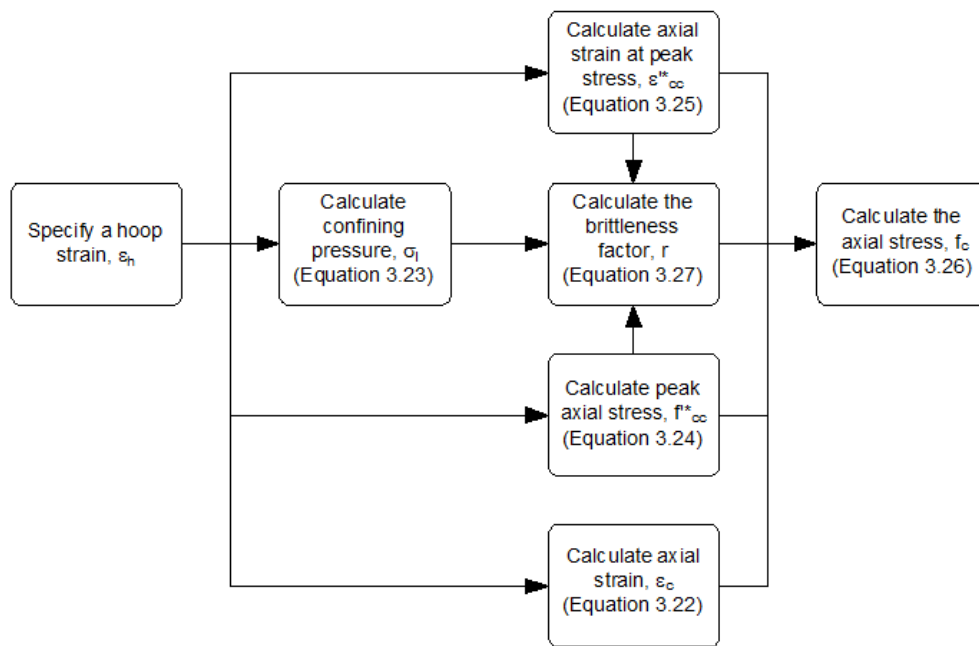


Figure 3.12: Analysis-Orientated Model Flowchart

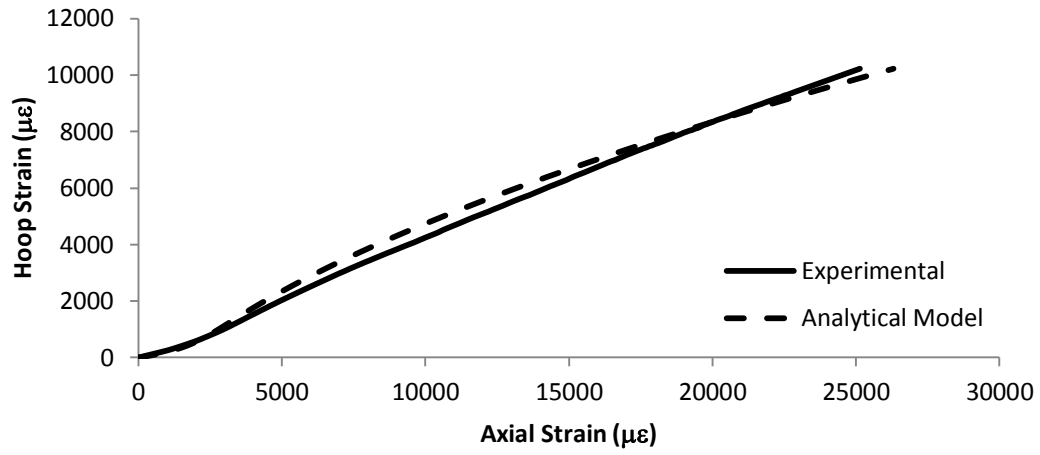


Figure 3.13: Column Type C2 Axial-Hoop Strain Relationship

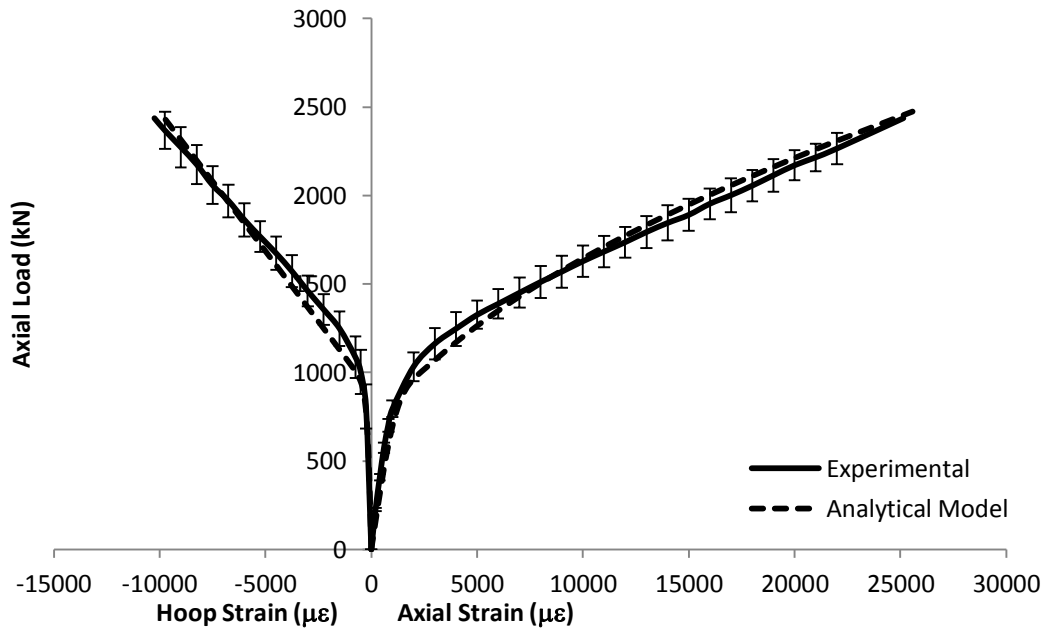


Figure 3.14: Column Type C2 Load vs. Strain Response

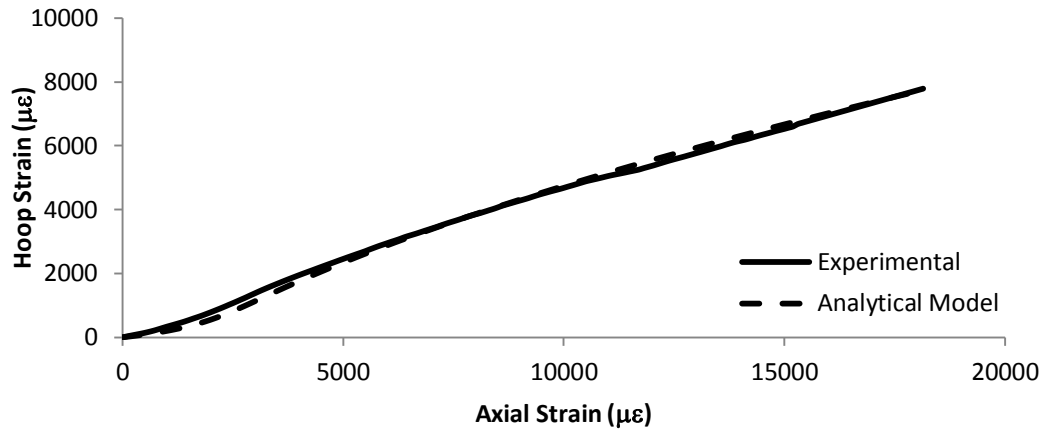


Figure 3.15: Column Type C4 Axial-Hoop Strain Relationship

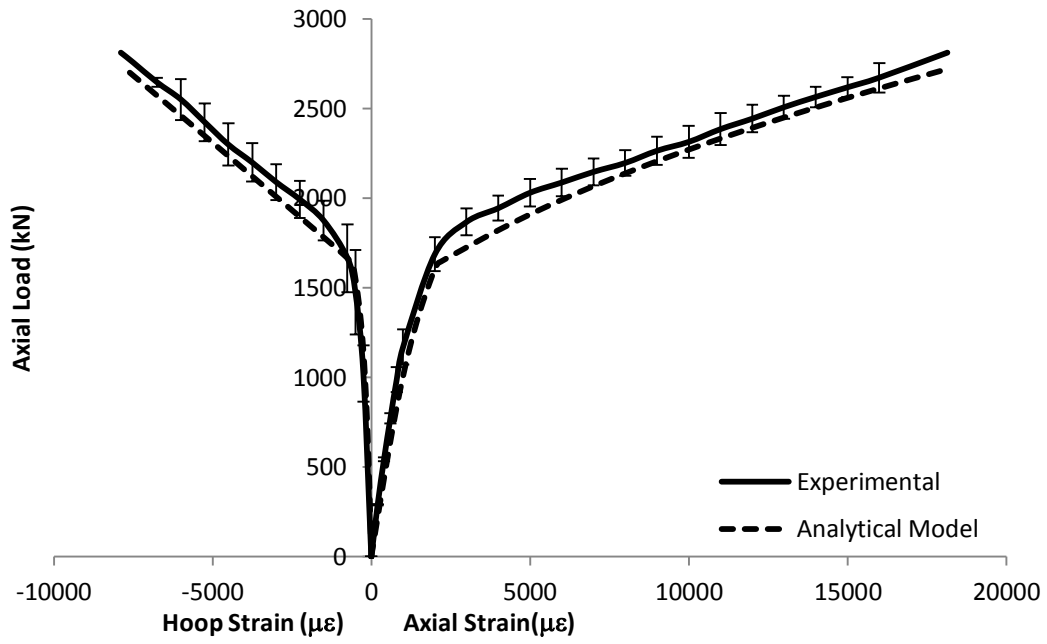


Figure 3.16: Column Type C4 Load vs. Strain Response

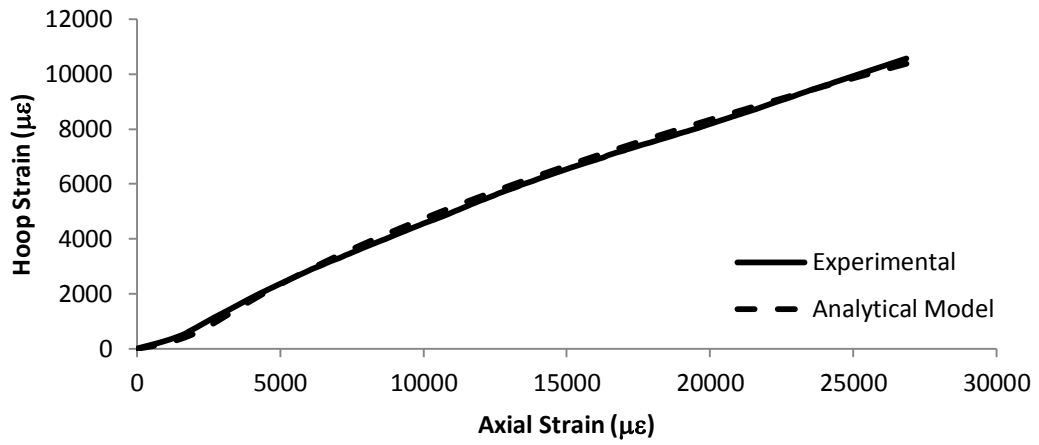


Figure 3.17: Column Type C6 Axial-Hoop Relationship for 2 Ply CFRP Jacket

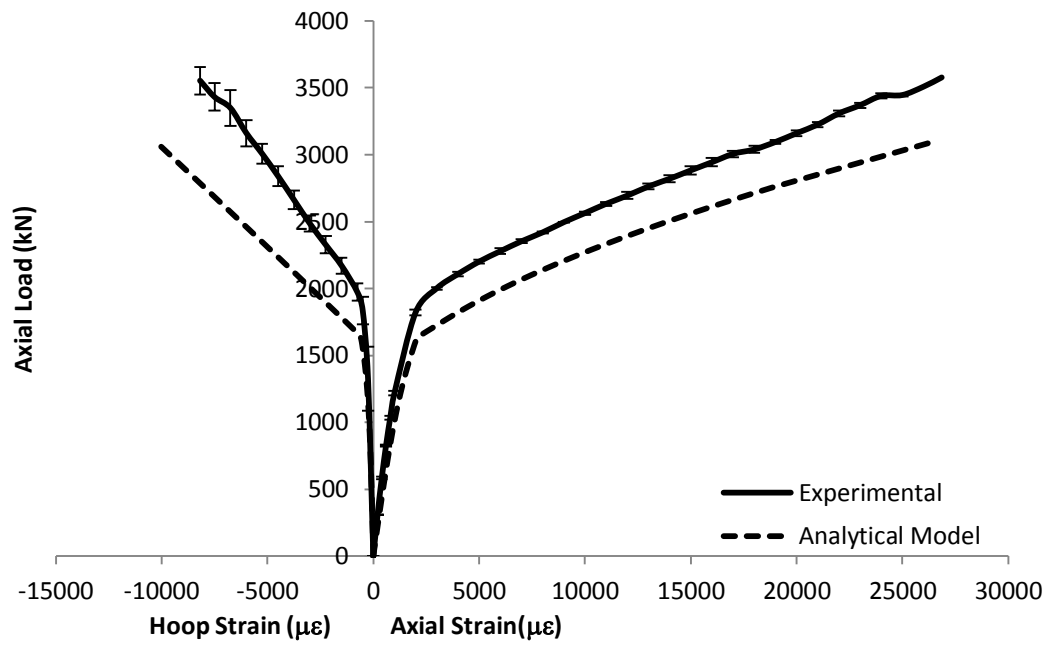
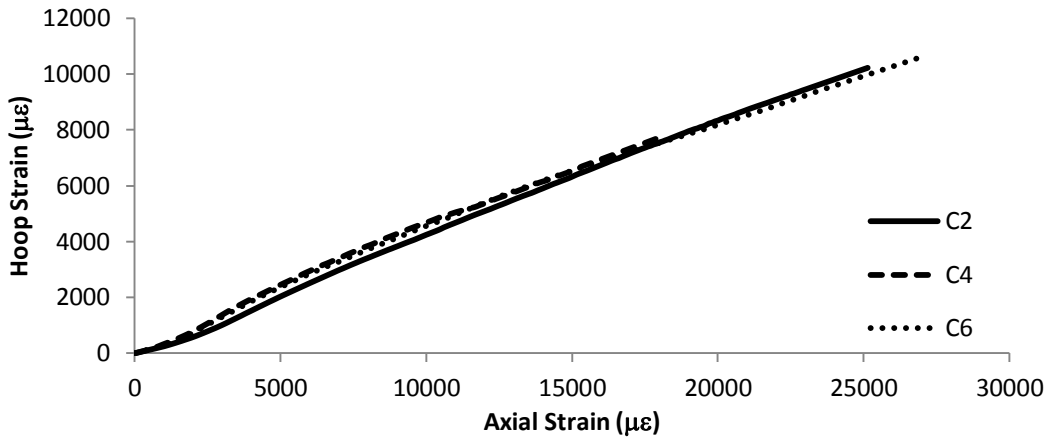
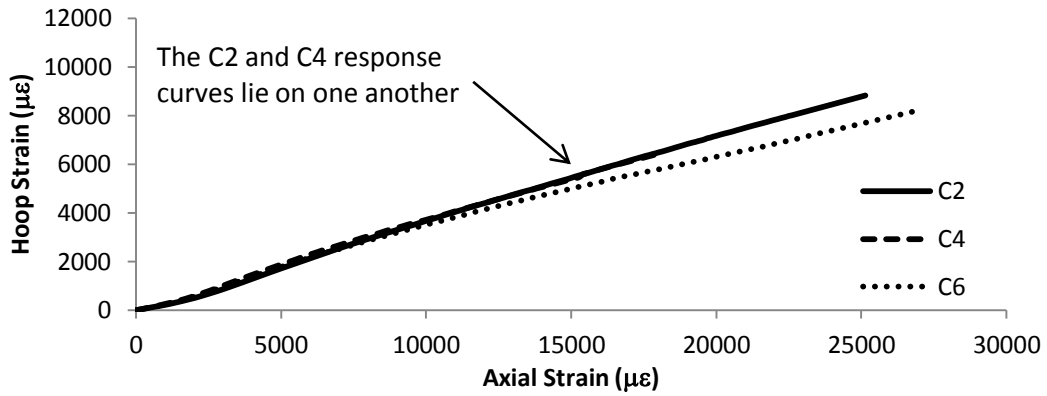


Figure 3.18: Column Type C6 Load vs. Strain Response Assuming 2 Ply CFRP Jacket



(a) Hoop Strain Averaged from only 2 Ply CFRP strain gauges



(b) Hoop Strain Averaged from all strain gauges

Figure 3.19: Comparison of Axial-Hoop Strain Relationship for Column Types C2, C4, and C6

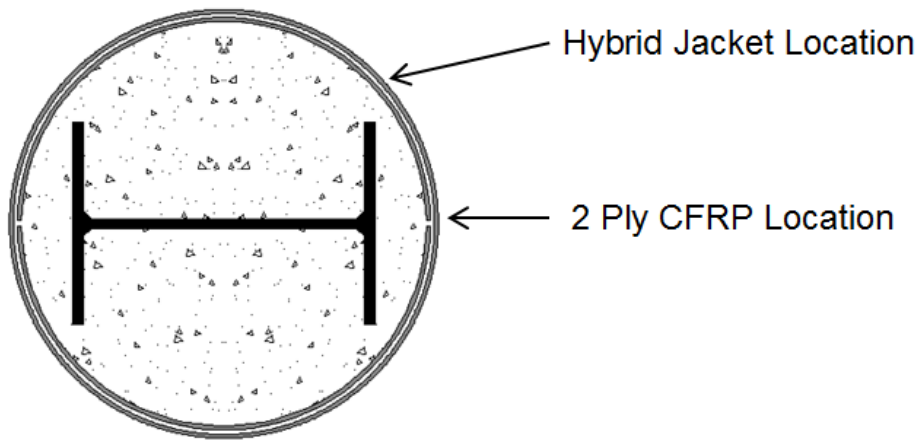


Figure 3.20: Column Type C6 Jacket Locations

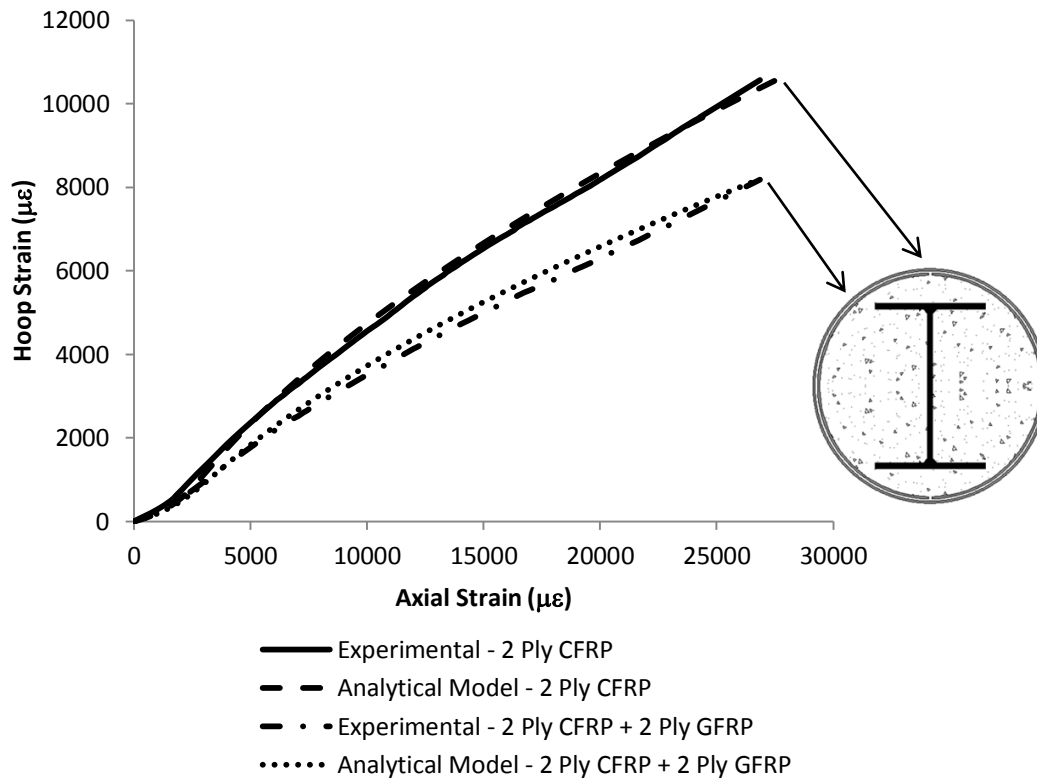


Figure 3.21: Column Type C6 Axial-Hoop Strain Relationship Comparison

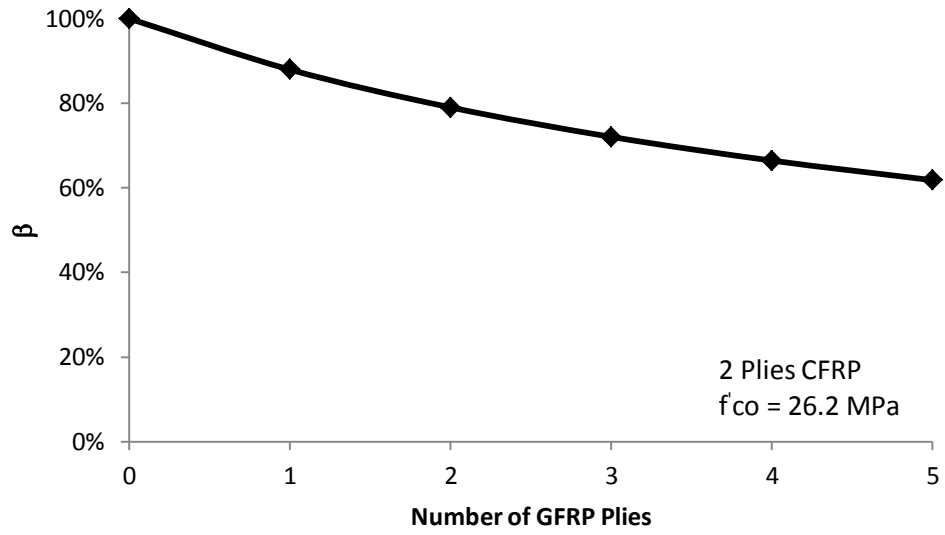


Figure 3.22: Influence of the number of GFRP Plies on the factor β

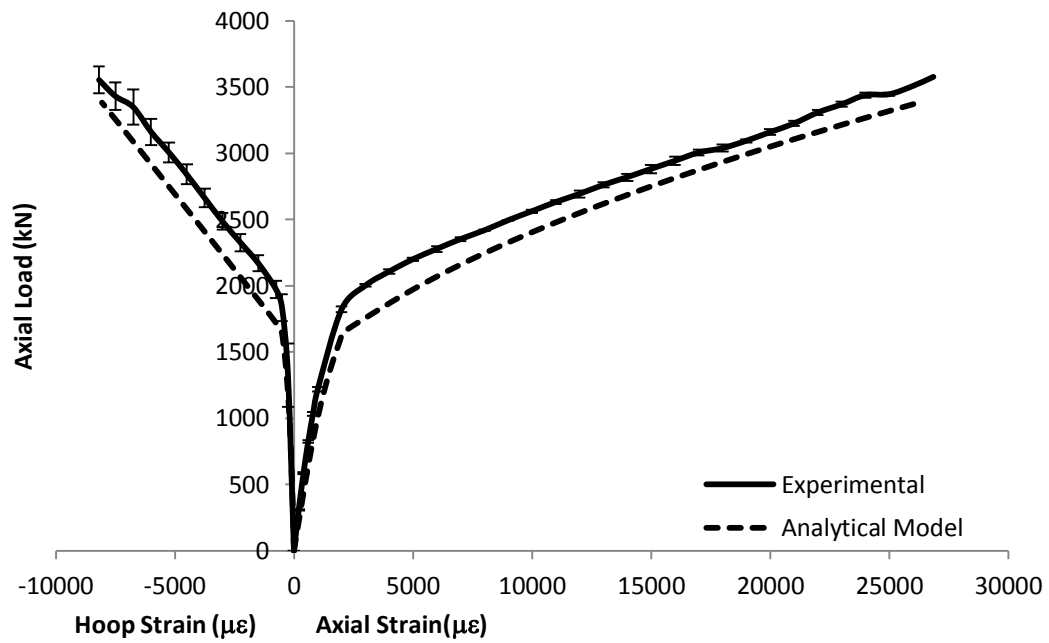


Figure 3.23: Column Type C6 Load vs. Strain Response Incorporating Increased Jacket Stiffness

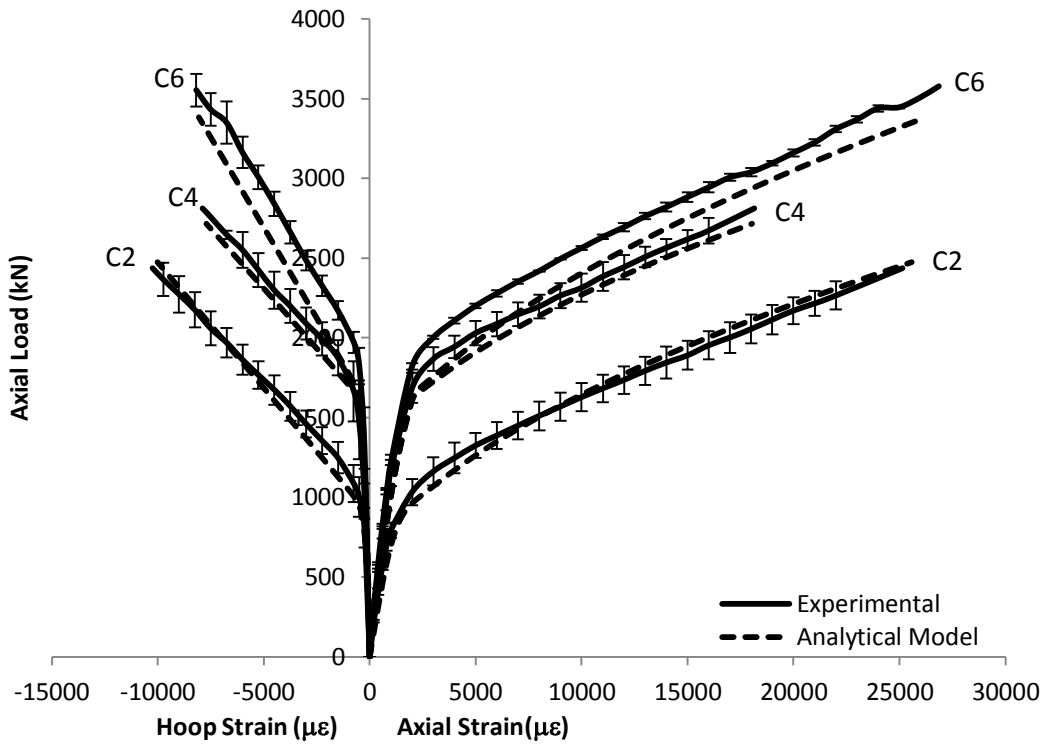


Figure 3.24: Analysis-Orientated Model Comparison

Chapter 4 - Retrofit Design

4.1 Introduction

This chapter investigates the design considerations of applying the composite column technique in a retrofit scenario. First, a parametric study investigates the influence of different parameters on the column response. Understanding the effect of different elements in the composite column aids the designer in achieving the desired response. Secondly, the experimental results are compared to code predicted values. The comparison demonstrates the suitability of current codes for use with the composite column technique.

Fam and Rizkalla (2001) proposed an analytical model to predict the response of short stub FRP-confined concrete columns under axial load. The passive confinement model is based on radial displacement compatibility and variable confinement using a stepping technique which analyzes the response at each strain increment as having constant confinement. The model is applicable for both FRP tubes filled with concrete and concrete columns wrapped with FRP. The model accounts for completely filled tubes as well as partially filled tubes with a central hole. A parametric study was performed with the model that investigated the effect of the stiffness of the FRP tube in the hoop direction, the effect of a central hole in the confined concrete cross-section, and the effect of

axially loading the FRP tube directly. As the hoop stiffness was increased, the initial portion of the axial stress versus axial strain response did not vary. The stiffness of the second portion of the response increased with an increase in hoop stiffness. The confinement effectiveness, measured as confined concrete strength divided by unconfined concrete strength, was enhanced with an increase in the hoop stiffness of the FRP tube. However, the rate of strength gain was diminished with increasing hoop stiffness. As the size of the central hole increased, the initial portion of the axial stress versus axial strain response did not vary. The stiffness of the second portion of the response decreased with an increase in the size of the central hole. The confining pressure and the confinement effectiveness decreased with an increase in the size of the central hole. The axial stress versus axial strain response curve of the confined concrete followed a similar initial trajectory with and without axial load being applied directly to the FRP tube. However, the response curve for the confined concrete that had axial load directly applied to the FRP tube reached a lower axial strain and a lower axial stress than the one which was not loaded directly.

Karimi et al. (2013) used an analytical model to predict the behaviour of FRP-confined steel-concrete composite columns classified as short, intermediate, or long. The cross-sectional behaviour of the confined concrete was adopted from the model by Lam and Teng (2003). The study

investigated the effects of the column diameter, the thickness of FRP tube, and the steel ratio. Increasing the composite column diameter reduced the confinement effectiveness which resulted in a decrease in confined concrete strength. Although the composite column capacity increased due to the increased cross-sectional area of the column, the capacity did not increase at the same rate as the increase in cross-sectional area due to the decrease in confined concrete strength. An increase in the thickness of the FRP tube resulted in an increase in the confinement effectiveness. This led to an increase in the confined concrete strength which resulted in an increase in cross-sectional capacity. It was also noted that the ultimate lateral confining pressure was proportional to the thickness of the FRP tube. The steel ratio had minimal influence on short and long composite columns. An increase in the steel ratio resulted in an increase in compressive capacity for intermediate columns; however, it also resulted in increased predicted expense due to the higher cost of steel relative to concrete. It was noted that a minimum amount of steel was recommended to satisfy ductility requirements.

The current parametric study utilizes the revised model presented in Chapter 3, which includes the stiffness contribution of the GFRP split tube elements.

4.2 Parametric Study

This chapter includes a parametric study using the revised analysis-orientated model presented in Chapter 3. This model is employed since it best predicted the response of column type C6. The properties for the column specimens are taken as those reported in Chapter 2 and Chapter 3. These properties include column diameter, CFRP and GFRP strength and stiffness, steel strength and stiffness, and unconfined concrete strength and strain. The parameters studied include the number of plies of GFRP in the split tube elements, the number of plies of CFRP wrap, the concrete strength, and the steel ratio of the composite column cross section. This study examines the influence of these parameters on the response of column type C6, CFRP-Wrapped Split-GFRP-Confined Concrete-Steel Composite column. The value of the parameter in question is varied while holding all other parameters constant at the values typical of column type C6. The effect of a parameter on a particular aspect of the column response is displayed using normalized plots. These plots are normalized to the response of the model using the properties of column type C6. These properties include a split tube comprised of 2 plies of GFRP; 2 plies of CFRP wrap; concrete strength of 26.2 MPa; and a steel ratio of 5.12%.

4.2.1 Number of Plies of GFRP in the Split Tube

The purpose of the GFRP split tube in the composite column is to provide a means of constructing an FRP jacket around an in situ steel *W* section. However, after the CFRP is wrapped around the GFRP split tube elements, the GFRP becomes an integral part of the hybrid FRP jacket. The GFRP provides additional stiffness to the majority of the circumference and in doing so it affects the column response. The effect of the number of plies of GFRP used to construct the split tube is investigated in this section. The number of plies in the CFRP wrap, the concrete strength, and the steel ratio are held constant at 2 plies, 26.2 MPa, and 5.12%, respectively. The plot in Figure 4.1 demonstrates the effect of the number of plies of GFRP on the column response. When the number of plies of GFRP is zero, the column response is that of a CFRP-confined concrete-steel composite column. An increase in the number of plies of GFRP does not affect the initial portion of the response curve as the confining action provided by the FRP has not sufficiently developed in this region of the curve. In the second portion of the response curve, an increase in the number of plies of GFRP leads to increased axial load for a given strain value. This results in an increase in the ultimate capacity as shown in Figure 4.2 (c). An increase in the number of plies of GFRP does not have an effect on the ultimate axial strain as shown in Figure 4.2 (b). This is inherently built into the model presented in Chapter 3 since it is

based on the assumption that the ultimate axial strain is constant with an increase in the number of plies in the split tube. Figure 4.2 (a) demonstrates that an increase in the number of plies of GFRP leads to a decrease in the hybrid ultimate hoop strain due to the increased jacket stiffness. The ultimate hoop strain of the jacket at the split location, which has 2 plies of CFRP, remains constant for a change in the number of plies of GFRP. Figure 4.2 (d) demonstrates that an increase in the number of plies of GFRP results in an increase in the confined concrete strength.

4.2.2 Number of Plies in the CFRP Wrap

The weak point in the hybrid FRP jacket dictates the ultimate confining pressure that the jacket can exert on the concrete core. The location of least strength in the cross-section is controlled by the number of plies of CFRP that are wrapped around the split GFRP tube in forming the hybrid FRP jacket. The number of plies of CFRP directly affects the strength of the jacket. The number of plies of the CFRP wrap also contributes to the jacket stiffness. The effect of the number of plies of CFRP used to wrap the split tube is investigated in this section. The number of plies of GFRP in the split tube, the concrete strength, and the steel ratio are held constant at 2 plies, 26.2 MPa, and 5.12%, respectively. The plot in Figure 4.3 demonstrates the effect of the number of plies in the CFRP wrap on the column response. An increase in the number of plies of CFRP does not affect the initial portion of the response curve as the confining action of

the FRP on the concrete in this region of the curve has not yet initiated. In the second portion of the response curve, an increase in the number of plies of CFRP leads to increased stiffness in the response due to the increased stiffness of the FRP jacket. This increased stiffness leads to an increase in ultimate capacity of the composite column as shown in Figure 4.4 (c). An increase in the number of CFRP plies also leads to an increase in the ultimate axial strain as shown in Figure 4.4 (b). Figure 4.4 (a) demonstrates that an increase in the number of plies of CFRP initially leads to an increase in the hybrid ultimate hoop strain and then asymptotically approaches the maximum value. Figure 4.4 (d) demonstrates that an increase in the number of plies of CFRP results in an increase in the confined concrete strength.

4.2.3 Concrete Strength

In a retrofit application, the designer must specify the concrete strength to be used therefore it is important to understand its effect on the column response. The effect of the concrete strength is examined in this section while the number of plies of GFRP in the split tube, the number of plies in the CFRP wrap, and the steel ratio are held constant at 2 plies, 2 plies, and 5.12%, respectively. The plot in Figure 4.5 demonstrates the effect of the concrete strength on the column response. In the initial portion of the response curve, an increase in concrete strength results in a stiffer response. An increase in concrete strength creates an increased Young's

modulus for the concrete which leads to the stiffer response. The concrete strength has minimal effect on the hybrid ultimate hoop strain as is shown in Figure 4.6 (a). The hybrid ultimate hoop strains for the concrete strengths shown are all within one percent of one another. An increase in concrete strength leads to a decrease in ultimate axial strain as is shown in Figure 4.6 (b). Figure 4.6 (d) demonstrates that an increase in concrete strength results in an increase in confined concrete strength. It follows that an increase in concrete strength also results in an increase in the ultimate capacity as shown in Figure 4.6 (c). However, Figure 4.7 demonstrates that the effectiveness of the confinement, as measured by confined concrete strength divided by concrete strength, decreases with an increase in concrete strength.

4.2.4 Steel Ratio

In a retrofit application the designer can control the steel ratio through the volume of concrete specified. Therefore, understanding the effect of the steel ratio on the composite column response will allow an optimized design in retrofit scenarios. The effect of the steel ratio is examined in this section while the number of plies of GFRP in the split tube, the number of plies in the CFRP wrap, and the concrete strength are held constant at 2 plies, 2 plies, and 26.2 MPa, respectively. The plot in Figure 4.8 demonstrates the effect that the steel ratio has on the column response. An increase in the steel ratio results in an increase in stiffness of the initial

portion of the load versus axial strain response curve since the steel section is behaving elastically in this region and contributes to the composite column stiffness. An increase in the steel ratio means that more of the cross-section responds at the Young's modulus of steel which is much higher than that of concrete. This results in an overall increase in column stiffness. At axial strains higher than the yield point, the response stiffness is identical for all steel ratios. In this region the steel is behaving plastically and adds no additional stiffness to the composite column response. The load versus axial strain response curves for the columns containing steel each exhibit a sharp bend at the point where the steel section begins to yield. This drastic change in stiffness is greater for columns with higher steel ratios since these columns were stiffer in the elastic portion of the response curve. Figure 4.9 (c) demonstrates that an increase in the steel ratio results in an increase in ultimate capacity. The steel ratio does not have an effect on the confined concrete behaviour. Therefore, the hybrid ultimate hoop strain, the ultimate axial strain, and the confined concrete strength are not affected by the steel ratio as is evident from Figure 4.9 (a), (b), and (d). This is inherently built into the model presented in Chapter 3 since the composite column response is determined by summing the contributions of the components.

4.2.5 Parametric Study Results

The results of the parametric study reveal that the different parameters control different portions of the column response curve. The stiffness of the initial portion of the response curve can be increased by increasing the steel ratio. Increasing the number of plies of GFRP or CFRP does not affect this region of the curve because the FRP jacket has not yet begun confining the concrete core. The stiffness of the second portion of the response curve can be increased by increasing the number of plies of GFRP or CFRP. Increasing the steel ratio does not affect the stiffness of this region of the curve because the steel is yielding and is not contributing any stiffness to the column response. An increase in either the number of plies of GFRP in the split tube or the number of plies in the CFRP wrap both result in an increase in column capacity. A comparison of Figure 4.2 (c) and Figure 4.4 (c) demonstrates that increasing the number of plies of CFRP has a greater influence on column capacity than increasing the number of plies of GFRP. An increase in the steel ratio also results in an increase in column capacity. An increase in the number of plies of CFRP results in an increase in ultimate axial strain whereas an increase in the number of plies of GFRP does not.

4.3 Code Predictions Comparison

Structural designers rely on code equations to calculate the factored resistance of a structural member to resist a factored load. This section

investigates the ability of current codes for confined concrete to safely predict the composite column capacity. Confined concrete is covered in the following three North American codes: ACI440.2R-08 in the United States and CAN/CSA S6-06 and CAN/CSA S806-12 in Canada. These codes cover the compressive behaviour of confined concrete as a strengthening technique for existing infrastructure but do not explicitly cover the compressive behaviour of confined concrete in new construction such as CFFT columns. The confined concrete strength calculated by a particular code is identical for column types C2 and C4 since they have the same column properties. The difference in the column capacity between these two column types comes from the increased compressive resistance offered by the steel section in column type C4. The shared properties of the specimens from column types C2 and C4 are used in the following sections to calculate the capacities given by these codes. The results are presented with the resistance factors as provided by each code as well as with the resistance factors set to unity.

4.3.1 The ACI440.2R-08

The ACI440.2R-08, Design and Construction of Externally Bonded FRP Systems (ACI Committee 440, 2008), has adopted Lam and Teng's (2003) design-orientated model as presented in Chapter 3 but has added an additional reduction factor, $\psi_f = 0.95$. The confined concrete strength, f'_{cc} , is determined as,

$$f'_{cc} = f'_c + \varphi_f 3.3 \kappa_a f_l \quad (4.1)$$

where f'_c is the unconfined concrete strength and κ_a is an efficiency factor to account for the geometry of the section and is given as 1.0 for circular cross sections. The maximum confining pressure, f_l , is given by,

$$f_l = \frac{2E_h t \varepsilon_{fe}}{d} \quad (4.2)$$

where t is the FRP jacket thickness, E_h is Young's modulus of the FRP jacket in the hoop direction, and d is the inner diameter of the FRP jacket.

The effective strain level, ε_{fe} , is given by,

$$\varepsilon_{fe} = \kappa_\varepsilon \varepsilon_{frp} \quad (4.3)$$

where ε_{frp} is the ultimate strain of the FRP as determined by coupon tests and κ_ε is the FRP strain efficiency factor given as 55%. The code also enforces a maximum axial compressive strain of 0.01 to prevent excessive cracking and the resulting loss of concrete integrity. When this limit is applicable the corresponding maximum value of f'_{cc} needs to be recalculated from the stress-strain curve.

The factored column capacity, P_r , is given as,

$$P_r = 0.8\phi[0.85f'_{cc}A_c + f_y A_s] \quad (4.4)$$

where A_c is the area of concrete, A_s is the area of steel, f_y is the yield strength of steel, and Φ is the material strength reduction factor which is given as 0.65 in ACI 318-05 (ACI Committee 318, 2005) for compression members with other reinforcement. The coefficient of 0.8 is a built in factor to account for imperfections in straightness or unintended eccentricity that do not allow the column to act in pure axial compression.

The factored capacity of column types C2 and C4 was calculated as 635 kN and 972 kN, respectively. The unfactored capacity, found with Φ set to unity, of column types C2 and C4 was calculated as 997 kN and 1515 kN, respectively.

4.3.2 The CAN/CSA S6-06

The CAN/CSA S6-06, Canadian Highway Bridge Design Code (Canadian Standards Association, 2010), gives the confined concrete strength as,

$$\frac{f'_{cc}}{f'_c} = 1 + 2 \frac{f_{l,FRP}}{f'_c} \quad (4.5)$$

where $f_{l,FRP}$ is defined as the confinement pressure due to FRP strengthening. It is calculated as,

$$f_{l,FRP} = \frac{2\phi_{FRP} f_{FRPu} t}{d} \quad (4.6)$$

where f_{FRP_u} is defined as the tensile strength of the FRP in the hoop direction and Φ_{FRP} is the resistance factor for FRP components which is given as 0.8.

The factored column capacity is given by,

$$P_r = 0.8(\alpha_1 \Phi_c f'_{cc} A_c + \Phi_s f_y A_s) \quad (4.7)$$

where Φ_c is the concrete material resistance factor taken as 0.65, Φ_s is the steel material resistance factor taken as 0.85, and α_1 is the compressive concrete factor given by,

$$\alpha_1 = 0.85 - 0.0015 f'_c \leq 0.67 \quad (4.8)$$

In addition, a confinement ratio between 0.1 and 0.3 is required. The lower limit ensures that enough FRP is used to provide sufficient confinement. The upper limit ensures that the factored resistance of the FRP-confined concrete does not exceed the equivalent normal strength of the unconfined concrete.

The factored capacity of column types C2 and C4 is calculated to be 715 kN and 1190 kN, respectively. The unfactored capacity, found with Φ_{FRP} , Φ_c , and Φ_s set to unity, of column types C2 and C4 is calculated to be 953 kN and 1473 kN, respectively.

4.3.3 The CAN/CSA S806-12

The CAN/CSA S806-12, Design and Construction of Building Components with Fibre-Reinforced Polymers (Canadian Standard Association, 2009), gives the confined concrete strength as,

$$\frac{f'_{cc}}{f'_c} = 0.85 + k_l k_c \frac{f_L}{f'_c} \quad (4.9)$$

where k_c is 1.0 for circular jackets and k_l is defined as,

$$k_l = 6.7(k_c f_L)^{-0.17} \quad (4.10)$$

where,

$$f_L = \frac{2f_F t}{d} \quad (4.11)$$

where,

$$f_F = \text{the lessor of } 0.006E_h \text{ or } \Phi_F f_{Fu} \quad (4.12)$$

where E_h is Young's modulus of the FRP jacket, f_{Fu} is the ultimate tensile strength of FRP composites, and Φ_F is the resistance factor for FRP composites which is given as 0.75. The factored resistance of the column can be calculated according to CAN/CSA A23.3 (CSA, 2004) as,

$$P_r = 0.8(\alpha_1 \Phi_c f'_{cc} A_c + \Phi_s f_y A_s) \quad (4.13)$$

The factored capacity of column types C2 and C4 was calculated as 868 kN and 1307 kN, respectively. The unfactored capacity, found with Φ_F , Φ_c , and Φ_s set to unity, of column types C2 and C4 was calculated as 1336 kN and 1836 kN, respectively.

4.3.4 Comparison

The factored resistance of column types C2 and C4 are determined with three North American codes. The factored capacity is compared to the response curve for each column type. Figure 4.10 (a) and Figure 4.11 (a) present this comparison for column type C2 and C4, respectively. The factored capacities of all three codes are within the elastic region of the response for column types C2 and C4. For column type C2, the factored capacities are near the transition point in the response curve. The factored code capacities for column type C4 are significantly lower than the transition point in the response curve, resulting in more conservative values. It should be noted that the contribution of the steel W section in column type C4 is applied in the code equations as the area of steel. The area of steel in these equations is typically the area of reinforcing bars in the column. The resistance factor for reinforcing steel is typically lower than that of structural steel which contributes to the conservative values for the factored capacity of column type C4.

For both column types, the capacities given by the different codes vary substantially. As code equations are based on modelling, improved code predictions will follow from better analytical models. Improved code predictions will result in better consistency between different codes.

The unfactored resistance of each column type is determined with three North American codes and compared to the response curve for column types C2 and C4 in Figure 4.10 (b) and Figure 4.11 (b), respectively. The unfactored resistance was calculated with all resistance factors equal set to unity. For these calculations, the equation coefficients and the various limits imposed by the codes were maintained. For both column types, ACI440.2R-02 and CAN/CSA S6-06 give comparable results to one another while CAN/CSA S806-12 gives a significantly higher column capacity. For column type C2, CAN/CSA S806-12 gives the greatest unfactored capacity of the three codes as 54.8% of the ultimate experimental capacity. For column type C4, CAN/CSA S806-12 gives the greatest unfactored capacity of the three codes as 65.3% of the ultimate experimental capacity. For both column types, all three unfactored code capacities are less than two thirds of the ultimate experimental capacity which indicates that there is a lot of conservatism built into the codes in addition to the resistance factors. The predictive capability of the codes will increase as research in this field continues. With better predictive capability, a code will be able to give a less conservative capacity.

4.4 Conclusions

First, a parametric study was performed on column type C6 using the analytical model developed in Chapter 3. Second, the experimental results of column types C2 and C4 were compared to composite column capacities predicted by three different North American codes.

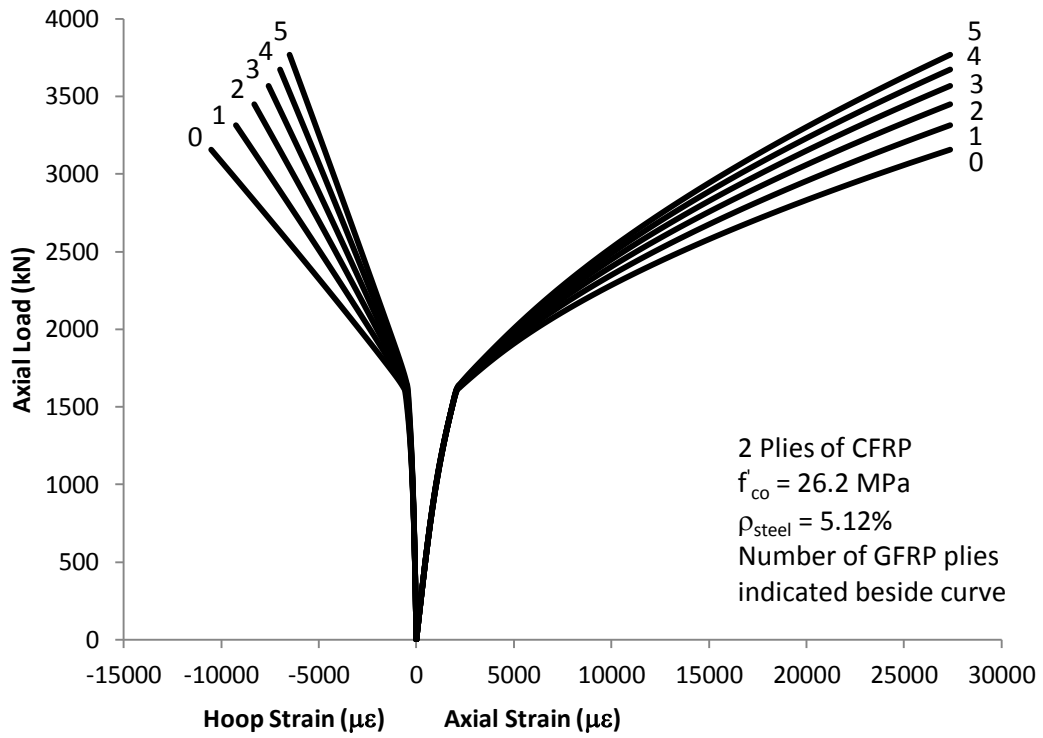
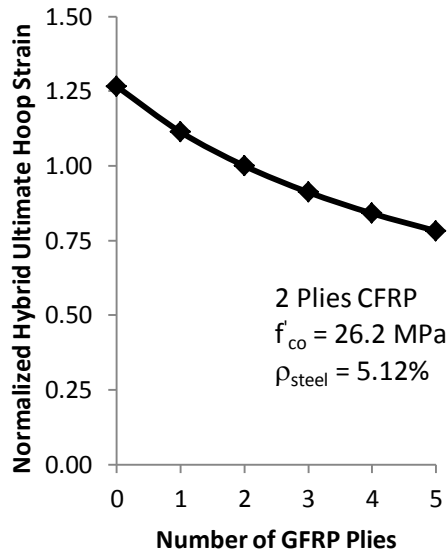
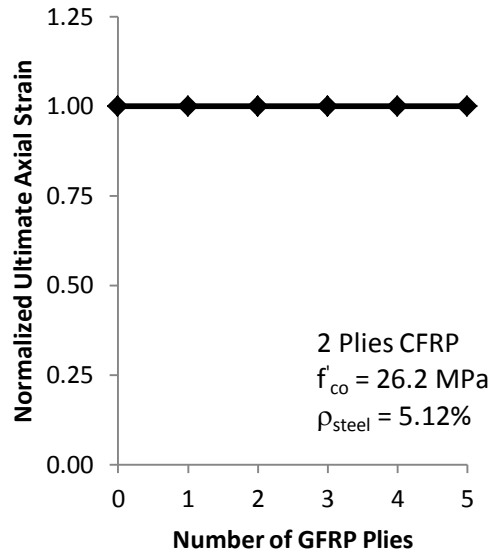


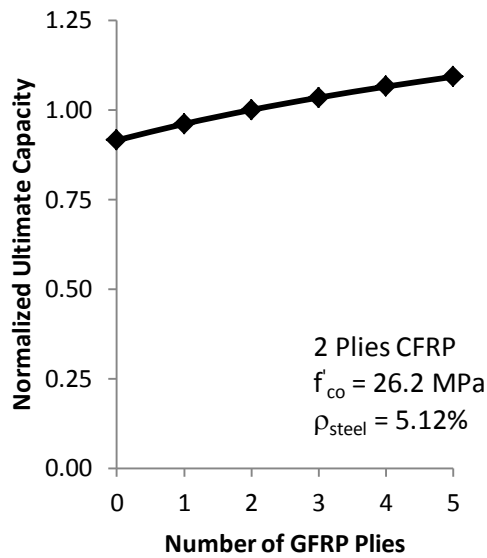
Figure 4.1: Effect of the Number of GFRP Plies on the Load vs. Strain Response



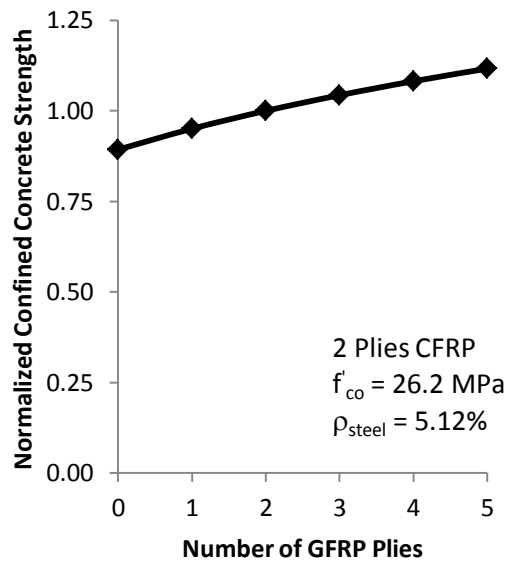
(a) Hybrid Ultimate Hoop Strain



(b) Ultimate Axial Strain



(c) Ultimate Capacity



(d) Confined Concrete Strength

Figure 4.2: Influence of the Number of GFRP Plies

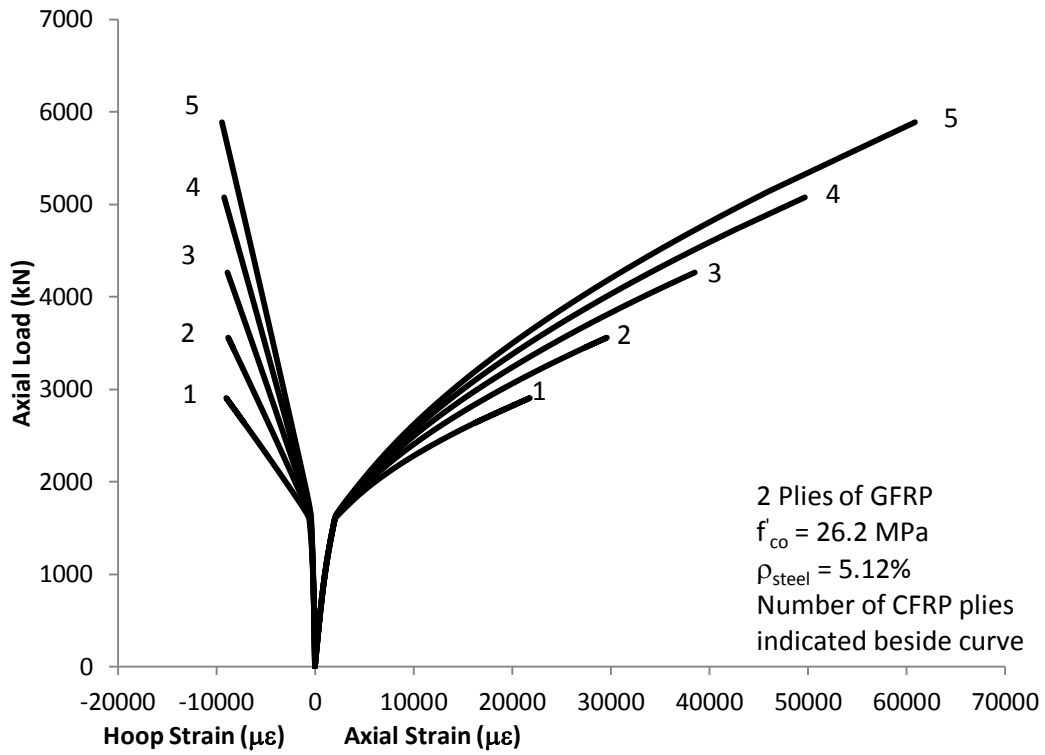
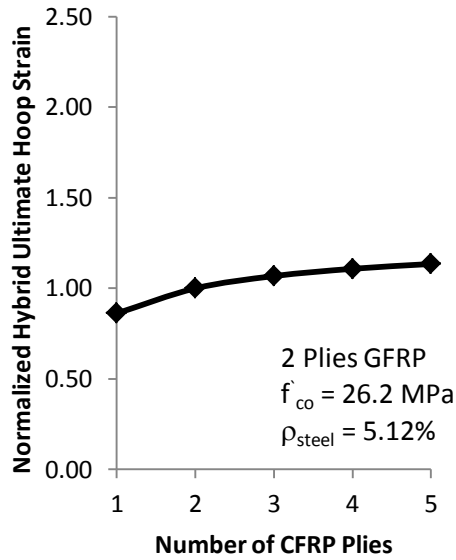
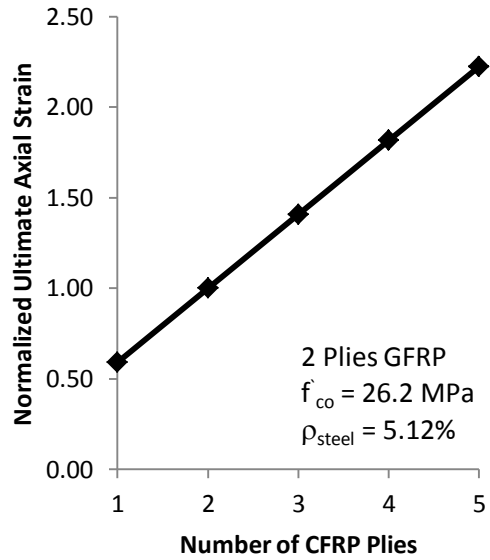


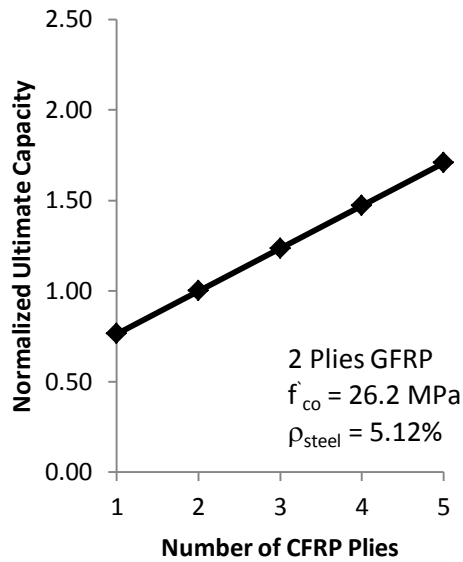
Figure 4.3: Effect of the Number of CFRP Plies on the Load vs. Strain Response



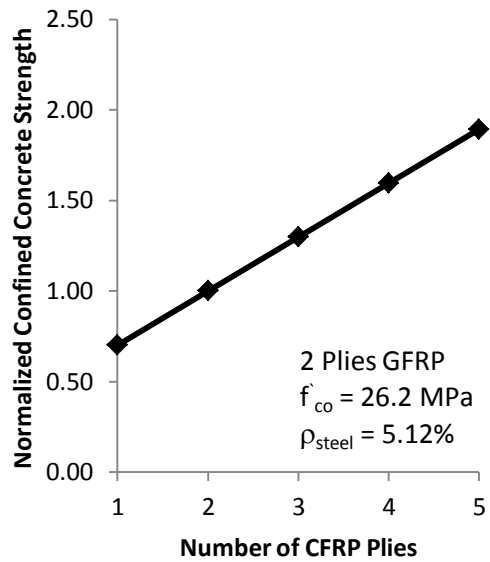
(a) Hybrid Ultimate Hoop Strain



(b) Ultimate Axial Strain



(c) Ultimate Capacity



(d) Confined Concrete Strength

Figure 4.4: Influence of the Number of CFRP Plies

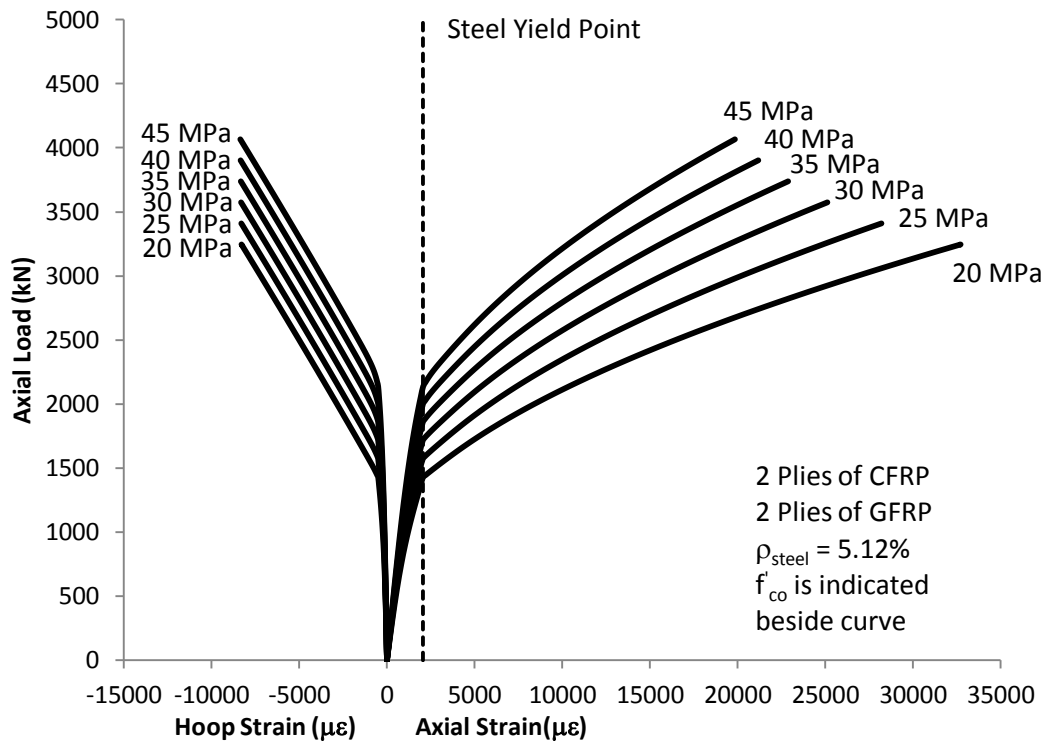
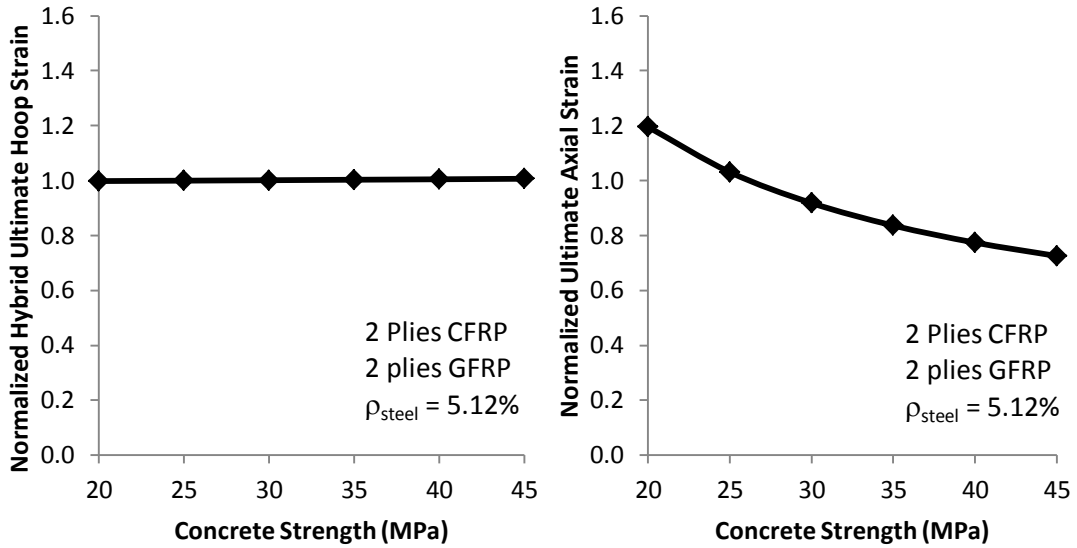
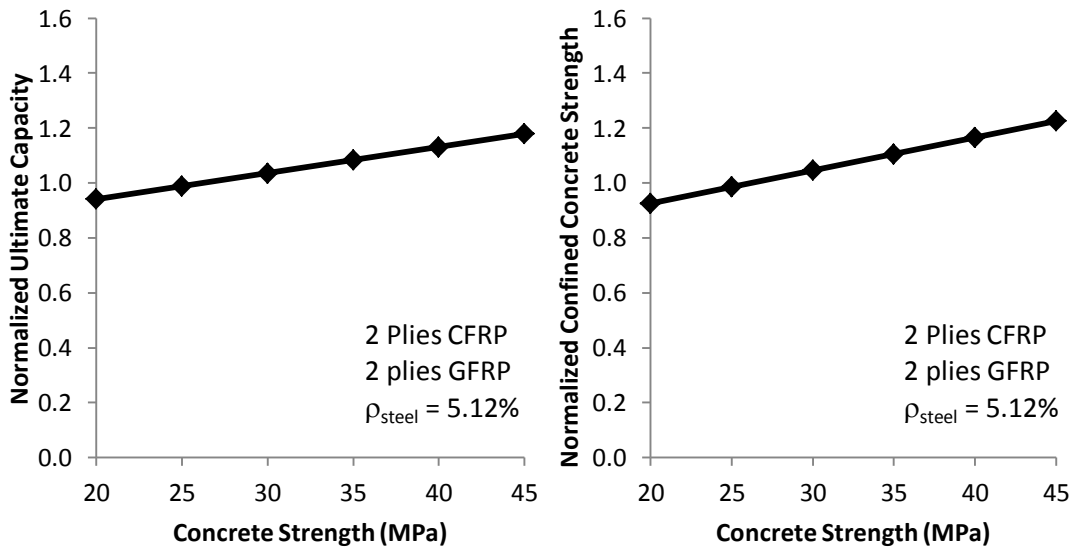


Figure 4.5: Effect of the Concrete Strength on the Load vs. Strain Response



(a) Hybrid Ultimate Hoop Strain

(b) Ultimate Axial Strain



(c) Ultimate Capacity

(d) Confined Concrete Strength

Figure 4.6: Influence of the Concrete Strength

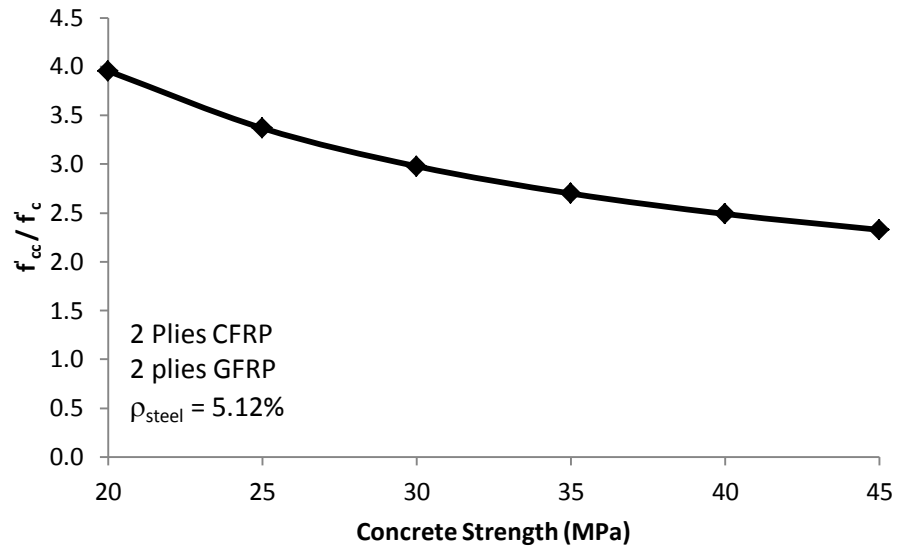


Figure 4.7: Influence of Concrete Strength on Split Tube FRP Jacket Confinement Effectiveness

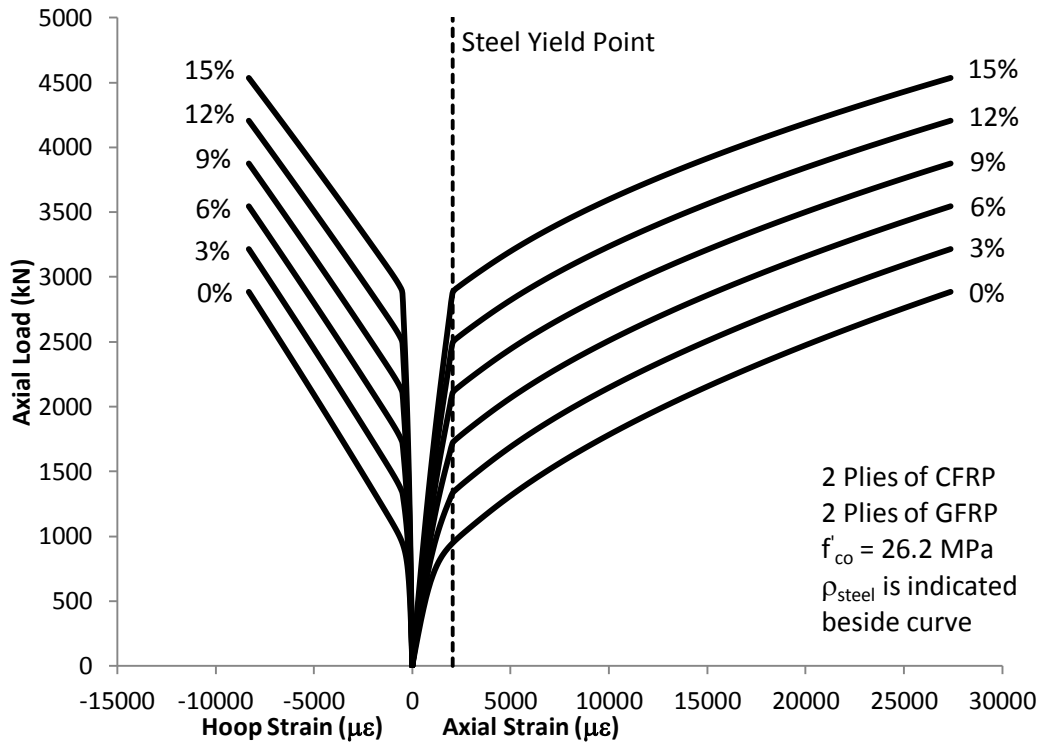
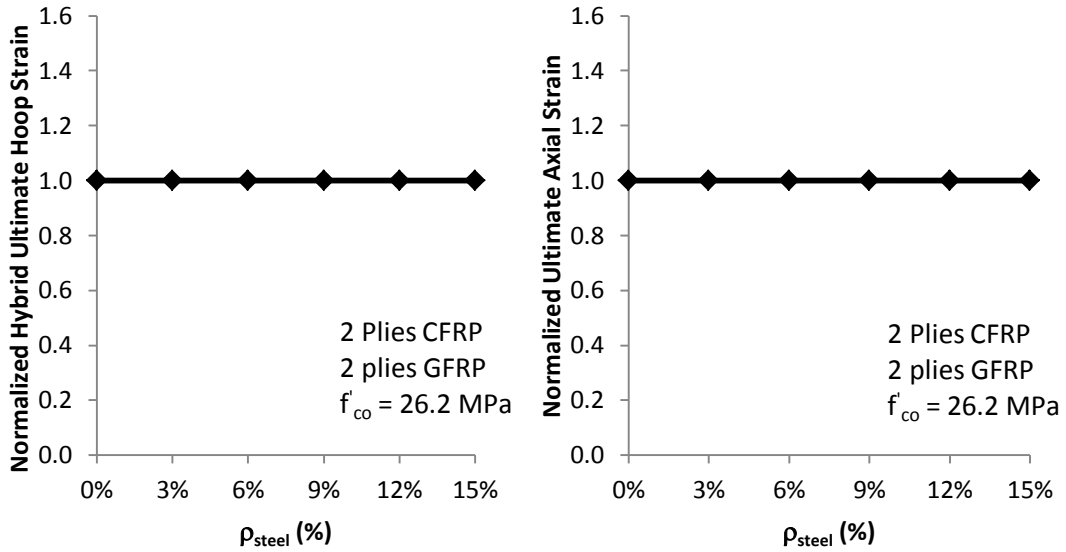
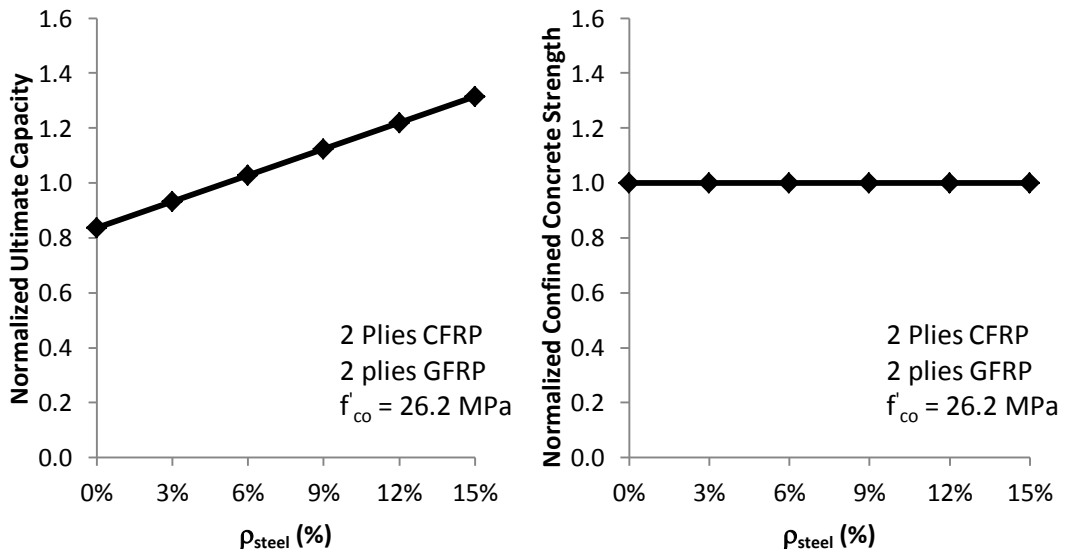


Figure 4.8: Effect of the Steel Ratio on the Load vs. Strain



(a) Hybrid Ultimate Hoop Strain

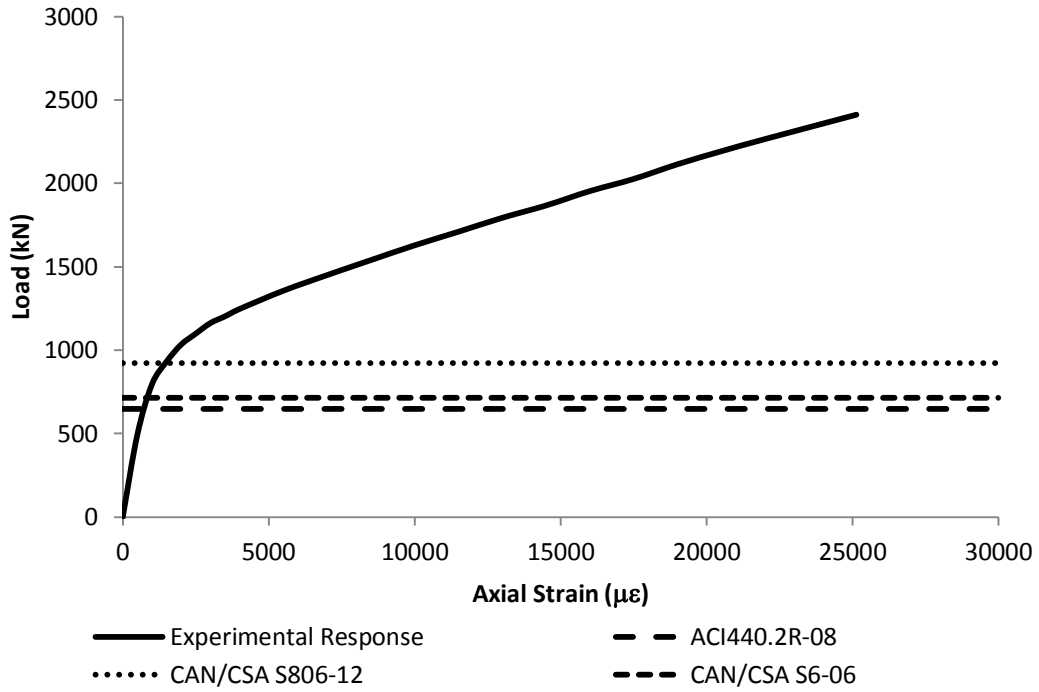
(b) Ultimate Axial Strain



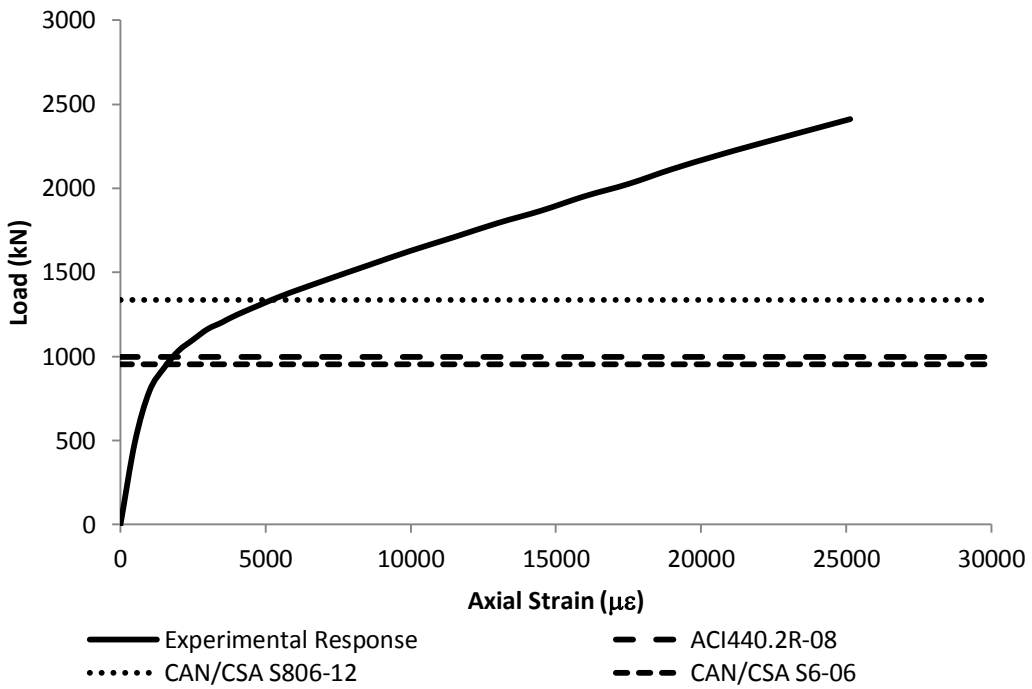
(c) Ultimate Capacity

(d) Confined Concrete Strength

Figure 4.9: Influence of the Steel Ratio

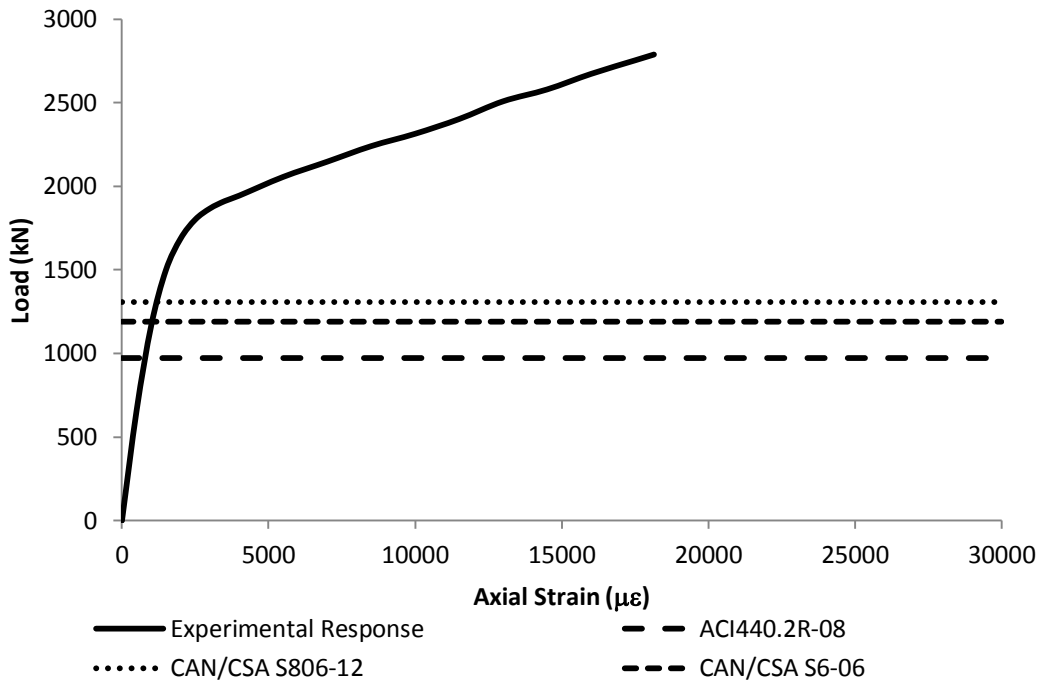


(a) Factored

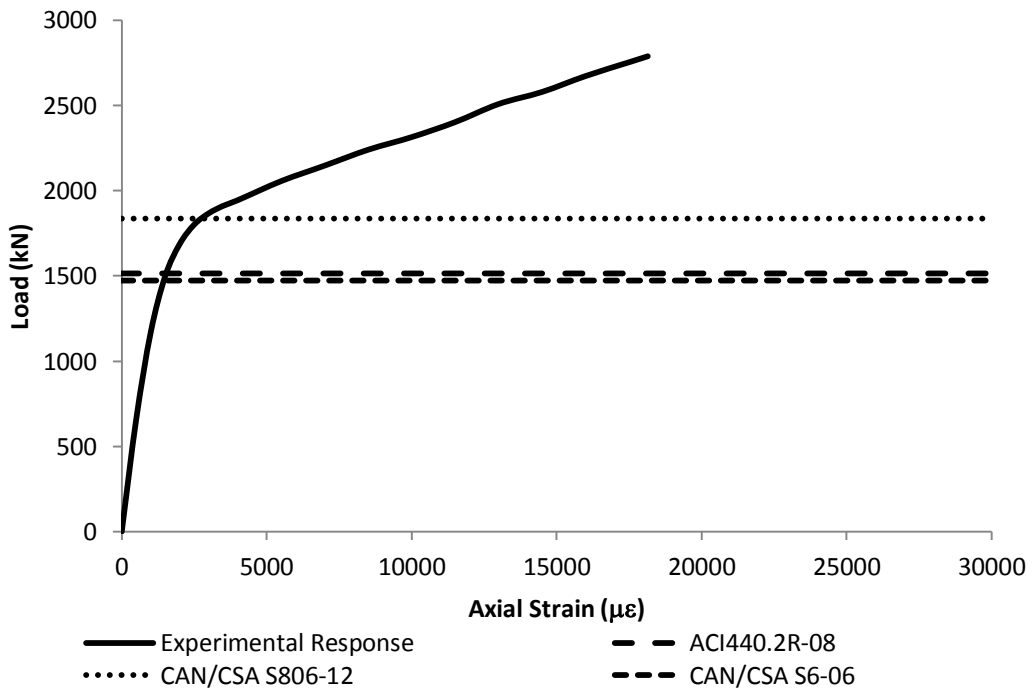


(b) Unfactored

Figure 4.10: Comparison of Experimental Response to Code Determined Resistance Values for Column Type C2



(a) Factored



(b) Unfactored

Figure 4.11: Comparison of Experimental Response to Code Determined Resistance Values for Column Type C4

Chapter 5 - Summary and Conclusions

5.1 Summary

The study included an experimental program, modelling work, a parametric study, and an investigation of code design predictive capabilities.

The experimental program was designed and performed in order to investigate three aspects of FRP-confined concrete-steel composite column systems, including: the effect of adding a steel W section to confined concrete; the effect of using a wrapped split tube system; and the effect of using concrete with shrinkage reducing admixture. A total of 18 stub column tests representing six unique column types were constructed and tested. The column types included: steel W sections; CFRP-confined concrete; CFRP-confined concrete plus shrinkage reducing admixture; CFRP-confined concrete-steel composite; CFRP-confined shrinkage reducing admixture concrete-steel composite; and CFRP-wrapped split-GFRP-confined concrete-steel composite.

The CFRP-confined concrete-steel composite column described in this study can be utilized in the repair and retrofit of steel compressive members in bridges. In particular, the CFRP-wrapped split-GFRP-confined concrete-steel composite system provides a practical application technique to apply this scheme in a retrofit scenario.

The load versus strain response of column types C2, C4, and C6 was investigated through the use of four analytical models. Two design-orientated models were examined: the first was the popular model by Lam and Teng (2003) and the second was a revised version of this model by Teng et al. (2009). Two analysis-orientated models were also examined in order to implement the effects of the increased jacket stiffness of column type C6. They included a model by Teng et al. (2007) and a revision to this model by Jiang and Teng (2007).

The parametric study investigated the effects of four parameters on the response of column type C6: CFRP-wrapped split-GFRP-confined concrete-steel composite. The study considered the number of plies of GFRP in the split tube elements; the number of plies of CFRP wrap; the concrete strength; and the steel ratio.

Three North American codes were investigated and applied to column types C2 and C4. These included ACI440.2R-08: Design and Construction of Externally Bonded FRP Systems; CAN/CSA S6-06: Canadian Highway Bridge Design Code; and CAN/CSA S806-02: Design and Construction of Building Components with Fibre-Reinforced Polymers. The investigation revealed that all codes gave a factored resistance in the elastic region of the composite column response for both column types.

5.2 Conclusion

Based on comparisons between the experimental results of different column types the following conclusions can be drawn:

1. The response of confined concrete that includes a steel W section is similar to the response of confined concrete plus the elastic-perfectly plastic steel contribution.
2. Confined concrete that includes a steel W section fails prematurely due to the stress concentrations in the confined concrete that arise from the buckling of the steel flanges.
3. The split tube system forces failure to occur along a predetermined line thus reducing the cumulative probability of failure which leads to an increased ultimate capacity.
4. The use of shrinkage reducing admixture in confined concrete has no distinguishable effect on the confined concrete strength.

Based on comparisons between the different analytical models considered, the following conclusions can be drawn:

1. The analysis-orientated modelling provides results that are in better agreement with experimental findings than the design orientated modelling for all column types.

2. The hybrid jacket stiffness can be utilized in the model for a split tube system if an appropriate reduction to the FRP efficiency factor is made.
3. The proposed β factor has an excellent ability to predict this reduction.
4. The analysis-orientated model which incorporates the increased hybrid jacket stiffness is in better agreement with experimental results than the model that ignores the split tube stiffness.

Based on the results of the parametric study, the following conclusions can be drawn:

1. An increase in the number of plies of GFRP leads to a decrease in the hybrid ultimate hoop strain and an increase in column capacity.
2. An increase in the number of plies of CFRP leads to an increase in column capacity as well as an increase in ultimate axial strain.
3. An increase in the concrete strength leads to an increase in column capacity and a decrease in ultimate axial strain
4. An increase in the steel ratio leads to increased column capacity but has no effect on the ultimate axial strain.

5.3 Recommendations for Future Work

1. Test and compare wrapped split tube confined concrete columns to wrapped split tube confined concrete-steel composite columns.

2. Test confined concrete columns with a 4 piece onion skin FRP jacket as shown in Figure 1.4. Extend analysis-orientated model incorporating increased stiffness to this jacket type.
3. Test and compare different diameter composite columns with the same steel W section.
4. If confined concrete-steel composite columns are to be tested, include strain gauges on the steel section to understand how the steel is behaving throughout the column response. Compare the encased steel response to the response of a steel section, such as column type C1 in this study, to help quantify the benefits of encasing the steel section in concrete.

Chapter 6 References

ACI Committee 318. (2005). ACI 318-05: Building Code Requirements for Structural Concrete.

ACI Committee 440. (2004). ACI 440.3R-04: Guide Test Methods for Fiber-Reinforced Polymers (FRP's) for Reinforcing Polymers (FRPs) for Reinforcing or Strengthening Concrete Structures.

ACI Committee 440. (2008). ACI 440.2R-08: Guide for the Design and Construction of Externally Bonded FRP Systems for Strengthening Concrete Structures.

ASTM International. (2008). ASTM Standard D3039/D3039M: Standard Test Method for Tensile Properties of Polymer Matrix Composite Materials. West Conshohocken, PA.

ASTM International. (2010). ASTM Standard D7565/D7565M: Standard Test Method for Determining Tensile properties of Fiber reinforced Polymer Matrix Composites Used for Strengthening of Civil Structures. West Conshohocken, PA.

BASF. (2010). TETRAGUARD AS20. Cheadle, UK.

Canadian Institute of Steel Construction. (2008). *Handbook of Steel Construction, Ninth Edition, Forth Printing*. Canada: Lakeside Group Inc.

Canadian Standard Association. (2009). *CAN/CSA S806-02: Design and Construction of Building Components with Fibre-Reinforced Polymers.*

Canadian Standards Association. (2010). *CAN/CSA S6-06: Canadian Highway Bridge Design Code.*

Chastre, C., & Silva, M. (2010). Monotonic axial behavior and modelling of RC circular columns confined with CFRP. *Engineering Structures*, 32, 2268-2277.

CSA. (2004). *A23.3-04: Design of Concrete Structures.*

De Nicolo, B., Oani, L., & Pozzo, E. (1994). Strain of concrete at peak compressive stress for a wide range of compressive strengths. *Materials and Structures*, 27, 206-210.

El Chabib, H., Nehdi, M., & El Nagar, M. (2005). Behavior of SCC confined in short GFRP tubes. *Cement & Concrete Composites*, 27, 55-64.

Fam, A., & Rizkalla, S. (2001). Confinement Model for Axially Loaded Concrete Confined by Circular Fiber-Reinforced Polymer Tubes. *ACI Structural Journal*, 451-461.

Federal Highway Administrative Bridge Programs National Bridge Inventory. (2012, Feb. 5). *FHWA Bridge Programs NBI Data.*

Retrieved July 17, 2012, from
<http://www.fhwa.dot.gov/bridge/britab.cfm>

Ford Motor Company. (1982). Energy Absorption in Composite Tubes.
Journal of Composite Materials, 16, 521-544.

Fyfe Co. LLC. (2010). *Tyfo SCH-41S Composite using Tyfo S Epoxy*.
California: Fyfe Co. LLC.

Fyfe Co. LLC. (2010). *Tyfo SEH-51A Composite using Tyfo S Epoxy*.
California: Fyfe Co. LLC.

Harries, K., & Carey, S. (2003). Shape and "gap" effects on the behavior
of variably confined concrete. *Cement and Concrete Research*, 33,
881-890.

Hu, H. (2011). *Development of a New Constitutive Model for FRP-and-
steel-confined Concrete*. Unpublished MSc Thesis. North Carolina
State University.

International Institute for FRP in Construction. (1998, Jan.). *Newsletters:
Vol. 6. Issue 1*. Retrieved July 17, 2012, from [http://www.iifc-
hq.org/news/](http://www.iifc-hq.org/news/)

Jiang, T., & Teng, J. (2007). Analysis-orientated stress-strain models for
FRP-confined concrete. *Engineering Structures*, 29, 2968-2986.

Karimi, K., Tait, M., & El-Dakhakhni, W. (2009). A Novel Retrofit Technique for Strengthening Steel Columns Using FRP. *CSCE 2009 Annual General Conference*. St. John's.

Karimi, K., Tait, M., & El-Dakhakhni, W. (2010). Experimental Investigation of Two FRP Retrofit Schemes for Strengthening Steel Columns. *9th U.S. National and 10th Canadian Conference on Earthquake Engineering*. Toronto, Canada.

Karimi, K., Tait, M., & El-Dakhakhni, W. (2010). Testing and Modeling of a novel FRP-encased steel-concrete composite column. *Journal of Composite Structures*.

Karimi, K., Tait, M., & El-Dakhakhni, W. (2011). Performance Enhancement of Steel Columns using Concrete-filled Composite Jackets. *ASCE Journal of Performance of Constructed Facilities*, 189-201.

Karimi, K., Tait, M., & El-Dakhakhni, W. (2012). Influence of Slenderness on the Behaviour of a FRP-encased Steel-Concrete Composite Column. *Journal of Composites for Construction*, 100-109.

Karimi, K., Tait, M., & El-Dakhakhni, W. (2013). Analytical modeling and axial load design of a novel FRP-encased steel-concrete composite

column for various slenderness ratios. *Engineering Structures*, 526-534.

Lam, L., & Teng, J. (2003). Design-oriented stress-strain model for FRP-confined concrete. *Construction and Building Materials*, 17, 471-489.

Lam, L., & Teng, J. (2004). Ultimate Condition of Fiber Reinforced Polymer-Confined Concrete. *Journal of Composites for Construction*, 8(6), 539-548.

Lee, S. (2012, Jan.). Current State of Bridge Deterioration in the U.S. - Part 1. *Materials Performance Magazine, National Association of Corrosion Engineers International*, pp. 62-67.

Li, H., Torres, S., Alaywan, W., & Abadie, C. (2005). Experimental Study of FRP Tube-encased Concrete Columns. *Journal of Composite Construction*, 39(13), 1131-1145.

Linde, J. (2011). *Influence of Shrinkage Reducing Agent on the Behaviour of Steel-Concrete-CFRP Composite Columns*.

Liu, X., Nanni, A., & Silva, P. (2005). Rehabilitation of Compressive Steel Members using FRP Pipes Filled with Non-expansive and Expansive Light-weight Concrete. *Advances in Structural Engineering*, 8(2), 129-142.

Mander, J., Priestley, M., & Park, R. (1988). Theoretical Stress-Strain Model for Confined Concrete. *Journal of Structural Engineering*, 1804-1826.

Marques, P., & Chastre, C. (2012). Performance analysis of load-strain models for circular columns confined with FRP composites. *Composite Structures*, 96, 3115-3131.

Mirmiran, A., Shahawy, M., Samaan, M., El-Echary, H., Mastrapa, J. C., & Pico, O. (1998). Effect of Column Parameters on FRP-Confined Concrete. *Journal of Composites for Construction*, 2(4), 175-185.

Mirza, S., ASCE, F., & Lacroix, E. (2004). Comparative Strength Analyses of Concrete-Encased Steel Composite Columns. *Journal of Structural Engineering*, 130, 1941-1953.

Mohamed, H. M., & Masmoudi, R. (2010). Axial Load Capacity of Concrete-Filled FRP Tube Columns: Experimental versus Theoretical Predictions. *Journal of Composites for Construction*, 14(2), 231-243.

Naguib, W., & Mirmiran, A. (2001). Effect of Advanced Composites on Creep and Shrinkage of Concrete. *2001: a Materials and Processes Odyssey: 46th International SAMPE Symposium and*

Exhibition: Long Beach Convention Center, Long Beach California, May 6-10, 2001, Book 2. Long Beach California.

Patnaik, A. K., & Bauer, C. L. (2004). Strengthening of steel beams with carbon fiber laminates. *Composite Materials in Bridges and Structures*. Calgary, Alberta.

Shaat, A., & Fam, A. (2006). Axial loading tests on short and long hollow structural steel columns retrofitted using carbon fibre reinforced polymers. *Canadian Journal of Civil Engineering*, 33(4), 458-470.

Teng, J., Huang, Y., Lam, L., & Ye, L. (2007). Theoretical Model for Fiber-Reinforced Polymer-Confined Concrete. *Journal of Composite Construction*, 11(2), 201-210.

Teng, J., Jiang, T., Lam, L., & Luo, Y. (2009). Refinement of a Design-Orientated Stress-Strain Model for FRP-Confined Concrete. *Journal of Composites for Construction*, 13(4), 269-278.

Xiao, Y., & Ma, R. (1997). Seismic Retrofit of RC Circular Columns using Prefabricated Composite Jacketing. *Journal of Structural Engineering*, 123(10), 1357-1364.

Xiao, Y., Wu, H., & Martin, G. R. (1999). Prefabricated Composite Jacketing of RC Columns for Enhanced Shear Strength. *Journal of Structural Engineering*, 125(3), 255-264.

Yang, H., Lam, D., & Gardner, L. (2008). Testing and analysis of concrete-filled elliptical hollow section. *Journal of Engineering Structures*, 30, 3771-3781.